Technical University of Denmark

DTU

Computational Design of New Materials for Ammonia Storage

Jensen, Peter Bjerre; Vegge, Tejs; Quaade, Ulrich

Publication date:
2014

Document Version
Publisher's PDF, also known as Version of record

Link back to DTU Orbit

DTU Library
Technical Information Center of Denmark

Computational Design of New Materials for Ammonia Storage

PhD Thesis

Department of Energy Conversion and Storage
Technical University of Denmark

Peter Bjerre Jensen

Computational Design of New Materials for Ammonia Storage

Author
Peter Bjerre Jensen
E-mail: pbjen@dtu.dk

Supervisors
Professor Tejs Vegge
Department of Energy Conversion and Storage
Technical University of Denmark
E-mail: teve@dtu.dk

PhD, Ulrich Quaade
Chief of Research
Amminex Emissions Technology A/S
E-mail: ujq@amminex.com

Atomic Scale Modelling and Materials
DTU Energy Conversion
Technical University of Denmark
Frederiksborgvej 399
4000 Roskilde
Denmark

Tel.:   (+45) 46 77 58 00
Web: www.ecs.dtu.dk
E-mail: info@ecs.dtu.dk

Center for Atomic-scale Materials Design
DTU Physics
Technical University of Denmark
Fysikvej 311
2800 Kongens Lyngby
Denmark

Tel.:   (+45) 45 25 33 44
Web: www.camd.dtu.dk
E-mail: info@fysik.dtu.dk

Abstract

Many renewable energy technologies are currently being developed, but most have the major drawback, that the energy is not generated when needed, and storage of the energy is therefore essential. For transportation applications, an energy carrier offering a high energy density is needed. Ammonia is one possible energy carrier offering high gravimetric and volumetric capacities. A major drawback regarding ammonia is however its toxicity requiring careful handling and storage.

Instead of handling the ammonia directly, it is possible to store it safely and completely reversibly in many different metal halide salts. The release temperatures vary significantly for the different materials and the release is often a multi-step reaction occurring over a broad temperature interval. The object of the present thesis has therefore been to design new mixed materials with improved release characteristics using Density Functional Theory (DFT), which offers a predictive accuracy at a limited computational cost. Initially strontium chloride, which is the state-of-the-art material for solid state ammonia storage, was studied in details. From the gained insights new solid solutions of strontium and barium chlorides were predicted to offer superior storage capacities, which subsequently were experimentally verified.

Inspired by the impressive properties offered by the binary mixtures an extensive computational screening was initiated searching for bi- and ternary metal halides. A large number of metals were allowed, resulting in search spaces containing many thousands of possible candidates, which cannot all be studied using DFT calculations due to consideration of the cumulative computational cost. Therefore a genetic algorithm (GA) was implemented to guide the search more effectively. To further decrease the need for computational resources a template based screening approach was used to set up the structures.

An initial test of the algorithm was performed searching for the mixed hexa ammine offering the highest storage capacity. The investigated search space contained almost 27 000 structures. By using the GA it was possible to identify the global optimum structure in three consecutive runs starting from different random populations, examining less than two percent of the candidates.

Following the successful initial test of the algorithm a more advanced screening was initiated. The complexity was increased by including checks of multiple intermediate ammine phases to determine the correct release patterns, resulting in a total of more than 100 000 structures to test. The objective of the search

was to find optimised materials releasing most possible ammonia in a narrow temperature interval. Again the robustness of the algorithm was confirmed by rerunning the algorithm, which showed a very high consistency in identifying the best candidates.

Interestingly, the algorithm correctly identified all the barium-strontium mixtures which were already known to exist from the previous studies as good candidates. Furthermore a ternary alkaline-earth mixture, $Ba_4CaSr_3Cl_{16}$ was identified, and the predicted release was verified experimentally. The two best found candidates, $Ca_4Cu_2Y_2Cl_{16}$ and $Sr_4Cu_2Y_2Cl_{16}$, are examples of materials, one would not suggest using chemical intuition. This shows that the algorithm is able to identify new materials by using the available operators, which are based on a combination of chemical knowledge and random events. The initial experimental tests of the identified candidates showed promising results, but did also reveal that the materials can be challenging to synthesize, and might degrade during ammonia desorption due to unwanted side reactions.

Resumé

Mange nye vedvarende energiteknologier er ved at blive udviklet, men de fleste har den store ulempe at energien ikke genereres, når den skal bruges, hvilket gør energilagring essentiel. Til transport er det vigtig at finde en energibærer, der tilbyder en høj energidensitet. Ammoniak er et eksempel på en mulig energibærer, som tilbyder høje gravimetriske og volumetriske kapaciteter. En stor ulempe ved ammoniak er dog dets toksicitet, hvilket kræver forsigtig håndtering og opbevaring.

I stedet for at bruge ammoniak direkte er det muligt at lagre det sikkert og reversibelt i mange forskellige metal halid salte. Frigivelsestemperaturerne varierer meget for de forskellige materialer og desuden frigives ammoniakken ofte i flere trin i et bredt temperaturinterval. Målet med denne afhandling har derfor været at designe nye blandede materialer med forbedrede frigivelsesegenskaber, ved brug af tæthedsfunktionale teori (DFT), der tilbyder en prædiktiv nøjagtighed ved brug af begrænsede computerressourcer. Til at begynde med studeres strontium klorid som er 'state-of-the-art' materialet for faststof-lagring af ammoniak. Ud fra den opnåede forståelse blev nye faststofforbindelser af strontium af barium klorid forudsagt, og efterfølgende eksperimentelt verificeret.

Inspireret af de binære blandingers imponerende egenskaber blev en stor computerscreening indledt, for at søge efter bi- og ternære metal halider. Et stort antal metaller var tilladt, hvilket resulterede i faserum med mange tusinde mulige kandidater, som ikke alle kan studeres med DFT beregninger der vil kræve for lang tid. Derfor blev en genetisk algoritme (GA) implementeret til at guide søgningen mere effektivt. For yderligere at reducere de nødvendige computerressourcer blev en skabelon-baseret tilgang anvendt til at sætte strukturerne op.

En indledende test af algoritmen blev foretaget ved at søge efter den blandede hexa amin, som tilbyder den højeste lagringskapacitet. Det undersøgte faserum bestod af næsten 27 000 strukturer. Ved at anvende den genetiske algoritme var det muligt at identificere den globalt optimale struktur i tre kørsler, startende fra forskellige tilfældige populationer, ved at teste mindre end to procent af kandidaterne.

Efter den succesfulde indledende test af algoritmen blev en mere avanceret screening udført. Kompleksiteten blev øget ved at inkludere flere intermediære amin-faser for at bestemme det korrekte frigivelsesmønster, hvilket resulterede i mere end 100 000 strukturer. Målet med screeningen var at finde optimerede materialer, som har mulighed for at frigive mest muligt ammoniak i et snæ-

vert temperatur-interval. Igen blev robustheden af algoritmen bekræftet ved gentagne kørsler af algoritmen, hvilket viste en meget stor succesrate i bestemmelse af de bedste kandidater.

Algoritmen identificerede strontium-barium blandingerne, som allerede var kendt som gode kandidater fra de tidligere studier. Yderligere blev en ternær jord-alkalimetal-blanding, $Ba_4CaSr_3Cl_{16}$, identificeret, og den forudsagte frigivelse blev bekræftet eksperimentelt. De to bedste kandidater, $Ca_4Cu_2Y_2Cl_{16}$ og $Sr_4Cu_2Y_2Cl_{16}$, er eksempler på materialer som man ikke ville foreslå ved brug af kemisk intuition. Dette viser at algoritmen er i stand til at foreslå nye materialer ud fra de tilgængelige operatorer, som er baseret på en kombination af kemisk viden og tilfældige begivenheder. De indledende eksperimentelle tests af de identificerede kandidater viste lovende resultater, men viste samtidigt også at materialerne kan være svære at syntetisere og kan blive nedbrudt under frigivelsen af ammoniak pga. uønskede sidereaktioner.

Preface

This thesis is submitted in candidacy for the PhD degree from the Technical University of Denmark (DTU). It is based on the work carried out between September 2011 and October 2014 in the Department of Energy Conversion and Storage, the Center for Atomic-scale Materials Design (CAMD) and with an external stay at Amminex Emmissions Technology A/S. The project was supervised by Professor and group leader of the section Atomic Scale Modelling and Materials at the Department of Energy Conversion and Storage, Tejs Vegge and co-supervised by Chief of Research at Amminex Emmissions Technology A/S, Ulrich Quaade. The work was financially supported by the Danish National Advanced Research Foundation (DNATF, Højteknologifonden).

First of all I would like to thank my supervisor Tejs Vegge for guiding me through the project and keeping me on track, when I have wanted to study some details, which might be interesting, but not important in the bigger picture. I would also like to thank my co-supervisor Ulrich Quaade for allowing me to gain insight into how the theory can be used do develop real-life products. Furthermore I appreciate that you made it possible for me to have my external stay at Amminex. I would also like to thank Agata Bialy and Bianca Larsen for taking care of me during the stay.

I will also thank my colleagues, both former and current, for a nice working environment. Especially thanks to the people I have cooperated with on different projects Steen Lysgaard, Didier Blanchard, Agata Bialy and Rune Johnsen. Also thanks to Jon Steinar Gardarsson Myrdal, Jakob G. Howalt, Nonni Bergmann and Dadi Sveinbjörnsson for various help the last years. Special thanks go to the people who have proofread the thesis Steen Lysgaard, Didier Blanchard and Rune Christensen, I am very grateful for your helpful comments and suggestions.

Last, but not least, Anette, thank you for your love and for choosing to spend your life with me.

Kgs. Lyngby, October 2014
Peter Bjerre Jensen

Contents

List of Tables

List of Figures

Introduction

1.1 Sustainable Energy

One of the major challenges for the continued growth and development all over the world is the need for a sustainable energy system [1]. Currently the main sources of energy are fossil fuels in form of oil, coal and natural gas (Figure 1.1) [1, 2], of which most have the major drawback that they are limited, and cannot be regenerated as fast as they are exhausted. Furthermore all of them have a possible negative impact on the environment, if they are not handled and converted to the needed form of energy very carefully.

A lot of research and development have been carried out in the area of renewable energy production and an increase in the total use of renewables has been observed over the last years [2]. Worldwide it is however still a very limited fraction of the total energy consumption, whereas some countries, including Denmark, have a larger fraction as a result of politics and/or easier implementation of renewable energy technologies (Figure 1.1). There are multiple reasons why fossil fuels are still used. First of all, fossil fuels have 'always' existed and therefore the technology to convert the energy to whatever needed form is well developed. Furthermore a major advantage is the very high energy density offered by the liquid fossil fuels, which is essential for e.g. transportation [3].
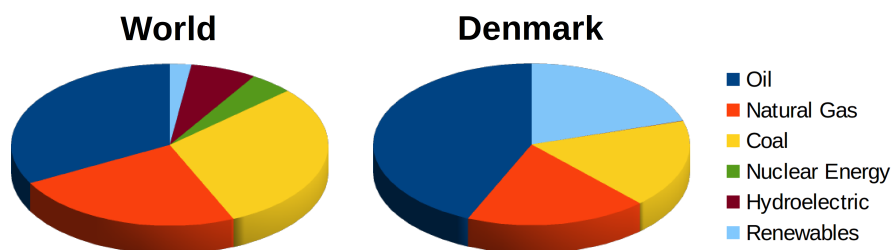
Figure 1.1: Energy sources used in Denmark and the world (2013). The data is obtained from [2].

1.2   Storing Energy

A major challenge regarding the renewable energy sources is that they are often fluctuating by nature, which require storage of the energy [4], and choice of the most optimal energy carrier [5]. Hydrogen is an energy carrier, which have attracted a lot of attention for transportation [3, 6, 7]. Hydrogen offers a high gravimetric energy density, whereas its volumetric density is significantly lower than other alternatives, as for example the existing liquid fuels. Furthermore there are several safety concerns related to transporting a compressed gas - however, the storage insecurity is probably similar to gasoline hazards.

Instead of storing hydrogen in its natural form, it is possible to absorb and store it in solid materials, with various complexity. The most simple solid storage is as metal hydrides, where the hydrogen is incorporated into a solid material. The problems with the hydrides are however, that they are very stable, requiring very high temperatures to release the hydrogen again, and furthermore the storage capacities are below 8 wt% [8]. It is also possible to store hydrogen by physisoption in various porous structures offering high surface areas. The problem with these materials is that the interaction is too weak, resulting in releases at very low temperatures, significantly below room temperature [9].

Another interesting class of hydrogen storage materials is the complex hydrides, where hydrogen is stored as a part of different chemical units in a solid host [10]. Many complex hydrides offer very high energy densities, and optimal release temperatures. The major drawback for the chemical storage is that the release is often not reversible, as the storage is a result of a complex chemical reaction. This would in practice require impractical off-board regeneration of the materials.

1.3   Ammonia As Energy Carrier

Ammonia is a very well-known chemical with many different applications, most importantly as a component in fertilizers, supporting the incredible growth of the world's population [11]. Because of the importance, the production has constantly been improved and optimized, following the early work by Haber and Bosch in the beginning of the 20th century [12]. More than 130 million tonnes of ammonia are produced yearly, consuming more than one percent of the total energy consumption in the world [13]. Ammonia can be stored either as a pressurized gas or as a liquid in isolated tanks [14]. A major drawback regarding ammonia is however its toxicity, requiring careful handling and storage [15]. Again the safety concerns are similar to the currently used liquid fuels, and ammonia have therefore frequently been suggested as an energy carrier for transportation due to the offered gravimetric and volumetric energy densities [14–23].

Similar to hydrogen, ammonia can also be absorbed in solid materials, forming the so-called metal halide ammines [14, 16–19, 24, 25]. By absorbing the ammonia in the solid material, the toxicity is lowered significantly, thereby al-

lowing easy handling and storage [17]. The storage in salts is safe, because the ammonia is bound in the crystal structures; this does however mean that heat should be supplied to release the ammonia. Depending on the metal halide, different release temperatures are observed, and the release might be a complicated multi-step process, which will be discussed in chapter 4.

The use of the metal halide ammines as energy carriers for transportation, require a method to extract the stored chemical energy. One possibility is to burn the ammonia in internal combustion engines [26], but this would result in similar issues regarding pollution and climate changes, as for the liquid fuels. A better solution would therefore be to extract the energy using a fuel cell. Both high-temperature solid oxide fuel cell (SOFC) [27] and direct ammonia fuel cell (DAFC) operating at lower temperatures (~400 °C) [14], allow the direct use of ammonia as the fuel.

It is also possible to decompose the ammonia to obtain hydrogen (and nitrogen) [14, 22, 28]. The obtained hydrogen can subsequently be used in polymer electrolyte membrane fuel cells (PEMFC), which is a much more mature fuel cell technology [29]. Furthermore PEMFCs has the advantage that they can be operated at low (< 100 °C) [30] or intermediate temperatures [31]. A challenge with the use of PEMFCs is however that they are easily poisoned by ammonia [32, 33], and the decomposition should therefore be complete, or the excess ammonia should be removed. The removal of ammonia could also be performed by another metal halide with higher release temperatures.

The recurring topic through this thesis is the design and study of improved metal halide ammines, to be used as future energy carriers. To achieve the highest possible system efficiency, the goal is to develop materials to work with low-temperature PEMFC, releasing the ammonia below 100 °C. However, the release should not be at too low temperatures, as this could result in safety concerns. For transportation the gravimetric density is the most important design parameter, and this will therefore be optimized.

As will be unveiled later, we will allow a large variety of different elements, in the search for a possible future energy carrier. To ensure that a material can be used it is however not only the storage and release properties which are important. If the material should be used throughout the transportation sector it is important that the used elements are abundant and not too expensive. As it is evident upon inspection of Table 1.1 the price is to some extent correlated to the abundance of the elements. The quoted prices should not directly be used to determine which metal to choose to obtain the cheapest metal halide, as some of the metals naturally occur as salts, and therefore will be much cheaper. We might identify mixtures of metals, naturally occurring together, further lowering the price of the material.

1.4 Computational Materials Design

When searching for a future energy carrier it is important to be open-minded, and not only search for compounds which are already known to exist, or re-

lated mixtures thereof, which are likely to exist, but would only result in slight improvements. It is important to include as many different material types and elements as possible in an initial screening study. However, as will be illustrated later, the defined search spaces do often contain thousands or millions of possible candidates, which *cannot* all be tested in real experiments. It is however possible to 'make' the experiments, or approximated experiments, by using computational methods, which have improved greatly over the last decades, now providing accuracy and speed suitable for investigating huge phase spaces and thereby lowering the number of candidates to test experimentally [35–52].

The computational methods do however still require the use of supercomputers for many hours, days or even months, and therefore it is always advisable to lower the total number of calculations, which have to be done. One possible way to navigate through the phase space, only testing relevant candidates, is by using the so-called genetic algorithms (GAs). As will be evident from this thesis, GAs are actually very well suited for this optimized search, significantly lowering the number of candidates to test.

Element	Symbol	Pure	Bulk	Abundancy
Rhodium	Rh	130 000	70 000	0.001
Palladium	Pd	58 330	15 710	0.015
Ruthenium	Ru	14 000	6500	0.001
Scandium	Sc	14 000	n/a	22
Beryllium	Be	7480	930	2.8
Titanium	Ti	6610	n/a	5600
Yttrium	Y	4300	n/a	33
Vanadium	V	2200	27	120
Zirconium	Zr	1570	160	165
Silver	Ag	1200	575	0.075
Strontium	Sr	1000	n/a	370
Barium	Ba	550	n/a	425
Cadmium	Cd	460	7.7	0.15
Molybdenum	Mo	440	n/a	1.2
Chromium	Cr	320	2.8	102
Cobalt	Co	210	44	25
Calcium	Ca	200	n/a	42 000
Niobium	Nb	180	n/a	17
Copper	Cu	97.6	6.6	60
Nickel	Ni	77	19	84
Iron	Fe	72	0.2	56 000
Manganese	Mn	65	2.8	1000
Zinc	Zn	53	1.8	70
Magnesium	Mg	37	2.9	23 000

Table 1.1: Prices for selected metals ($/kg). The price is reported for the pure metal and a bulk price representing the natural occurring form. The abundance in the earth's crust is also included (ppm by weight). Data taken from http://chemicool.com [34].

1.5 Thesis outline

Chapter 2 will introduce Density Functional Theory (DFT) and discuss the important choice of a suitable exchange-correlation functional. Furthermore the choice of calculation parameters and the general structure optimisation used throughout the thesis will be presented.

Chapter 3 will introduce the topic of computational materials design, initially discussing template based screening. The majority of the chapter is devoted to the introduction of genetic algorithms (GAs) and the discussion of the present implementation used in paper III and IV.

Chapter 4 presents a detailed study of the state-of-the-art solid ammonia storage material, $Sr(NH_3)_8Cl_2$, which is described in details in paper I. The study is focussing on the experimentally observed anisotropic expansion, which can be explained by the local coordination of the ammonia molecules.

Chapter 5 is based on paper II and demonstrates that the mixing of barium and strontium chloride results in materials superior to the pure metal chlorides. The chapter contains extra information regarding stabilisation of a specific polymorph by doping with a third metal, including initial experimental tests.

Chapter 6 discusses the initial GA screening study searching for improved hexa ammines, presented in paper III. The approach is verified, proving that the global optimum can be identified by testing less than two percent of the phase space. Furthermore, initial experimental testing of one of the identified candidates is presented.

Chapter 7 presents the adaption of the algorithm to perform a search for optimised mixed metal halide ammines including stability checks for multiple intermediate phases. As presented in the chapter and paper IV, the algorithm do successfully identify multiple mixtures with improved release characteristics, which subsequently are experimentally validated.

Chapter 8 presents a check of the reliability of the screening results, which are based on multiple assumptions. Some of the assumptions are adequate, whereas others might have introduced relative large uncertainties. Possible improvements of the template based screening approach are furthermore discussed.

Chapter 9 summarises the findings of this thesis and discusses possible future studies and improvements.

1.6 Included Publications

The following papers are included in the appendix of the thesis:

Paper I
Temperature- and Pressure-Induced Changes in the Crystal Structure of $Sr(NH_3)_8Cl_2$
Rune E. Johnsen, Peter Bjerre Jensen, Poul Norby and Tejs Vegge
The Journal of Physical Chemistry C, **118**:24349-24356, 2014

Paper II
Solid solution barium–strontium chlorides with tunable ammonia desorption properties and superior storage capacity
Agata Bialy, Peter Bjerre Jensen, Didier Blanchard, Ulrich J. Quaade and Tejs Vegge
Journal of Solid State Chemistry **221**:32-36, 2015

Paper III
Designing Mixed Metal Halide Ammines for Ammonia Storage Using Density Functional Theory and Genetic Algorithms
Peter Bjerre Jensen, Steen Lysgaard, Ulrich J. Quaade and Tejs Vegge
Physical Chemistry Chemical Physics **16**:19732-19740, 2014

Paper IV
Accelerated DFT-based Design of Materials for Ammonia Storage
Peter Bjerre Jensen, Agata Bialy, Didier Blanchard, Steen Lysgaard, Ulrich J. Quaade and Tejs Vegge
Submitted to Energy and Environmental Science

Quantum Mechanical Calculations

2.1 Introduction

Throughout this thesis various properties of different ammonia storage materials will be described using advanced quantum mechanical calculations. In the following the principles of the employed methods will be introduced, focusing on the trade-off between desired accuracy and computational cost. In theory a very high accuracy can be achieved, but often the available computational resources will call for various approximations. The introduction of different cost-saving approximations is crucial, especially for big screening studies as presented in this thesis. However, the approximations will decrease the accuracy, and it is thus important to have an understanding of the effect of the applied approximations, and the resulting accuracy.

In principle all ground state properties of a given material can be derived by solving the time-independent Scrödinger equation [53]:

$$\hat{H}\Psi = E\Psi \tag{2.1}$$

The Hamilton operator, $\hat{H}$, allows the evaluation of the total energy of a system described by the wavefunction, Ψ, which in general contains information of the position of both the electrons and nuclei. However, due to the fact that the electrons are much lighter than the nuclei, and therefore respond almost instantaneously when the nuclei are moved, the movements can be decoupled. This is normally referred to as the Born-Oppenheimer approximation [54]. Using this approximation the electronic Hamilton operator is in atomic units given as

$$\hat{H} = \hat{T}_e + \hat{V}_{e-e} + \hat{V}_{e-nuc} \tag{2.2}$$

$$\hat{H} = -\frac{1}{2}\sum_j \nabla_j^2 + \frac{1}{2}\sum_{j\neq j'} \frac{1}{|\mathbf{r}_j - \mathbf{r}_{j'}|} - \sum_{j,l} \frac{Z_l}{|\mathbf{r}_j - \mathbf{R}_l|} \tag{2.3}$$

where $\mathbf{r}_j$ and $\mathbf{R}_l$ are the positions of the electrons and nuclei respectively, and Z_l is the atomic number of the nuclei. $\hat{T}_e$ describes the kinetic energy of the electrons, $\hat{V}_{e-e}$ the Coulomb repulsion of the electrons and $\hat{V}_{e-nuc}$ the interaction between the electrons and nuclei. Solving this problem is still a very complicated task, as Equation 2.3 depends on the interactions of all electrons.

2.2   Density Functional Theory

To reduce the complexity of solving the Schrödinger equation it has been suggested to reformulate the problem and use the ground state electron density, $\rho(\mathbf{r})$, instead of the more demanding wavefunction, Ψ. This makes it possible to describe a system of N electrons by using 3 spatial coordinates instead of the 3N spatial coordinates used in Ψ. This opens up for faster calculations and allows the study of very big systems, containing hundreds of atoms. Because of this, the method known as Density Functional Theory (DFT), have gained enormous interest in different scientific disciplines during the last decades [43].

DFT is based on the work by Hohenberg and Kohn [55], who demonstrated that (i) all ground state properties of a system can be described by a functional of the electron density, and (ii) the energy of the system is minimized by the correct ground state charge density. The major drawback related to DFT, is that no one, have been able to determine a universal functional. This results in the exact theory to be used as an approximation in practice. From the second theorem a practical way of tackling the problem arises using the variational principle beginning with a qualified guess of the true ground state density.

The variational problem is normally solved by following the Kohn-Sham scheme [56], describing the system as a sum of fictitious non-interacting one-electron orbitals, $\phi_i(\mathbf{r})$, reproducing the charge density:

$$\rho(\mathbf{r}) = \sum_{i=1}^{N} |\phi_i(\mathbf{r})|^2 \tag{2.4}$$

The one-electron Kohn-Sham orbitals are given by a set of single particle Scrödinger equations:

$$\left\{ -\frac{1}{2}\nabla^2 + v(\mathbf{r}) \right\} \phi_i(\mathbf{r}) = \epsilon_i \phi_i(\mathbf{r}) \tag{2.5}$$

where $v(\mathbf{r})$ is the effective potential due to all the particles in the system:

$$v(\mathbf{r}) = \int \frac{\rho(\mathbf{r}')}{|\mathbf{r} - \mathbf{r}'|} d\mathbf{r} + v_{\text{ext}}(\mathbf{r}) + v_{\text{xc}}(\mathbf{r}) \tag{2.6}$$

where the first term is describing the interaction of the electron and the mean electron density. $v_{\text{ext}}(\mathbf{r})$ describes the interaction with an external field, which is normally the potential between the nuclei and the electron. The last term, $v_{\text{xc}}(\mathbf{r})$, is the exchange-correlation potential describing the many-electron interactions (correlation) and Pauli-exclusion effects (exchange). The potential is a functional derivative of the exchange-correlation energy:

$$v_{\text{xc}}(\mathbf{r}) = \frac{\delta E_{\text{xc}}\left[\rho(\mathbf{r})\right]}{\delta \rho(\mathbf{r})} \tag{2.7}$$

Starting from an initial guess of the electron density it is possible to obtain an initial set of orbitals using Equation 2.5. Using these orbitals a new density can be calculated using Equation 2.4, which in turn can be used to obtain a new set

of orbitals. Solving the Kohn-Sham equations in this iteratively fashion might eventually result in a converging electron density. In practice the calculations are stopped when the density and corresponding energy are converged within some tolerance.

2.3 Exchange-Correlation Functionals

To follow the Kohn-Sham scheme presented in the previous section, it is necessary to apply an exchange-correlation functional to obtain the corresponding potential from Equation 2.7. As mentioned, the exact functional is unknown and has to be approximated. Various approximations with different accuracy and computational cost have been suggested. The most common, which are relevant for the work presented in the thesis, will be shortly discussed in the following.

A simple approximation is the Local Density Approximation (LDA), treating the local environment as an uniform electron gas [56]. This approach should be appropriate if the system has a slowly varying density, which is only the case for a very limited number of systems. However, the functional provides reasonably accurate results for many systems due to significant error cancellation [57].

An improved description is obtained with the General Gradient Approximation (GGA), which also takes into account the gradient of the density. A common GGA functional is PBE [58], which is used for many calculations in this thesis, as it is known to accurately describe the local geometries [39]. Due to the necessity of knowing not only the density, but also the gradient, the GGA calculations are more computationally demanding, but nonetheless a very popular class of functionals, often providing an optimal balance between desired accuracy and speed.

There are, however, important phenomena, which are not correctly described by PBE and GGA functionals in general. Due to the semi-local description, the long-ranged non-local dispersion and van der Waals (vdW) interactions cannot be described correctly. It is crucial to include vdW effects to obtain a correct description of the metal halide ammines investigated in this thesis, as they contain many hydrogen bonds. Several ways of including the non-local description have been proposed and have resulted in increased accuracy at some extra computational cost [41, 59, 60]. Throughout this thesis the vdW-DF functional [61] has been used. The functional combines LDA and GGA, and adds a non-local correlation:

$$E_{xc}^{\text{vdW-DF}} = E_x^{\text{revPBE}} + E_c^{\text{LDA}} + E_c^{\text{nl}} \qquad (2.8)$$

The exchange is from revPBE [62], which is a GGA functional fitted to exact exchange calculations. The added non-local correlation is by construction vanishing for a uniform electron density, and the local correlation is therefore optimally described using LDA. Many other choices of GGA exchange is of course available, and different vdW functionals have emerged. However, depending on the system and searched property different functionals will be the optimal choice [59]. vdW-DF has been used in the current work, as it has

previously been shown to describe the type of investigated materials very well [63, 64].

Due to the evaluation of the non-local correlation between all electron density pairs, the computational cost is further increased for this class of functionals. As will be shown in different examples throughout the thesis it is often adequate to perform single point vdW-DF energy calculations on the PBE-relaxed structures, if only the correct energetic description is searched and the local coordination is of less importance. This approach lowers the total computation time, which is very desirable when investigating thousands of structures, as have been done in the presented screening studies. However, when a detailed description of the local coordination is of interest, it is crucial to relax the structures with a vdW-corrected functional.

As discussed, when designing a vdW functional, different choices of exchange and correlation are possible (Equation 2.8). BEEF-vdW is a functional with a certain choice of fitted parameters. In addition, BEEF-vdW allows the user to calculate an estimate of the error to be expected on the energy calculated self-consistently with BEEF-vdW [65]. The functional has intrinsically embedded the possibility to non-self-consistently calculate energies for an ensemble of functionals with different parameters. The ensemble can be generated with low computational cost. From this ensemble statistical methods can be used to estimate functional dependent discrepancies.

If a more accurate description of the vdW interactions is needed, a range of more advanced methods exist. One way of increasing the accuracy (and the computational cost) is by including the kinetic energy density to obtain the so-called meta-GGAs. M06-L is a meta-GGA which describes the vdW interactions quite accurately as a result of fitting the underlying parameters to various organic and organometallic systems [66]. A meta-GGA version of the BEEF-vdW functional, mBEEF, has also been developed with similar error estimates from ensemble statistics [67]. Going beyond the pairwise addition of dispersion interactions used for the discussed vdW functionals, even higher accuracy is possible by using the Random Phase Approximation (RPA) [68, 69]; this is however very computationally demanding, and prohibits its use for larger systems.

2.4   Calculations Details

All calculations presented in this thesis have been executed through the Atomic Simulation Environment (ASE) [70] using the Grid-based Projector Augmented Wave method (GPAW) [71, 72], which is a real space implementation of the PAW method [73]. The PAW method is a technique developed to perform DFT calculations efficiently and accurately. This is achieved by the use of pseudo wavefunctions and applying the frozen-core approximation. The use of real-space grids in GPAW enables efficient parallelisation, on the cost of introducing small inaccuracies in the forces and energies, due to the so-called egg-box error.

As will be discussed in section 3.1, the ground state structures are normally not available. Therefore a calculation is normally started from a guess of the initial structure. To ensure the correct description, this initial structure is initially relaxed, to obtain the ground state properties. In general a three-step optimization is used to obtain a relaxed structure[1]:

1. **Initial relaxation:** Internal relaxation of the atomic positions in the initial structure (with a fixed unit cell).

2. **Volume relaxation:** The unit cell is optimized, either hydrostatically or one direction at a time, depending on whether the symmetry should be fixed.

3. **Final relaxation:** Internal relaxation of the atomic positions in the new unit cell.

The accuracy of a calculation depends on a number of different parameters, which will be described in the following. All parameters have been checked for convergence for representative systems - complete verification for all systems investigated in the screenings, is not feasible. The Brillouin-zone is sampled using a Monkhorst–Pack grid [74] with at k-point density of approximately 25 k-points per Å^{-1} using a grid spacing of 0.18 Å. To optimize the convergence a number of empty bands are included in the calculation; depending on the system size 20-50 empty bands are included. The structures are relaxed as described above[2], by using a quasi-Newton optimization algorithm [75] until the forces are less than $0.05 \text{ eV} \cdot \text{Å}^{-1}$. In general the calculations are performed for unit cells subjected to periodic boundary conditions (PBC); however, to calculate the gas phase energy of an ammonia molecule, the molecule is placed in box disabling the PBC, to ensure a correct description with no interactions with periodic repetitions.

---

[1]Sometimes the initial guess might be poor or a very complex structure might be present. This will result in more complex relaxations, which might make it necessary to repeat the cycle two or three times. For complex systems this is simply checked by re-running the optimization cycle, to determine when the structure and energy have converged.

[2]As discussed in section 3.1, the full relaxation is not performed for all structures in the template based screening studies presented in chapter 6 and 7.

Computational Materials Design

3.1 Template Based Screening

As mentioned in the introduction, the main goal of the studies presented in this thesis is to design new materials for ammonia storage using computational methods. As described in the previous chapter, DFT is the chosen method for the computations because it gives an accuracy suitable for such screening studies. However, DFT is still a computational demanding method - even with the use of supercomputers, and it is therefore necessary to lower the time consumption and number of calculations as much as possible, while sustaining the required accuracy of the predictions. One of the most time-consuming parts of a standard DFT investigation of some chemical system is the structural relaxation, requiring the calculation of the energy and the forces acting on all atoms at multiple configurations determined by some optimization algorithm. The number of evaluations is dependent on the efficiency of the optimization algorithm and the initial guess. A good starting guess can lower the calculation time significantly, as the algorithm needs fewer steps to approach the minimum [76–78].

The problem is however typically that the ground state structure is not known, and it might therefore be very hard to come up with a good initial guess [79]. Different ways of constructing an initial structure based on templates have been proposed, and shown to be successful for identifying the (sometimes new) global minimum [19, 80–87]. In general the proposed methods are based on analysing the constituents of the material and identifying important parameters which need to be correct to ensure an accurate description of the system. The parameters can for instance be important bond lengths between ligands and the metal they coordinate to or the orientation of the ligands, e.g. optimizing the number of hydrogen bonds to a maximum.

For the metal halide ammines investigated in this thesis, especially the distance from the coordinating metal atom to the ammonia molecules is very important, as will be described in more details in chapter 4. In general the ammine phases can be described as a lattice consisting of the halide atoms coordinating to different oriented polyhedra constructed of the metal atoms and the coordinating ammonia molecules. An example of a fully DFT optimized

mixed octa ammine structure is shown in Figure 3.1, which illustrates this picture. As is evident from the optimized structure the two different metals have similar coordination, but show different bond lengths, resulting in slightly bigger polyhedra for the larger metal. Because of these similarities in the fully relaxed structure, it is possible to come up with a very qualified initial guess for new unknown mixed structures, by using the bond lengths and unit cell volumes from the pure structures.
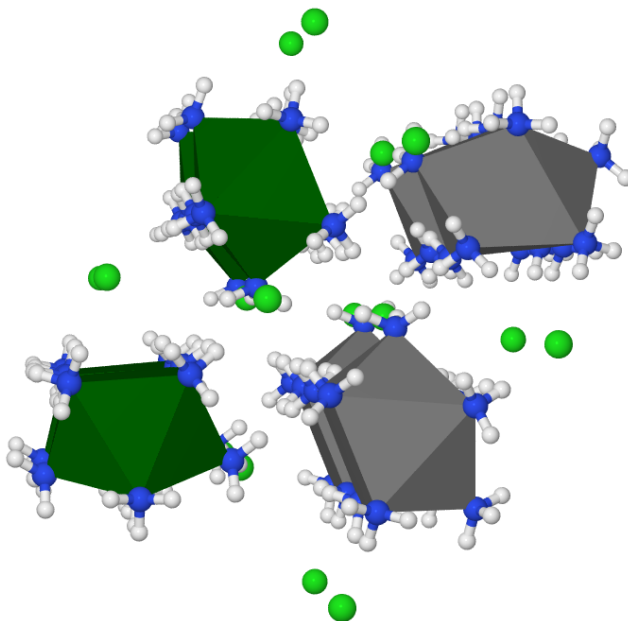
Figure 3.1: Example of a relaxed mixed strontium-barium chloride octa ammine (for details about the relaxation consult section 5.3). Sr is in the centre of the dark green polyhedra, Ba in the grey polyhedra, N is depicted blue, H white and Cl light green.

If the pure structures are not known, the best initial guess is obtained by initially relaxing the pure structure in a known crystal structure with fixed symmetry. This is exactly the approach used in the big screening studies presented in chapter 6 and chapter 7, where the pure structures, for all the investigated phases, are initially optimized in the fixed symmetry and stored in a database. To set up a new mixed trial structure, the implemented algorithm substitutes the chosen elements into the template, and scales the volume and metal to nitrogen distances, while keeping the local symmetry. The volume is set to the average of the constituents, and the metal to nitrogen distances are scaled individually to the optimal values obtained from the pure structures. As will be proven in section 8.3 this approach is actually resulting in mixed structures very close in energy to fully relaxed structures, and therefore providing a very reasonable starting guess.

If a very big screening study is intended, it is often not feasible to fully optimize every trial structure, as this would increase the total calculation time signif-

icantly, even when the optimizations start from intelligently prepared structures. Therefore the only possibility, especially in initial screening studies with huge search spaces, would often be to calculate single point energies for the investigated structures. This might not be as bad as one would think immediately, because the interesting properties are often obtained by calculating differences between different phases, which probably would result in error cancellation, because the template structures would have similar errors in the different phases. Even if the sought-after property is only calculated from one single structure, the template based screening might give useful information of the relative changes observed, thereby allowing to select material with optimized characteristics [48, 88].

3.2 Genetic Algorithms

If brute force screening is not an option, it will be useful to have a method, which can optimize and guide the search in a defined search space, if too many candidates exist. Even if it is possible to perform the calculations on all possible trial structures, it might be useful to optimize the search to lower the needed calculation time; however, it is very important to ensure that the search space is correctly sampled and the optimal candidate(s) has been identified, which in general *cannot* be ensured without testing all candidates. In some cases it is however possible to de-select candidates prior to actual performing the time-consuming calculations, if it is known that the suggested trial structure cannot in any way get better properties than the so far best candidate.

One example favouring such a pre-selection could be a search for a material with the highest possible amount of stored ammonia, releasable within some specific temperature interval, but the actual temperature is of lower or no importance at all; if this is the case, one can determine the maximum possible release of a trial candidate prior to the calculation, and de-select the candidate if the possible release does not exceed the best candidate so far. If a collection of improved candidates instead is wanted one should perform the comparison with some tolerance, specifying that the candidate should have the possibility of having e.g. at least 95 % storage capacity compared to the best so far observed. Furthermore, one should take care when de-selecting candidates, because the search algorithms would often use information from the already investigated compounds, when suggesting new trial structures, which might benefit from using information from semi-good structures.

A genetic algorithm (GA) is one example of a search method, providing the ability to guide the search through the search space, using information from the already tested candidates. The method is also known as an evolutionary search, because of its origin in biology, inspired by the observations by Charles Darwin describing the evolution of all species as a result of natural, *Darwinistic*, selection favouring the survival of the most fit species, which have the ability to adapt to the changes in the environment [89]. The introduction of the theory as a computational tool to simulate a broad range of different phenomena is ascribed to the work by J. H. Holland [90]. Since then, GAs have been used in many different areas, including very different topics such as biology, economics

and politics [91, 92].

Also within chemistry, physics and material science GAs have become an important tool used to solve different problems, when other methods are either too slow, or simply not able to solve the defined problem. GAs have for example been successfully used to predict folding of (small) proteins [93], determine the optimal alloy in a fixed structure [35], identify the preferred crystal structure for a fixed composition [94–97] or even solving the complex issue of predicting the most stable structure both identifying the crystal structure and the composition for bimetallic compounds [98]. Also the stability and shape of nanoparticles have been investigated quite a lot using GAs, both in the gas phase [99–103] and for supported particles on surfaces [104–109] or inside metal-organic-frameworks (MOFs) [108, 110, 111].

As mentioned, it might in some cases be of interest to locate many local minima structures, because they might be observed at finite temperatures, because of the thermal energy, or because they are kinetically trapped, as the transformation to the thermodynamic ground state involves crossing huge barriers, requiring further increased temperatures. Also when determining the optimal elements and optimizing the composition in a fixed structure, the goal would often be to identify a limited number of structures, as using the fixed structure unavoidable introduces a higher uncertainty in the predictions. In both cases the use of GAs are recommended, as the method automatically will investigate multiple different compositions, which all can be ranked according to different criteria after a GA run, thereby identifying multiple candidates, which subsequently can be further analysed computationally or experimentally, depending on the number of remaining candidates.

The problem of determining the optimal configuration of a collection of elements hold together in nanoparticles or molecules, is one problem which is very difficult to solve with ordinary optimization algorithms, which navigate in the search space by following the energy gradient downhill [76, 77]. The challenge for these structural optimizations is the existence of an enormous amount of local minima, in which the algorithms will get stuck. This results in algorithms only able to locate the global minimum, when starting from a structure similar to the optimal structure, which indeed require very good initial guesses. One possible solution to avoid ending up in local minima is to introduce a fictive temperature, which allows the crossing of the thermodynamic barriers between different minima. The problem is however often to determine what temperature is needed, and furthermore the simulation of the cooling down has to be controlled carefully. A number of temperature based methods exist, including the Monte Carlo method, simulated annealing, basin hopping and the more recent minima hopping method, which have been introduced and compared to the other mentioned methods by S. Goedecker [112].

3.3 GA Implementation Adapted to Mixed Ammines

This section will describe the main thoughts and choices made during the design and implementation of a genetic algorithm to predict new mixed metal halide ammines. The implemented algorithm is based on an algorithm initially designed by Lysgaard et al. to optimize nanoparticles [101, 113]. The details of the adapted algorithm is described in paper III, which should be read to have a complete understanding of the implementation. In the paper and chapter 6 the performance is also tested in a relatively small study, which allows subsequent confirmation of the success of the algorithm, proving its ability to find the global optimum by testing less than two percent of the candidates. In paper IV and chapter 7 a bigger screening study searching for improved ammonia storage materials is presented, together with experimental validation of some of the best identified candidates.

In the following important design criteria used in both of the screening studies are introduced and discussed. The general flow of the algorithm is illustrated in Figure 3.2, where it should be noted that a very small population of only three individuals is shown for clarity. As shown, the full description of a material is solely given by a string representing the included elements and their internal ordering. To encode these strings and perform a calculation to determine the sought-after properties, the algorithm needs a set of template structures as described in section 3.1. In both studies presented in this thesis the search spaces are quite big, and we do therefore not take permutations of the string in to account, and assign the same fitness for mixtures containing the same mixture of elements. This approach is however dangerous, because changing the local ordering of the elements is likely to change the energy significantly. However, we use the same ordering in all phases, resulting in structures where the metals have the same internal coordination. This might result in error cancellation, still providing adequate estimates for the investigated reactions. The validity of this approach is tested for selected candidates in chapter 8.
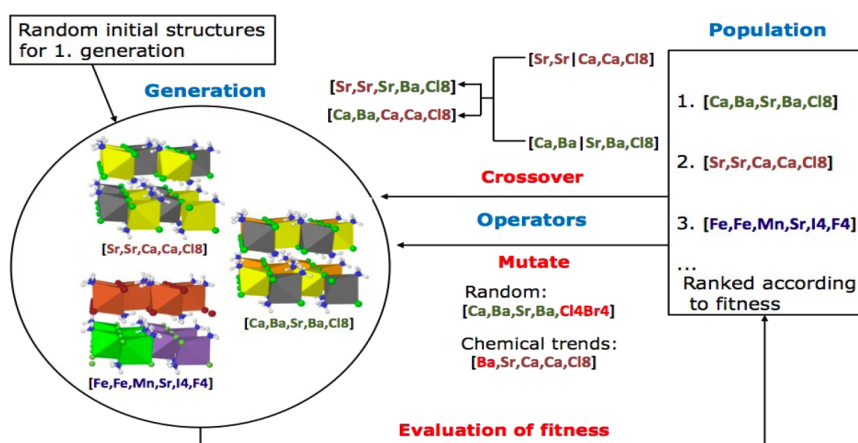
Figure 3.2: Illustration of the implemented algorithm, only showing a population containing three structures for clarity.

3.3.1   Screening Objectives

One of the first things that has to be decided, when designing a GA, is naturally what the goal of the search is, and what should be searched for. It is required that a method is available to calculate a value for the sought-after properties, which is known as the fitness. This method could for example be DFT, which is used to perform a calculation on a specified mixture, to determine e.g. the reaction temperature. From the calculated temperature, one could assign a fitness being the deviation from an optimal release temperature, resulting in a screening focused on finding the mixture having the optimal release temperature.

The goal of a screening is often to improve several properties simultaneously, for instance increasing both the stability, minimizing the weight and volume and lowering the number of reaction steps if multiple phases are considered. Furthermore, if the screening should be of general interest, and not only a scientific study, also the price of the elements and the possible toxicity is of great importance, if there should be any chance that the material could be commercialised. In general it is possible to include all these parameters in a fitness function, but it is difficult to compare the different properties all having different units, and weighting the relative importance of them in a combined fitness function. One option could be to use a multi-population approach, optimizing multiple objectives separately, but allowing the sub-populations to communicate and interbreed with each other, ultimately identifying the Pareto-optimal candidates [114, 115].

Instead of trying to optimize multiple objectives simultaneously it might be possible to reformulate the objective and optimize one single parameter, and place some restrictions related to other parameters, determining which structures to accept for further progress. This approach has been taken in the work presented in this thesis, where the fitness is simply defined as the available amount of hydrogen by weight stored in a material, as this ultimately is the most important criteria to optimize. To ensure that the predicted materials can be used as future energy carriers for transportation, we impose some requirements related to the release temperature and the amount of expensive metals in the mixture. Furthermore the stabilities of the mixed phases are also checked, to ensure that the mixture will not decompose (see section 6.2 for details). It is important to notice that such rules do not directly guide the search, but only restrict where *not* to search. Again, one should be cautious when de-selection candidates, because the offspring of two semi-bad parents might produce an optimized offspring, and furthermore there might be uncertainty of the calculation of some properties. Therefore one should allow some flexibility on the requirements, and be careful not to impose too strict rules.

3.3.2   Controlling the Population

The starting point of a GA run is the definition of an initial population (Figure 3.2). Normally a random population is chosen, to improve the success of locating all the best structures. It is however possible to define a starting population, by using already established knowledge. Defining a starting population

only consisting of already known, and maybe very similar structures, would result in a high probability of making only slight or no improvement at all, because the algorithm most likely will end up in a pre-converged state. Because the goal of the screening studies presented in this thesis has been to find compounds with great improvements compared to the already known compounds, random starting populations have been chosen, to enhance the probability of locating structures with significant increases in the sought-after properties.

Another important parameter is the population size, which determines how broad the search will be. If a too narrow population is sustained there is a low probability of finding the global optimum. On the other hand, if the population is very big, a lot of candidates have to be tested, leading to very slow convergence. Therefore the population size should be chosen big enough to prevent pre-convergence, but small enough to minimize the total computation time. As a general rule of thumb, the population size, S, should be in the range $log_2(N) < S < 2log_2(N)$, where N is the total number of combinations in the search space [116].

In some cases it might be advisable to choose a relatively small population size, and rerun the algorithm several times starting from random, and thereby different populations. This might be preferred if the search space is very big, resulting in a very big population size using the general rule stated above, which would result in an algorithm with a high probability of finding the global optimum, but on the cost of a very long run time. Choosing a (too) small population size on the other hand, would most likely result in relatively short runs, because the algorithm gets stuck in local minima. However, for very big search spaces, this might be the only choice, hopefully allowing the location of interesting local minima with improved properties. In general rerunning is also interesting to test the performance and reproducibility of the algorithm, starting from different populations. Both the presented screening studies in paper III and IV (and chapter 6 and chapter 7), have been shown to locate similar structures starting from random populations, validating the general performance of the algorithm.

3.3.3   Creating Offspring

As mentioned, a GA search evolve by using the information of the previously tested structures to generate new offspring, similar to natural evolution. New offspring are generated by mating two parents using the crossover operation, or by introducing a more or less random mutation [92]. After a new trial structure is generated the fitness is calculated, and if it is a more fit structure, it will be used to generate offspring in the next generation (Figure 3.2).

We apply a standard crossover operator, combining genetic information from two parents to generate a new offspring (Figure 3.3). The operator is randomly picking a point in the atom strings, thereby allowing the use of more information from one parent than the other. The current implementation, is a single-point crossover combining the first part from one parent with the last part from the other. This is working well for relatively short atom strings, but might need improvements if materials with more genetic parts are defined. If

the atom string is very long, two-point cuts should be implemented, thereby allowing the passing on of central information.

The mutation operator is creating an offspring using the information from a single parent, introducing a more or less random mutation. We apply two different mutations, namely a normal random mutation and a so-called neighbor mutation (Figure 3.3). Both operators randomly choose an atom to be mutated into another; the random mutation exchanges the atom with a random element, whereas the neighbor operator exchange the atom to a neighbor element in the periodic table (up, down, left or right). It is expected that both operators are important for the algorithm. The random operator should prevent getting stuck in local minima, whereas neighbor mutations should optimize the structures more locally, by using chemical knowledge.

[Mg | Mg, Mn, Mn, Cl$_8$]
[Sr | Sr, Ba, Ba, Cl$_8$]   Crossover   **[Mg | Sr, Ba, Ba, Cl$_8$]**
                                               [Sr | Mg, Mn, Mn, Cl$_8$]

[Mg, Mg, Mn, Mn, Cl$_8$]   Random m.   **[Mg, Fe, Mn, Mn, Cl$_8$]**

[Mg, Mg, Mn, Mn, Cl$_8$]   Neighbor m.   **[Ca, Mg, Mn, Mn, Cl$_8$]**
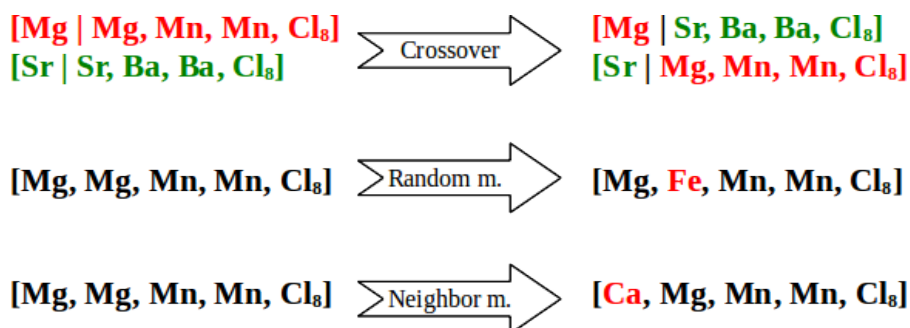
Figure 3.3: Illustration of the different operators acting on random input strings.

The operators available in the algorithm are working locally (crossover and neighbor) or randomly (random mutation)[1], both being very important. However, the local operators are most important for the general optimization of candidates, and should be used more than the random operators. If the goal of a screening is to find the global optimum, it might be relevant to implement a 'concentration operator' allowing the optimization of the composition of a material, increasing the concentration of one element and decreasing the other, e.g. $Sr_5Ca_2BaCl_{16} \longrightarrow Sr_4Ca_2Ba_2Cl_{16}$. This would further increase the success of optimizing a composition to the local minimum, which could be difficult only using the present operators, especially for longer atom strings. This has not been implemented in any of the presented work, but might have further improved the reproducibility of the screening presented in paper IV and chapter 7, where many of the best found mixtures consists of the same elements in different ratios.

3.3.4 Ensuring Diversity

As touched upon it is very important to ensure that the algorithm explores different regions of the search space and not ends up in some pre-converged state.

---

[1]In addition a totally random operator is also availble to ensure the diversity, see end of section 3.3.4 for details.

As mentioned a sufficient large population initialised randomly and the use of mutation operators can be some ways of preventing this, but other important techniques are available. The selection of parents used for offspring generation is very important, and in general it is important to use a relatively diverse population for offspring creation. This can either be achieved by having a big population, or by banning similar structures.

In general one determines a population after each generation, containing the most fit structures, and selects parents from this population, to generate new offspring. The selection can either be random or dependent on the fitness, with a higher probability of selecting the most fit candidates. If the global optimum is wanted it is favoured to use the latter selection, whereas the random selection generally will make the search more broad. To further ensure the diversity, and prevent pre-convergence, a possibility is not only to select parents from the best structures, but select some from all tested structures. In the present implementation we have found it practical to select approximately one fifth of the parents with a probability equal to

$$ \frac{exp\left(\frac{fitness}{best_{fitness}}\right) - 1}{e - 1} \tag{3.1} $$

where $best_{fitness}$ is the fitness of the so far best candidate. Furthermore a very small fraction of totally random structures are produced by a special offspring operator, not using any information from the tested candidates (similar to the random initialisation).

3.3.5 Convergence Control

One of the main drawbacks related to GAs is that you can never be guaranteed that you have found the global optimum, without testing all possible candidates[2]. Furthermore it is difficult to determine when to stop the algorithm and no general rules exist. Normally the GA is stopped when no new improved structures are generated for some time. Dependent on whether the goal is to suggest a collection of improved structures or to locate the global optimum, the algorithm should be checking whether new structures enters the best population used for offspring generation, or only a part of it, maybe only checking if the best structure is improved.

Because of the lack of guidance, the best one can do is to start from a qualified guesses for the convergence parameters, and subsequently test it, by rerunning from different starting populations. This approach will of course increase the total computation time, but as shown in the convergence analysis presented in section 6.3, it was possible to verify the applicability of the parameters, testing less than 4 % of the total search phase. This was possible by rerunning the algorithm three times, with the possibility of reusing already calculated data (see section 3.4 for details regarding reusing data). So despite the fact that it is necessary to rerun the algorithm, GAs are very effective, drastically lowering

---

[2]One exception to this is if the phase space can be lowered during the run as improved candidates are found, as discussed in the beginning of section 3.2, and used to confirm the location of the global optimum in search presented in paper III and chapter 6.

the number of candidates to test. In section 7.3 the effect of changing the convergence criteria will also be analysed.

Another possibility when rerunning the algorithm, might be to iteratively lower the search space. This could for example be possible if it is found that certain metals are never part of the materials in the best population, or if some mixtures with certain metals are found to be unstable no matter what the other constituents are. When doing so one should be very careful, because of the risk of de-selecting materials, and therefore it is only advisable to do so if it is 100 % certain that the materials cannot fulfil the requirements, or if more tests cannot be done simply because of the lack of time. It could also happen that the objectives are changed after a first run, because of the gained knowledge. This could for example be the case if one initially have defined a maximum price of the material, but during the search found many improved materials with a much lower price - then it might be chosen to generally lower the maximum price, as the very best material is not necessarily needed.

3.4 Automating the Materials Design

As described in the previous sections, the only input required to start a GA run is the initial population. From this population the algorithm will automatically determine which structures to test. This allows for automation of the algorithm, thereby reducing the necessity of human interaction. To enable the automation, some initial setup is however needed. It is necessary to have a system for storing the current status of the algorithm and determine the new structures to test, when the fitness from the previous calculations are available. Furthermore a system to generate the scripts to perform the calculations of the fitness is needed, and optimally the scripts should automatically be submitted for calculation. If a proper method to handle errors is implemented, this allows for fully automated computational materials design.

The optimal way of controlling and storing data is by using a database. The current implementation[3] uses the Computational Materials Repository (CMR) [117], which is an open source database implementation for electronic structure calculations. All structures, including the pure reference structures, are stored and retrieved from the database during the GA run. This has several advantages including easy monitoring and post-processing of the data, reuse of already calculated data (both from the current and older GA runs) and easy sharing among colleagues. All of this can be done both from a web interface or locally using scripting.

---

[3]Recently CMR, have been deprecated, as a database have been included in ASE. The current GA implementation, has been adapted to this database, and a is freely available through ASE at https://wiki.fysik.dtu.dk/ase.

Strontium Chloride Ammines

4.1 Pure Metal Halide Ammines

It has been known for a long time that most pure metal halide salts of the general formula MX_2 have the possibility to absorb ammonia and release it again at elevated temperatures [24, 25, 118]. Depending on the atomic radii of the elements [119], the salts have the possibility to coordinate up to 10 ammonia molecules, this do however require a very big cation and some of the ammonia molecules are often weakly bound, leading to complexes that are only stable at low temperatures [25]. Normally a maximum of 8 ammonia molecules is observed for systems like $Ca(NH_3)_8Cl_2$ [19, 120], $Sr(NH_3)_8Cl_2$ [63, 121] and $Ba(NH_3)_8Cl_2$ [121], whereas smaller metals can only coordinate 6 molecules as observed for a range of different materials [122–124] - however, because the smaller metals are often lighter, the hexa ammines often have a competitive gravimetric hydrogen density (wH), as e.g. the 9.2 % observed for $Mg(NH_3)_6Cl_2$ [16, 124, 125], which was the first metal ammine to be proposed as an indirect hydrogen storage material in 2005 [16].

As mentioned in the introduction, having a material with a high energy density is of no use, if the energy cannot be released in a controlled manner at ambient temperature. The release temperatures vary quite a lot for the different materials, and as mentioned, the release is often a multi-step reaction occurring over a broad temperature interval [14, 18]. The release temperatures are determined by the change in enthalpy, ΔH_{des}, and entropy, ΔS_{des}, during the desorption. These define the free energy of the reaction, which can also be related to the equilibrium constant of the reaction. Using the vapour pressure to define the equilibrium constant, one obtains the van 't Hoff equation,

$$\ln \frac{p}{p^\circ} = -\frac{\Delta H_{\text{des}}}{RT} + \frac{\Delta S_{\text{des}}}{R}, \tag{4.1}$$

where a reference pressure $p^\circ = 1\,\text{Pa}$ has been defined for metal ammines. It should be stressed that the enthalpy and entropy values are defined as per released NH_3. This entails that the entropy at standard conditions is calculated as $\Delta S_{des} = (S_{\text{final}} - S_{\text{initial}})/x + R \ln \frac{10^5\,\text{Pa}}{1\,\text{Pa}}$, where x is the number of released ammonia molecules during the reaction and $S_{\text{final/initial}}$ are absolute entropies (in J/(mol · K)). Relatively small variations in ΔS_{des} are observed for a range

of investigated pure metal halide ammines [25], and using a representative value of $230\,\mathrm{J/(mol \cdot K \cdot NH_3)}$, would often be accurate enough for most applications. It is important to remember that this description of the reaction is solely based on thermodynamics, whereas real systems might display slow kinetics, possibly resulting in increased release temperatures.

4.2   Strontium Chloride

Strontium chloride is often regarded as the best of the pure metal halide ammines for ammonia storage, due to its relatively high total hydrogen density (wH=8.2 %). As for most other pure metal halide ammines the release of ammonia occurs in multiple steps:

$$\mathrm{Sr(NH_3)_8Cl_2(s) \longleftrightarrow Sr(NH_3)_2Cl_2(s) + 6\,NH_3(g)} \qquad \mathrm{(C\,4.1)}$$

$$\mathrm{Sr(NH_3)_2Cl_2(s) \longleftrightarrow SrNH_3Cl_2(s) + NH_3(g)} \qquad \mathrm{(C\,4.2)}$$

$$\mathrm{SrNH_3Cl_2(s) \longleftrightarrow SrCl_2(s) + NH_3(g)} \qquad \mathrm{(C\,4.3)}$$
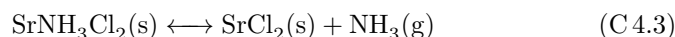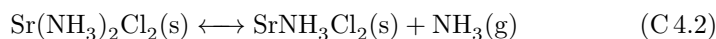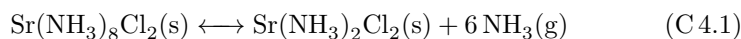
Strontium chloride is preferred over other materials, because the first two reactions occur at more or less the same temperature, which has led to discussion in the field debating whether a di ammine exists or not. However, recently it has been verified that the di ammine do exist, but only in a very small interval dependent on the reaction conditions [63]. Furthermore it is only observed during desorption, whereas the octa ammine is formed directly from the mono ammine during absorption. The existence of the mono ammine phase is however certain, and the last ammonia molecule is bound very strongly, and released a temperature approximately 100 degrees higher than the first seven molecules. For practical reasons, it is therefore often chosen to leave this ammonia molecule, and never use it, as the full release would require supplying a lot of heat. This would furthermore require a lot of engineering to ensure that the full system is not degraded and to control the non-steady stream of ammonia upon release; because of this, the practical hydrogen density in strontium chloride is only 7.2 %, but it is still the best material as other materials with higher theoretical wH, have even lower available densities.

4.3   Ammonia Coordination

To gain further insight in the desorption process of strontium chloride a combined experimental and computational study was conducted, which led to paper I. *In situ* X-ray Powder Diffraction (XRPD) was used to study the observed changes in the crystal structure during desorption. XRPD gives information about the the average positions of the atoms in the crystal, by analysing the position and intensity of the Bragg peaks observed when a X-ray beam interacts with the electrons in the irradiated crystals. The scattering power is dependent on the electron density, resulting in different scattering power for the different elements. Because hydrogen has only one electron, it is practically invisible when it is delocalised in the structure and e.g. NH_3 is therefore refined as one rigid molecule.

From the Rietveld refinement of the diffraction pattern, the previously proposed [63, 120] space group with orthorhombic *Pnma* symmetry, was confirmed for the octa ammine. In this space group the strontium atom is directly coordinated to the eight ammonia molecules forming the so-called double capped trigonal prisms as shown in Figure 4.1. The Sr-N distances for the six 'standard' ammonia molecules (N3,N4,N5) are of approximately equal length and coupled two by two by a mirror plane. The distance to one of the cap atoms (N2) is also similar, resulting in seven distances ranging from 2.71 to 2.79 Å at 275 K. The last ammonia molecule (N1) is significantly further away from the strontium atom, with a Sr-N1 bond length of 2.95 Å. As shown in the figure the position of the hydrogen atoms are not fixed for the two cap atoms, because NH_3 has the possibility to coordinate to different chloride atoms, with only small energy differences.
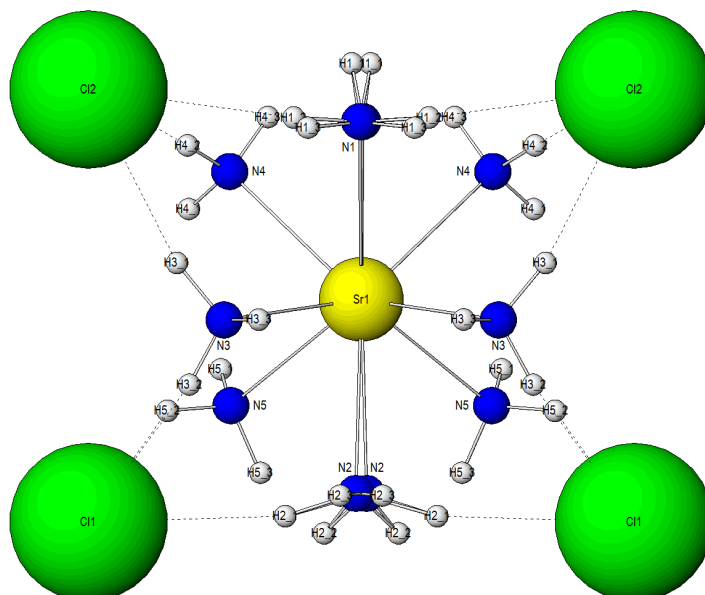
Figure 4.1: Ammonia coordination at 275 K around the strontium atom, showing the three different ammonia types: Weak (N1), Cap (N2) and Standard (N3,N4,N5). Sr is depicted as yellow, Cl green, N blue and H white.

Starting from the experimentally observed structure, and fully relaxing it using the vdW-DF functional [61], both allowing the atoms to move and the cell parameters to change, gives a similar picture. Averaging over a cell containing 8 formula units, the seven short bonds are in the range of 2.77 Å to 2.86 Å, whereas the distances to the weakly bound ammonia molecule are significantly longer ranging from 2.97 Å to 3.00 Å. Comparing to experiments reveal that the short bonds are approximately 0.1 Å longer, whereas the long bond is at maximum 0.05 Å longer. Thus the XRPD and DFT results are in really good aggreement showing the high accuracy for DFT, which is a result of using the advanced van der Waal's functional, capable of describing the hydrogen bonds between the ammonia molecules and the negatively charged chloride atoms.

The energy potential for the different types of bonds was studied to understand the origin of the longer one. To obtain the local potential for one ammonia molecule, single point energies are calculated while moving the molecule and fixing the rest of the structure, both compressing and elongating the bond from the equilibrium value, obtained from the full relaxation (Figure 4.2). Comparing the energy potentials for standard and cap atom it is clear, that they are very similar, especially during compression. Elongating the cap bond length is easier than for the six standard molecules, probably because the crystal structure has more void space around the cap atom. From the energy potential regarding the weak bound molecule (N1), it is indeed clear that it is weakly bound, requiring less energy both during compression and expansion, requiring approximately half the energy to displace the ammonia the same distance as the seven other bonds. However, on the absolute scale it seems from the calculations that it is actually harder to compress the weak bond significantly. This extra energy required is probably not the correct picture, but more realistically coupled to the way the single point energies are calculated. If the system was not fixed, but allowed to relax, some of the other ammonia molecules would probably move away from the central metal atom, to compensate for the shorter Sr-N1 distance. Regarding expansion of the Sr-N1 it is again evident that the molecule is weaker bound, and has more void space around it, similarly to the cap atom (N2). However, it is not completely free to move the weak molecule, which can be seen as the curve is not flattening out. This is likely the reason why an ammine phase with seven ammonia molecules is not observed, as the ammonia molecules can only escape after major restructuring of the cell [63].
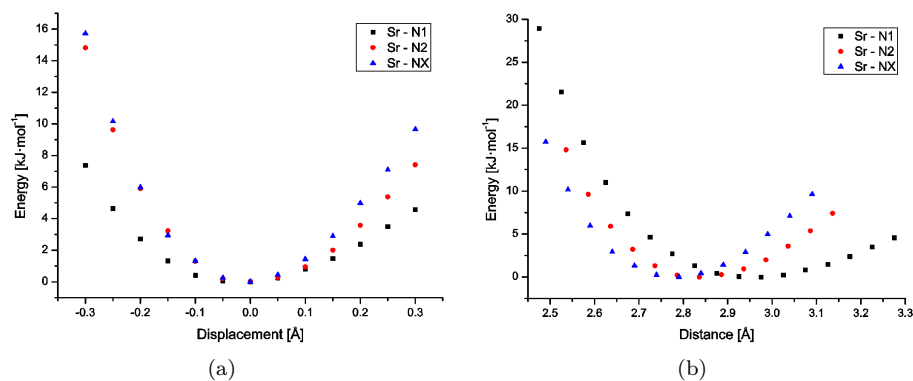
Figure 4.2: The calculated energy required to change the Sr-N bond distance relative to its equilibrium distance, for three different types of ammonia molecules, both shown at a relative (a) and absolute scale (b). The standard bond is shown with blue triangles, cap with red circles and weak with black squares.

4.4 Anisotropic Thermal Expansion

To get further insights in to the consequences of having different ammonia bond strengths, the octa ammine was heated while observing the changes in

the structure both regarding the internal coordination and the total cell expansion (Figure 4.3). Again it is evident that the weakly bound ammonia molecule (N1) behaves distinctively, and that the Sr-N1 bond distance increases to 3.50 Å at 322 K, whereas the other bond lengths are almost constant during heating. Looking at the unit cell expansion it is evident that the cell is not expanding isotropically, but relatively more in the a direction. Changing the a parameter would have the greatest effect on elongating the Sr-N1 bond, as it is almost parallel with to that direction. In other words, the expansion of the cell is closely related to the local environment in the cell, where one ammonia molecule is a lot easier to move as described.

(a)   (b)
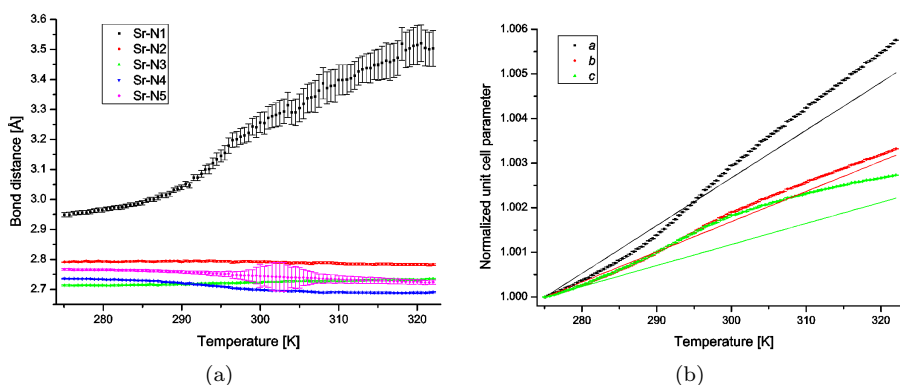
Figure 4.3: Heating $Sr(NH_3)_8Cl_2$ does not expand the structure isotropically. Most Sr-N distances (a) are constant while the distance to weakly bound ammonia molecule (N1) is increasing significantly. Also the lattice parameters (b) expand differently (shown with scattered symbols) and can be approximated from calculations (solid lines).

In general it is very interesting if one can predict the anisotropic expansion of a crystal, without the need of studying every bond in detail. Following the recent work by Zarkevich et al. [126], we tried to predict the anisotropic parameters from the ground state structure. The proposed method is based on calculating the energy for structures with slightly distorted lattice constants, one direction at a time. By fitting the energy as a function of the distortion to a third order polynomial, it is possible to obtain an equation of state, which in turn allows the estimation of the linear thermal expansion coefficient for the different directions, from the coefficients in the polynomial. The theory only holds for very small deviations, and it is therefore important to make very small distortions. Furthermore it is important to fix the shape and orientation of molecular units, as e.g. NH_3 in the strontium octa ammine, to ensure that the symmetry is not broken, which would result in too high energies for distortions. In Figure 4.3 the results obtained by distorting the structure +/- 0.5, 1.0, 1.5 and 2.0 % in each direction is shown together with the experimentally observed expansion. The absolute values calculated with DFT does not fit perfectly, as expected as the expansion is all the way from 0 K; however, the relative expansion is predicted very well, clearly capturing the greater expansion in the a direction.

Through this chapter the strontium chloride octa ammine has been described in detail, comparing the experimentally obtained structures to the models we use. In general the structure is well described using van der Waal's corrected DFT, capable of describing the important hydrogen bonds present in the system. Because there are so many hydrogen bonds in the system it is important to have a good starting point for the structure, to ensure the correct description, as setting up the structure with equal Sr-N bonds would probably give the wrong result. Therefore it is necessary to have the local structure correct, if one intends to perform template based screening for new unknown structures, which is the focus of the rest of the work that is presented in this thesis.

Mixed Strontium-Barium Ammines

5.1 Mixed Metal Halide Ammines

The recurring theme of the work presented in this thesis is the search for new improved ammonia storage materials. As discussed in the introduction and chapter 4, most of the pure metal halide consisting of one metal and one halide, have been studied in details, but none of them have the needed properties for use as an energy carrier, releasing the stored ammonia at suitable temperatures and preferably in one step. It is natural to look into the sources of the pure metal halides; by doing so, is quickly realized that most metal halides are present in the earth's crust as a mixture of similar metals and halides. These observations have led to experimental tests of the ammonia storage properties of mixed materials, both mixing the cation and anion, resulting in materials which do *not* simply behave as the average of the constituents [127, 128].

5.2 Mixed Sr/Ba Chloride Salts

In paper II the mixed system obtained by mixing strontium chloride with barium chloride is investigated. The reason for choosing this system is first of all that $BaCl_2$ and $SrCl_2$ naturally occur together, making the material cheaper, as no or limited purification is needed. Furthermore both systems display interesting features individually, with both systems allowing coordination of eight ammonia molecules, with $BaCl_2$ releasing all the stored ammonia in one step, but at a too low temperature, and $SrCl_2$ displaying increased release temperatures, and thereby higher safety, on the expense of a need of supplying relatively much heat to desorb the ammonia. Therefore it was hoped that mixing the two materials would produce a stable mixture still allowing the uptake of eight ammonia molecules and releasing them in one step at intermediate temperatures. Furthermore it is expected that it will be easier to get the mixtures approved by the authorities, when the barium content is lowered; this is an important aspect even though most barium minerals have very low solubility, because even small concentrations of dissolved barium is extremely toxic for humans and animals [129].

To be successful, it is important that the two salts can form a stable solid solution, which might be difficult to obtain due to the fact that the two salts

do not share the same preferred crystal structure. $SrCl_2$ is primarily found in the cubic fluorite structure (*Fm-3m*) [130, 131], but at very high pressures an orthorhombic polymorph can be formed [132]. $BaCl_2$ is more complicated in the sense that four polymorphs exist around standard conditions depending on the preparation. The orthorhombic (*Pnma*) polymorph is the thermodynamic ground state structure, but two cubic and one hexagonal structure can relatively easy be prepared from the hydrated salt, by changing the drying conditions [133]. The mixed barium-strontium chloride salt have been synthesized many years ago, but have not been very well characterized [130, 134], which might be due to the fact that it is difficult to form the solid solution.

Two methods were employed to produce the solid solution, of which only spray drying of the aqueous solutions was successful, giving more stable mixtures, which were not degraded during ab- and desorption of ammonia. The other employed method is based on mixing the solid salts, using a technique known as high energy planetary ball milling. Ball milling is a relatively simple technique where the solid salts are mixed by enclosing them in a rotating container containing metal balls, which effectively turns the salts into a fine grinded powder. The attempt to form the solid solutions by ball milling were unsuccessful and basically the two precursors were co-existing after the milling. This resulted in a release, which seemed to be the two individual releases, meaning that no, or only minor mixing had occurred; furthermore the total uptake of ammonia was less than half of the expected eight ammonia molecules [135]. It should however be stressed that the experiments are not as simple as described here, but is the result of many different parameters, which if changed could result in changed performance; therefore one cannot be sure that one technique is better than the other.

The spray dried solid solutions were studied using XRPD, and as shown in Figure 5.1, the mixed salts are not consisting of one single phase as desired; the only exception being very low barium concentrations, where the barium atoms are incorporated in the cubic strontium structure, only resulting in a slight increase in the lattice parameters, due to the fact that barium is a bigger element. For intermediate concentrations the cubic strontium and the orthorhombic barium structure type co-exist. Increasing the concentration of barium results in increased volumes for all concentrations, indicating that barium is incorporated into both structure types. Going to very high barium concentrations, the hexagonal structure is also observed - again with increased volume at higher barium concentrations. In conclusion it was therefore *not* possible to form a mixture with one single structure type, but mixing was occurring as indicated by the increase in volume, showing the formation of co-existing solid solutions.
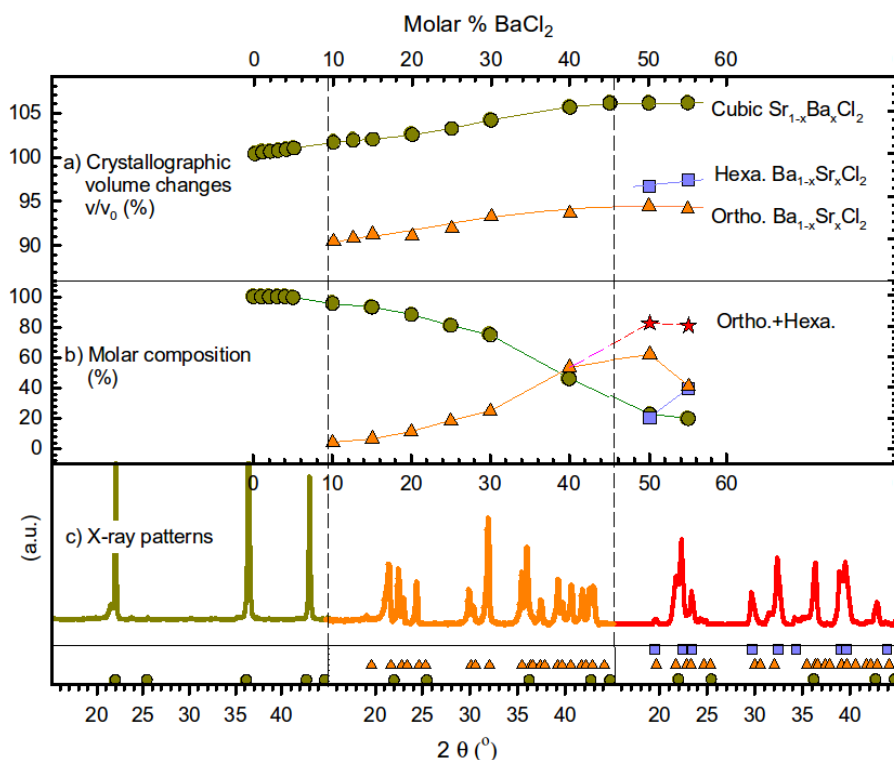
Figure 5.1: Observed structure types for the different synthesised mixtures. In (a) the observed volume changes are reported. The approximated molar composition is shown in (b), which have been deduced from the intensities of the different peaks corresponding to the different phases as shown in (c). Green circles signify the cubic phase, orange triangles the orthorhombic phase and blue squares the hexagonal phase.

5.3 Modelling the Ammonia Release

In order to predict the correct release patterns for the mixed barium-strontium system it is important to have good candidate structures to start from, as described in the previous chapters. For this system this is however challenging as ammoniated phases have only been reported for the strontium system [63]. The best starting guess for all mixtures, including the pure barium structures, is therefore based on the known strontium ammines. The approach starting from known (expected similar) crystal structures have previously been shown to give acceptable predictions of desorption enthalpies for different metal halide ammines, and especially the observed trends and shifts observed for different elements can be accurately described using a semi-local GGA functional [19, 87, 136]. However, the GGA functional underestimates the desorption enthalpies, but it is known that using a van der Wall's corrected functional gives the correct description of the binding energies of the ammonia molecules resulting in accurate absolute desorption enthalpies [63, 113].

To set up a new structure the relevant number of elements were substituted into the relaxed strontium structures, and the unit cell was scaled with a factor related to the radii of the elements [119]. The obtained structures were subsequently optimized in an iteratively cycle both regarding internal relaxation and optimization of the unit cell until convergence was ensured (see Figure 3.1 on page 14 for an example of a relaxed mixed octa ammine). Relaxing both the internal coordinates and the lattice parameters, one direction at a time, is important, as this makes it possible to break the initial symmetry. This is important as the mixed phases might not share the crystal structures observed for the pure phases, as was shown for the salts in Figure 5.1; however, in the calculations only one structure is allowed, which is anticipated to give a correct description of the average observed.
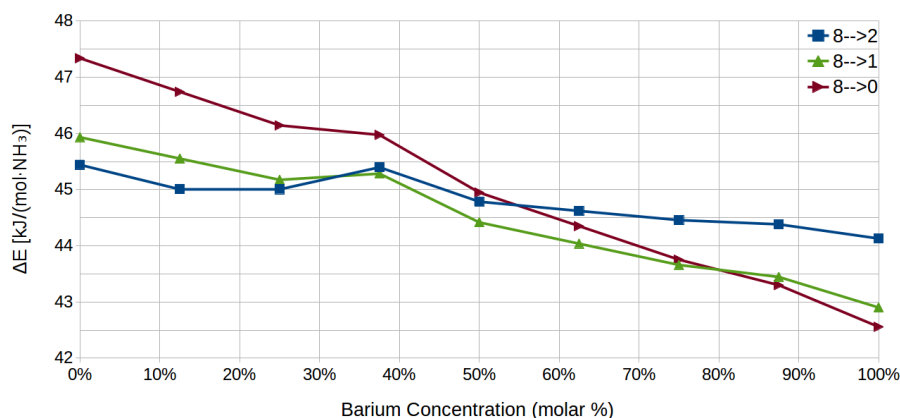
Figure 5.2: Calculated desorption energies from the octa ammine (8) of mixed strontium-barium ammines, to either the di ammine (2, blue), the mono ammine (1, green) or directly to the salt (0, dark red). The lines connecting the markers are only shown for clarity.

The expected release patterns are determined by calculating the difference in energy between an initial and final phase including the energy of the free ammonia molecules, for all possible reactions (similar to reaction C 4.1-C 4.3). The expected desorption route can then be determined by analysing the reaction energies, starting from the octa ammine, and determining whether the reaction proceeds to a lower ammoniated phase or directly to the salt. As is evident from Figure 5.2, the calculated routes are very close in energy only separated by a few kJ/(mol · NH$_3$). From the figure the $8 \rightarrow 0$ reaction is correctly predicted for the pure barium system. For the pure strontium chloride the separation is clear, and it is expected to see both a di and a mono ammine. As a general rule of thumb the reactions need to be separated by more than 1 kJ/(mol · NH$_3$), to be observed under normal reaction conditions. Using this rule, introducing just 25 % of barium into the strontium chloride, would result in a one-step release. This material would be superior to both SrCl$_2$ and BaCl$_2$ with an one-step release at an intermediate temperature, with an increased practically available gravimetric storage capacity.

5.4 Mixed Materials Superior to Constituents

To test the ammonia storage properties of the synthesized mixed materials, an experimental technique known as temperature programmed desorption (TPD) was employed. This technique monitores the changes in either the pressure or the mass during ammonia ab- or desorption, thereby allowing the calculation of the amount of stored ammonia at a certain temperature and pressure. In the results from paper II presented here the later method, also known as thermogravimetric analysis (TGA), was used. As evident from Figure 5.3 the predictions from DFT fit the observation very well, showing a two-step release for 12.5 % barium resembling $SrCl_2$, whereas both 25 % and 50 % of barium give a release similar to pure $BaCl_2$. For 50 % the release is clearly one-step, whereas 25 % shows a small shoulder, indicating a semi-stable mono ammine. As discussed in the previous section, and as shown in Figure 5.1, the salts did not mix perfectly, which might result in degradation during cycling. However, as shown in the inset in Figure 5.3, the desorption profile does not change during cycling, demonstrating a very stable system[1].
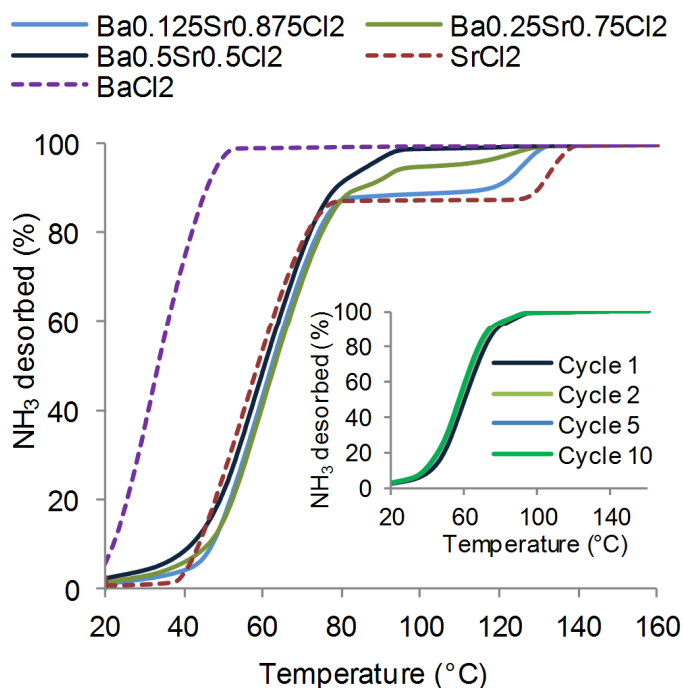
Figure 5.3: Experimental tests of the mixed ammines, using temperature programmed desorption (TPD). The inset demonstrates the stability during cycling for $Ba_{0.5}Sr_{0.5}Cl_2$.

As discussed earlier the ammonia density is a very important criteria determining if a material is interesting as an energy carrier. Thus both the gravimetric

---

[1]Actually, a small change is observed from the first to the second cycle, which probably is associated with formation of a stable porous structure, similar to what is known to occur for pure metal halides [19].

and volumetric densities for the compacted salts were measured for the different concentrations. As shown in Figure 5.4 some of the mixed materials show an increase in both the available gravimetric and volumetric densities compared to having the pure $SrCl_2$ or $BaCl_2$. Interestingly introducing a small amount (up to ~15 %) of barium into $SrCl_2$ initially has no effect on the desorption, resulting in a lower energy density. At higher barium concentrations the desorption is changed to a one-step release occurring when the concentration exceeds ~35 %. For intermediate concentrations not all the ammonia is released in the defined temperature interval (20° to 100 °C), but still the available density is increasing. For even higher concentrations, the release cannot be improved further, as all the ammonia is already released, resulting in a lower density, because of the introduction of the heavier barium. In conclusion it has been shown, that it is possible to form mixed strontium-barium ammines with volumetric densities similar to that of liquid ammonia and available gravimetric densities superior to previously reported compounds, corresponding to a weight percent of hydrogen exceeding 7.7 %, all releasable in one step at relatively low temperatures.

Comparing the calculated and experimentally observed volumetric densities in Figure 5.4b, it seems like it is possible to form more compact materials than predicted from DFT. This should not be understood as any kind of super materials, but more probably as an error in the volumes predicted from DFT, which in general is known to be up to ten percent off (corresponding to an error on the lattice parameters of some percent), normally overestimating the volumes [39]. It has however been shown, that van der Waal functionals similar to the used vdW-DF [61] underestimate the equilibrium volumes for simple alkali and alkaline metals [137]. The predicted densities for the relaxed octa ammines are also slightly underestimated, but falls within the accuracy of the experimental measurements; therefore it cannot be concluded whether the functional is underestimating the volumes for the ammines, or the error is on the experimental site. The accuracy of the predictions are quite impressive, surely suitable to use for computational screening for new materials.
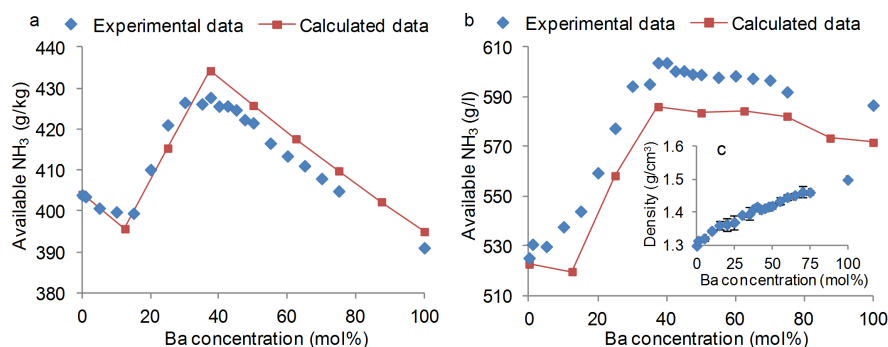
Figure 5.4: Available gravimetric (a) and volumetric (b) ammonia content for the different concentrations predicted from DFT (red) and the experimental observations (blue). Also the densities of the fully ammoniated mixtures are shown in (c).

5.5 Stabilising a Single Polymorph

As described in section 5.2 it is difficult to synthesize the mixed strontium-barium chloride salts, due to the existence of multiple polymorphs. In the concentration range from 10-40 % barium the mixture is a combination of cubic *Fm-3m* and orthorhombic *Pnma*, dominated by the orthorhombic polymorph at high concentrations (Figure 5.1). As discussed, it is preferred to have one single polymorph to prevent degradation of the mixed material upon cycling. Because of this it was investigated whether doping the mixed material with another metal could enhance the chances of forming a mixture only containing the orthorhombic polymorph. A range of different alkali, alkaline earth and d-block metals was tested as dopants. Because of computational limitations, a cell with 8 metal atoms in total was chosen, resulting in a 'doping' of 12.5 %. Furthermore the structures were relaxed using the PBE functional, followed by calculation of vdW-DF single point energies of these minima.

Before studying the effect of dopants, it is important to understand the description of the two-metal system. As is shown in Figure 5.5 the cubic symmetry, is actually preferred for all concentrations, according to the calculated vdW-DF energies of the PBE minimized structures. However, the relative energy between the two polymorphs is not constant, and *Pnma* is 'less unfavourable' at higher barium concentrations, which fits with the experimental observation, showing exactly this behaviour favouring the orthorhombic structure at higher barium concentrations (Figure 5.1). The reason for not predicting the correct ground state structure, is probably related to the fact that the calculations are at 0 K and finite temperatures effects have not been included. However, as shown by the correct relative shifts towards the orthorhombic phase, the calculations, can still be used to get an estimate of the relative stabilization.
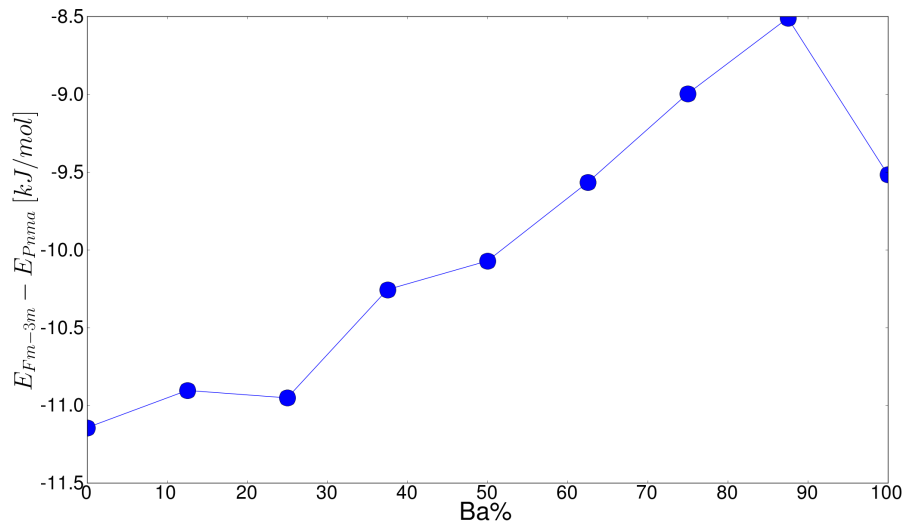
Figure 5.5: Relative energy of the mixed strontium-barium chloride in space group *Fm-3m* compared to *Pnma*. The lines connecting the markers are only shown for clarity.

For the doped salts the cubic phase is also preferred for all dopants, and therefore the relative stabilization is again considered. Figure 5.6 shows the relative stabilization defined as the energy difference between the cubic and orthorhombic phase for the doped system compared to the difference for the undoped Sr-Ba salt. Using this definition, a material with a high negative value for stabilization, has a greater probability of being found in the orthorhombic *Pnma* symmetry. For clarity, only the dopants offering high stabilization are shown. As can be seen, lithium has the greatest effect of the stabilization of the wanted *Pnma* phase, for all concentrations except doping into pure $SrCl_2$. The highest effect can be seen for the pure $BaCl_2$, which is also expected as this salt naturally occurs in the orthorhombic structure.
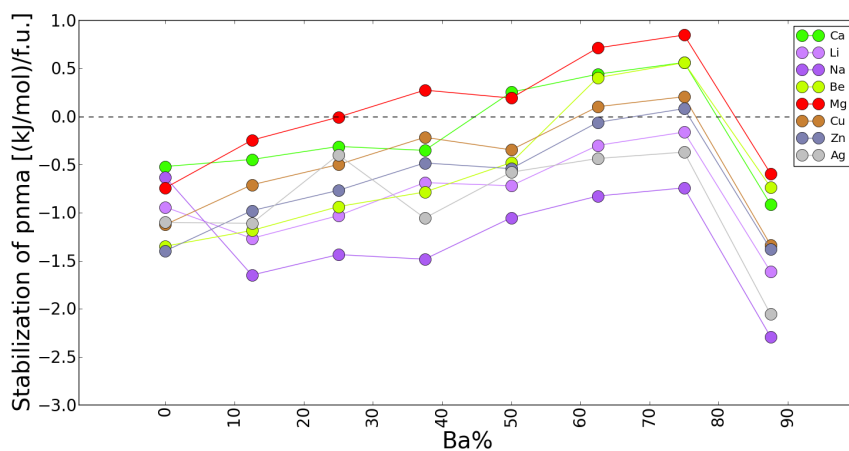
Figure 5.6: Relative stabilization of the mixed salt, $Ba_xSr_{0.875-x}M_{0.125}Cl_2$, in space group *Pnma* compared to *Fm-3m* for selected dopants. Having a more negative value for the stabilization, results in a greater probability of observing the mixed material in *Pnma*. The lines connecting the markers are only shown for clarity.

To test the predictions $Ba_{0.375}Sr_{0.5}Zn_{0.125}Cl_2$ was synthesized by ball milling, which, as described in section 5.2, resulted in a poor mixing for the undoped Sr-Ba salt. The reason for choosing zinc even though many other of the tested materials had higher predicted stabilization (Figure 5.6), was, that the calculations were performed on a system always forced to be neutral and with fixed symmetry, resulting in the oxidation state +2 for all metals; of the metals normally found in this oxidation state, Ag and Be is predicted to give a larger stabilization, but silver prefers +1 and beryllium is toxic, and is therefore disregarded, leaving zinc as the best candidate.

The doped system was not thoroughly tested, because it was realized that it was possible to form a stable barium strontium mixture by spray drying as discussed in section 5.2. However, from the initial investigations [135] it was clear that the orthorhombic phase was preferred with more than 90 % of the mixture found in this symmetry after cycling as compared to around 60 % for $Ba_{0.5}Sr_{0.5}Cl_2$. The ammonia storage properties of the zinc-doped material, were found to be quite poor only allowing an uptake of four ammonia

molecules per metal atom, which is lower than the expected eight molecules. However, the doped mixed octa ammine was not investigated computationally, and might be unstable compared to having the pure metal octa ammines separated. However, it might be interesting to study the system in greater details both computationally and experimentally, as this could give insights into the effect of dopants. Furthermore the system would have an gravimetric hydrogen density increased by 3 %, which might be worth pursuing as zinc might be cheaper (Table 1.1), resulting in a cheaper material with better properties, but maybe at the cost of a more complex synthesis and reaction.

Designing Mixed Hexa Ammines

6.1 Testing the Genetic Algorithm

This chapter will describe the initial test and validation of the implemented genetic algorithm, described in chapter 3 and presented in paper III. The goal of the screening was to test the algorithm on a realistic system, designing new hexa ammines, with improved ammonia storage and release properties compared to the pure metal halide ammines, which generally show multi-step releases at too high temperatures (see chapter 4). Therefore the search was focused on identifying the best hexa ammine releasing all the stored ammonia in one step at a temperature suitable for use as an energy carrier for transportation.

Mixtures containing up to three different metals and two different halides were investigated, with limitations on the concentration of expensive metals. A broad range of elements were allowed (Figure 6.1), and primarily metals expected to be stable in the enforced oxidation state +2 were included [138]. In total the search space contains almost 27 000 combinations, which is a suitable size for these initial tests. Furthermore, as will be described in the following sections, the chosen fitness function made it possible to verify that the algorithm succeeded in finding the same global optimum from random starting populations, validating the applicability of the GA.

Figure 6.1: Selected elements from the periodic table included in the screening.

6.2 Genetic Algorithm Setup

As described in chapter 3, a range of different parameters and reference data are needed before the algorithm can be started. In the following selected parameters and the generation of reference data will be described, the interested reader may consult paper III, to get the complete description. An example of one of the investigated mixed hexa ammines is shown in Figure 6.2.
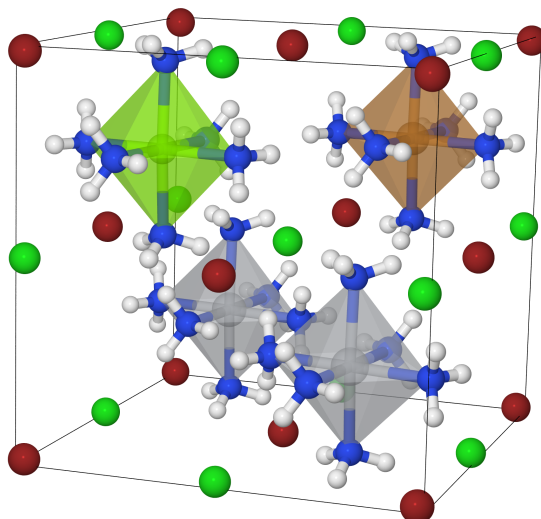
Figure 6.2: Example of a mixed hexa ammine, $Ti_2CuMgCl_4Br_4$, in the template structure. Metals are centred in the polyhedra surrounded by ammonia molecules, Ti is depicted grey, Mg light green, Cu brown, Cl green, Br dark red, N blue and H white.

The goal of the screening was to design mixtures with high ammonia storage capacities, and the ability to release the stored ammonia in one step at relatively low temperatures. This is ideally achieved by using the combination of a single-objective fitness function optimizing the weight percent of hydrogen, wH, and an additional set of rules the materials should obey to be accepted for further progress. The most important thing to check is that the release is within an acceptable temperature interval determined from the calculated reaction enthalpy by using the van 't Hoff equation (Equation 4.1).

Another important thing, which should be fulfilled in order to have an interesting material, is that the mixture should be stable in all phases, compared to having the pure metal halide ammines in the reference structures. The reference data for the pure structures are generated as described in section 3.1, and stored in a database (see section 3.4). By comparing the energy of a trial mixed structure to the sum of the pure references, the decomposition energy can be determined, by studying a reaction similar to the following:

$$Mg_3Be(NH_3)_{24}Cl_8(s) \longleftrightarrow 3\,Mg(NH_3)_6Cl_2 + Be(NH_3)_6Cl_2 \qquad (C\,6.1)$$
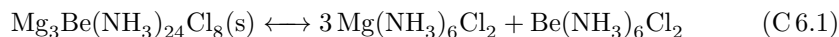
A similar comparison is performed for the mixed salt, and the material is considered stable, if both phases are stable against decomposition. Given the use

of predefined template structures, we also include marginally unstable mixtures (up to 0.5 eV per formula unit containing one metal atom) in order not to exclude candidates that may potentially display stability following full relaxation of all structures.

As mentioned in chapter 4 some metal halides can coordinate eight ammonia molecules and form octa ammines. This is also very important to take in to account when judging if the material is stable against decomposition. If for example a hexa ammine mixture of strontium and magnesium chloride is decomposed the result would most likely be a mixture of strontium octa ammine, strontium salt and magnesium hexa ammine:

$$\mathrm{Mg_2Sr_2(NH_3)_{24}Cl_8} \longleftrightarrow 2\,\mathrm{Mg(NH_3)_6Cl_2} + \tfrac{3}{2}\mathrm{Sr(NH_3)_8Cl_2} + \tfrac{1}{2}\mathrm{SrCl_2} \quad (\mathrm{C\,6.2})$$
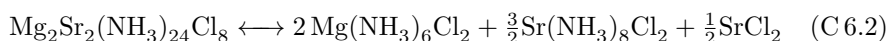
Because all the pure metal halides in the search space have not been experimental tested, it is determined whether an octa or hexa ammine is expected from the calculated energies. This is done by comparing the energy of the octa ammine to the energy of the hexa ammine and two ammonia molecules in the gas phase, and as evident from Figure 6.3 most of the investigated metal halides are expected to form hexa ammines. The decomposition energy is always calculated relative to the most favourable way of splitting up the constituents, especially important for materials containing different halides and metals simultaneously.
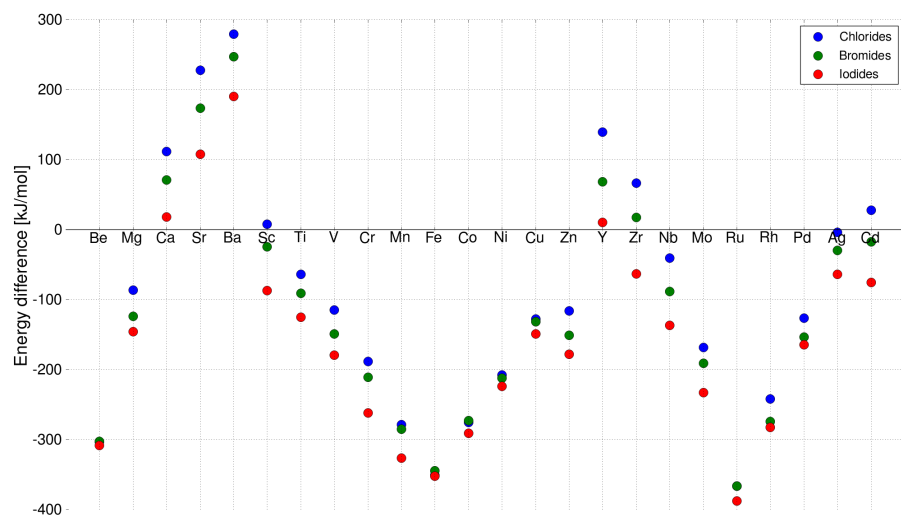
Figure 6.3: Stability of octa vs. hexa + 2 $\mathrm{NH_3(g)}$. If energy difference > 0 octa is preferred.

6.3   Searching the Phase Space

If a GA should be powerful, it is important that it samples all relevant parts
of the phase space. The topology of the phase space defined in section 6.1 can
be described using the fitness, wH, which can easily be calculated for all the
different combinations of elements. Studying Figure 6.4 it is evident that the
distribution allows one to pick a material with a very specific wH ranging from
just below four percent up to more than nine percent.

However, it is not expected that all these materials are stable against decom-
position, and have releases at suitable temperatures. In Figure 6.5 the release
temperatures for all of the investigated materials fulfilling the decomposition
criteria, are shown together with the observed fitness. The first thing to ob-
serve from the figure is that many structures with relatively high fitness have
been tested by the algorithm. This is a result of choosing wH as the fitness
function, which results in structures with higher and higher weight percent
being analysed, as more and more accepted structures with high fitness enters
the population, resulting in offspring with high wH. It is also evident that the
search is divided in almost horizontal bands, despite the fact that all values of
wH should be possible (Figure 6.4). The different bands represents different
combinations of the halides, which have a drastic effect on wH, resulting in the
algorithm jumping from a lower band to a higher, continuing the search there.

Another important thing indicated in Figure 6.5, is the reproducibility. The
algorithm was started three times, to test the convergence from different ran-
dom starting populations, and interestingly a lot of overlap is seen between the
runs. Especially many of the high fitness structures have been tested by all
three runs, proving that the algorithm is able to find the same optimal struc-
tures starting from different areas of the phase space. However, the approach
towards the optimal mixtures is not the same, and the different runs require
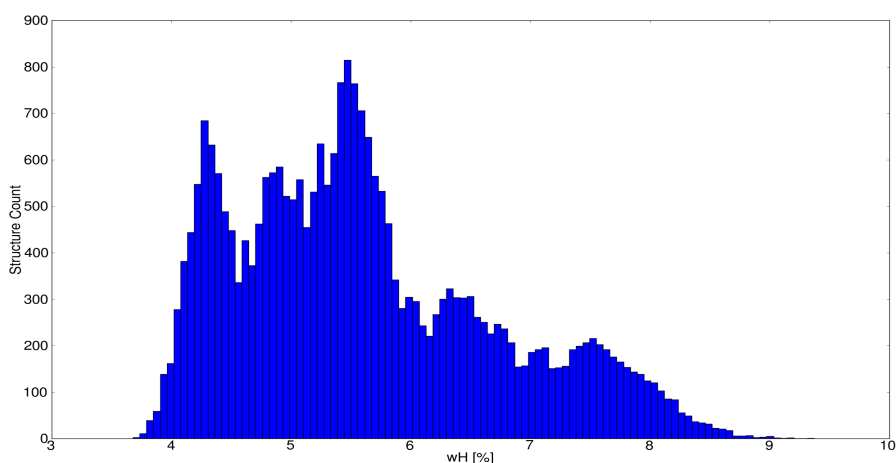
Figure 6.4: Distribution of the weight percent of hydrogen (wH) for all struc-
tures in the defined search space.

different number of generations as shown in Figure 6.6. There are, however, similarities in the routes taken, and they behave similar after some initial focussing of the search, after which the optimal building blocks are identified, and the local minima are found. The first run was continued until a new structure entered the top five best structures, which was used to determine, when the algorithm was expected to be converged. To find a new structure almost 50 % extra generations were needed - therefore rerunning the algorithm multiple times is generally more advisable, especially in the used setup allowing reuse of old data (see section 3.4).
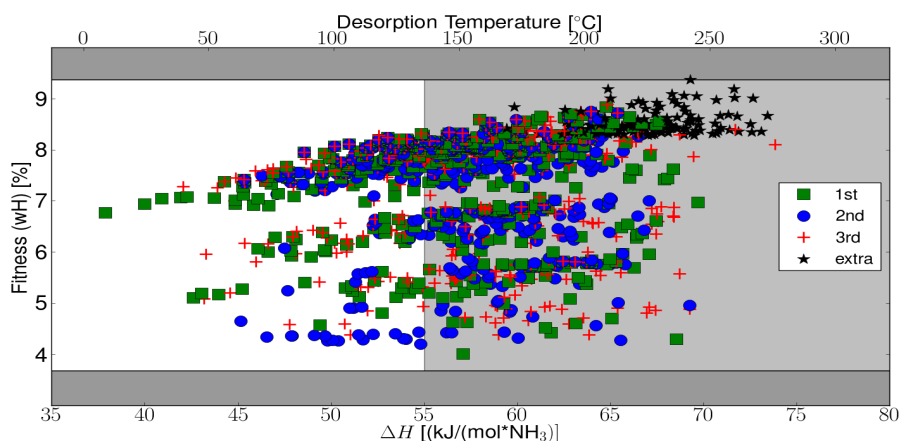
Figure 6.5: Visited parts of search space, for all the three runs and the extra manual search described in section 6.5. The dark grey area indicates wH not accessible within the defined search space (see Figure 6.4). The white window indicates structures with acceptable release temperatures. Only structures which fulfil the decomposition stability criteria are shown.
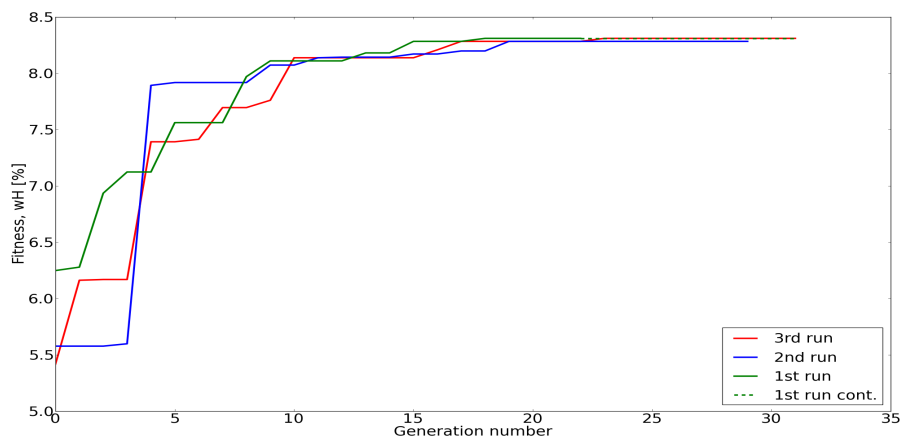
Figure 6.6: Fitness (hydrogen weight percent, wH) of the best individual as a function of generation number. As indicated by a dotted line, the first run was continued for a longer time to test the convergence.

6.4   Optimal Identified Mixtures

As indicated in Figure 6.5 the three different runs identified many of the same structures. Most of the identified mixtures do unfortunately bind the ammonia hard, and the release temperatures are therefore too high. However, as it is only the stable mixtures which are shown in the figure, it is evident that many mixtures with high wH are available, which might be relevant for other applications. In this search the release temperature is however very important, and it is therefore important to apply the selection rules. Table 6.1 shows the top ten candidates identified in the three different runs, which fulfil the two criteria regarding stability against decomposition and release temperature. As can be seen, there is a high dominance of titanium rich structures, which is not surprising because it is one of the lightest elements in the search space, and apparently the mixtures have acceptable release temperatures. Furthermore only chlorides are present, which reveals that the chlorides are stable and show acceptable release temperatures, and because it is the lightest halide, it dominates the screening. In future screenings, the other halides might be disregarded, if wH is the ultimate criteria.

With the chosen stability criteria the algorithm accepts structures which are slightly unstable in the templates, but might be stable upon full relaxation. However, the structures which are strictly stable are undoubtedly the most interesting. If the selection is made strict in all phases (bold in Table 6.1), it is very interesting to see that the three runs find the same top four candidates, disregarding Ti_4Cl_8 only found by the second run[1]. It has been shown that similar mixtures are synthesisable, e.g. $TiMgCl_4$ [140] and pure titanium(II) chloride has been observed in the $MgCl_2$ structure [141] used as template in the screening; this indicates that the suggested materials can be synthesized, and the templates used should give reasonable estimates of the reaction enthalpies.

As discussed in section 6.1 many of the pure metal halide ammines have the disadvantage that one or more intermediate ammine phases are observed during the release. Because of this, it was tested whether mono or di ammines would be expected for the top ten candidates. These tests showed that the best identified mixture, $Ti_2CuMgCl_8$, and a couple of other structures would have two-step releases passing through di ammines. For $Ti_2CuMgCl_8$ this results in a lowering of the practical available ammonia density, as the last two molecules are released at too high temperatures ($>200\ °C$). This shows that it is indeed relevant and important to check for the stability of intermediate phases if possible. Ultimately it would be preferred to check this for all structures, while the algorithm is running. In order to speed up the calculations, this was not done in this initial testing. Only a limited number of the investigated structures showed stable intermediates, therefore the results would probably not have changed significantly.

---

[1]$TiCl_2$ does not form a hexa ammine, but only a tetra ammine; however, $TiCl_3$ do form the hexa ammine [139].

1st run		2nd run		3rd run	
Structure	Fitness (wH)	Structure	Fitness (wH)	Structure	Fitness (wH)
TiScTiCaCl8	8.31	**TiTiCuMgCl8**	**8.28**	CaTiTiScCl8	8.31
TiTiCuMgCl8	**8.28**	ScTiTiTiCl8	8.24	**CuTiTiMgCl8**	**8.28**
TiTiTiScCl8	8.24	**TiTiTiTiCl8**	**8.21**	ScNiCaCaCl8	8.28
TiScTiVCl8	**8.21**	**ScTiTiVCl8**	**8.21**	TiTiTiScCl8	8.24
TiScTiCrCl8	8.20	ScTiTiCrCl8	8.20	CaTiCuCaCl8	8.21
TiTiTiVCl8	**8.18**	**TiTiVTiCl8**	**8.18**	**TiTiVScCl8**	**8.21**
TiTiTiCrCl8	8.17	TiTiTiCrCl8	8.17	CrTiTiScCl8	8.20
ScCuCuMgCl8	**8.17**	**ScCuCuMgCl8**	**8.17**	**VTiTiTiCl8**	**8.18**
VTiTiVCl8	8.15	TiVVTiCl8	8.15	CrTiTiTiCl8	8.17
VTiTiCrCl8	8.14	TiVTiCrCl8	8.14	**ScCuCuMgCl8**	**8.17**

Table 6.1: Optimal structures with the highest fitness (hydrogen weight percent, wH), from three different runs, starting from random initial populations. The structures in bold are structures that are strictly stable against decomposition in both phases.

6.5 Global Optimum

A validation of the method and the results can be performed because the weight percent is chosen as the fitness, since it is possible to determine which structures in the search space have a higher weight percent and could potentially have acceptable stabilities and release temperatures (Figure 6.4). It turns out that only 253 structures in the search space would have higher wH than the best candidate, $Ti_2CuMgCl_8$, and 83 of these have already been tested by the three runs, leaving us with 170 candidates. Because it is this very limited number of structures, we manually tested all of these candidates. As shown as stars in Figure 6.5, none of these structures were found to be better, primarily due to high release temperatures. This demonstrates that the global optimum structure was found by the algorithm in all three GA runs, thereby proving that the suggested algorithm is very efficient, and rerunning is not necessary if only the global optimum is wanted.

Only ~400 out of the ~27 000 structures were tested on average for a genetic algorithm run in this search space. The top-down validation approach is naturally only possible in this special case because of the simple fitness function. The goal of a screening is often to find multiple candidates, which would favour the use of the genetic algorithm; in this specific example it would require 254 calculations to get the best, 337 to get top two, 372 to get top three and 401 to get top four, which is more than the average length of one run, which in all cases find the top four candidates. Furthermore, the GA would also find stable structures, with lower, but still high wH (Figure 6.5), which is a lot better than the top-down approach leaving us with only one to four stable structures.

6.6   Preliminary Experimental Tests

Prior to performing the tests on possible intermediate phases, it was decided to test $Ti_2CuMgCl_8$ experimentally, which was thought to be the best candidate. Attempts to synthesise the mixed salt were performed by ball milling the precursor salts (all dichlorides), in the specified ratios. After the milling, none of the precursors could be detected in the XRD pattern (Figure 6.7), indicating that some mixing had occurred. However, from the XRD it was clear that metallic copper was present; no other phases could be identified with certainty. Most likely the copper was formed from reduction by titanium chloride:

$$TiCl_2 + CuCl_2 \longrightarrow TiCl_3 + \tfrac{1}{2}CuCl_2 + \tfrac{1}{2}Cu \qquad (C\,6.3)$$
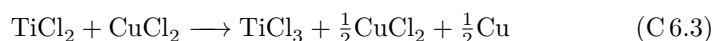
As indicated, titanium chlorides exist in different metastable oxidation states [142], but none of them could be identified in the XRD. This indicates that a mixed system with unknown composition exists.

The ammonia storage properties of the obtained mixture were analysed, but the absolute ammonia uptake/release cannot be trusted, due to the uncertainties regarding the constituents - however, the relative amounts released in the steps, should be correct. Figure 6.8 reveals that the release is a multi-step process. The predicted two-step release at 136 °C and 214 °C seems to fit with the experimental observations during the first cycle; however, the release is clearly also starting at lower temperatures, which might be due to the incomplete mixing. As mentioned, the absolute values cannot be trusted, but the ratio between the release steps seems to fit reasonably well with the predicted 6→2→0 release.

In Figure 6.8 the effect of cycling is also presented. As indicated the first cycle was from room temperature up to 300 °C, whereas higher temperatures were applied in the following cycles, to determine if some of the ammonia could be released at higher temperatures. Studying the figure it is evident that some degradation occurred. The degradation can also be observed from the XRD analysis of the cycled salt (Figure 6.7), revealing presence of CuCl and $MgCl_2$, which were not present earlier; furthermore the metallic copper content is also increasing during cycling. The copper dichloride decomposes above 570 K [138]:

$$CuCl_2(s) \longrightarrow CuCl(s) + \tfrac{1}{2}Cl_2(g) \qquad (C\,6.4)$$
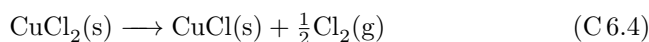
The reaction is irreversible, because the gas escapes from the system during the experiment. It is therefore very likely that we observe this degradation in cycle #2-5, which were heated to higher temperatures. Partial reduction by titanium could also yield CuCl, but this should also occur during milling, and no significant amount of CuCl was detected for the freshly milled sample. As discussed in section 6.4, other of the identified materials from the screening have shown to be more interesting, as no intermediates are expected. Despite of this, the experimental testing of $Ti_2CuMgCl_8$ has shown that the template based approach seems to give accurate release temperatures, but also reminded us that one should be aware of possible destructible side reactions and segregation of the phases.
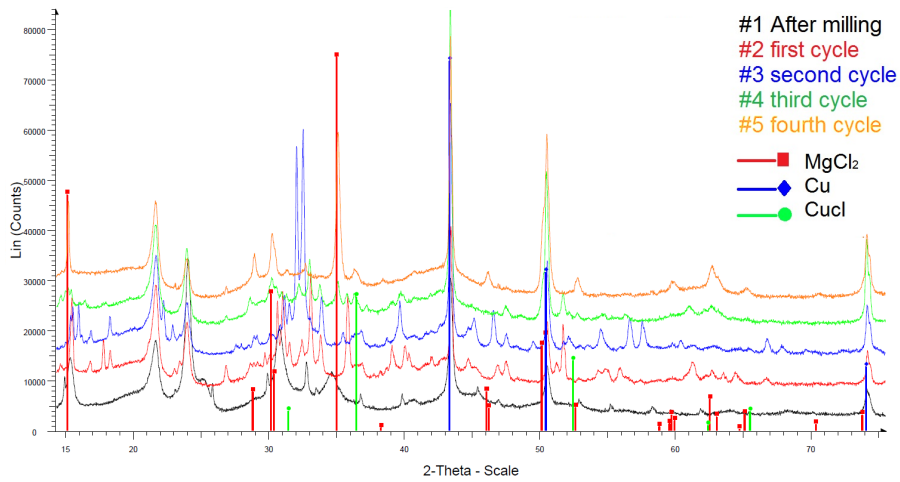
Figure 6.7: XRPD patterns for $Ti_2CuMgCl_8$ before and after cycling. The Bragg peaks for the identified phases are marked with vertical lines.
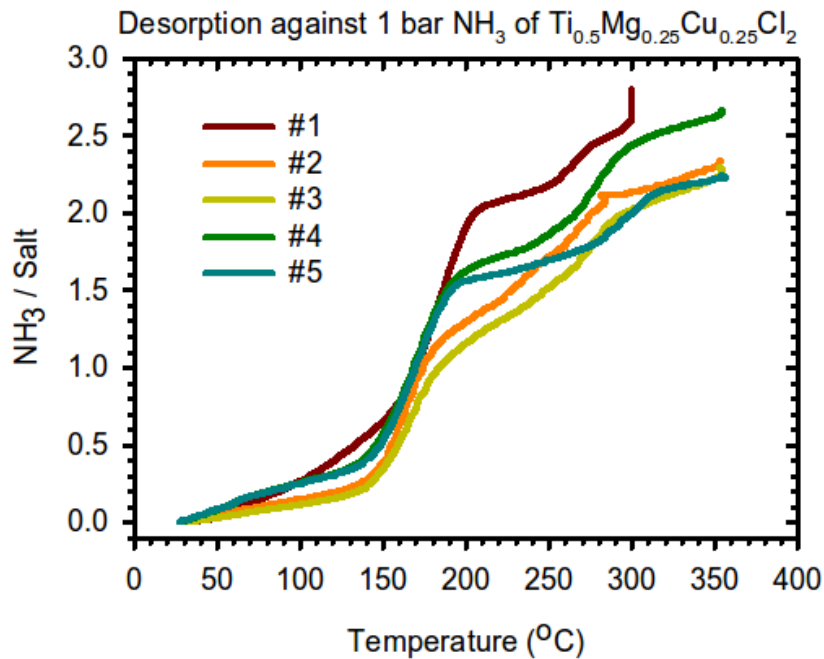
Figure 6.8: Initial experimental testing of $Ti_2CuMgCl_8$, including cycling experiments. The sample was only heated to 300 °C in the first cycle (and kept at this temperature for some time). The amount of desorbed NH_3 is calculated as if the mixed salt was formed, and does not take into account the inactive part of the sample, due to the presence of metallic copper and the possible release of $Cl_2(g)$.

Designing Improved Mixed Metal Ammines

7.1 Introduction

After the successful initial test of the algorithm, presented in the previous chapter, the complexity of the screening is increased and a more complete screening is performed. In paper IV a screening is presented, where the goal is to find the best mixed metal halide ammine, which is able to release as much ammonia as possible in a narrow temperature interval. The screening includes checks on the stability of multiple intermediate phases, to get a complete description of the expected release patterns. In this chapter the main results and the adjustments of the genetic algorithm are presented. Furthermore the experimental testing of a selection of the best candidate materials are presented, further proving the success and applicability of the GA to predict new materials for ammonia storage.

In this screening the same metals as in the hexa study are allowed (Figure 6.1), but only chlorides are considered, as it was found that many stable mixtures existed. The complexity is not only increased by including stability checks on multiple intermediates. The system size is also doubled, resulting in a unit cell containing eight metal atoms, and up to 280 atoms in total, which is the maximum feasible cell to use in a screening study of this size with the current available technology. This opens up for testing materials with at minimum 12.5 % of one metal, which might result in interesting release properties; it is not really dopant level, but might still provide insight in interesting dopant elements, which could be tested in lower concentrations experimentally.

To further ensure that the identified materials can be used as energy carriers, the definition of expensive metals has been changed. The number of expensive metals is increased to 11 different metals, still allowing a maximum concentration of 25 % (also allowing mixtures with 12.5 % of two different expensive metals). In total the defined search space contains more than 17 000 different combinations, resulting in more than 100 000 structures to test. If all structures should be tested with brute force screening, approximately ten million CPU hours would be used - therefore it is ideal to use our GA to perform

an optimized search, thereby lowering the total number of calculations to be performed.

7.2   Adaption of the Genetic Algorithm

In the following the adaption of the algorithm to perform the multiphase screening will be described. Most of the setup is similar to the hexa study, and only the changes will be described in the following. To get a complete understanding of every facets of the algorithm, the interested reader is referred to paper IV (and chapter 6 and paper III, if they have not been studied).

The most important change was made to allow the investigation of multiple intermediate phases for every structure. The energies of all investigated phases are calculated, and subsequently the release pattern is determined. When it has been determined which phases will be observed, it is determined at what temperatures, the interchanges between the observed phases are occurring. Finally the fitness is defined as the available ammonia released in the temperature interval, converted to a weight percent of available hydrogen. This principle is similar to the one applied in paper II comparing the barium-strontium system, to existing pure metal halide ammines. With this setup the fitness of for instance $Sr(NH_3)_8Cl_2$ will be 6.2 % even though the stored amount of ammonia corresponds to wH = 8.1 %. The reason is that only the release to the di ammine is predicted to occur in the specified temperature interval (see chapter 4).

All other pure metal chlorides have also been tested, as they are needed as reference data to determine the stability of the mixed phases, which is determined for all phases, by studying reactions similar to Equation C 6.1. A new mixed material is regarded as stable if all observed phases are stable again decomposition; again semi-stable structures are allowed, as they may show stability upon relaxation. Out of the pure metal chlorides the highest possible fitness is 7.3 % for $Ca(NH_3)_8Cl_2$ releasing the first six ammonia molecules. $Ba(NH_3)_8Cl_2$ is the only octa ammine having a predicted one step release, resulting in a fitness of 7.0 %. As already known, mixing barium and strontium chloride results in a material superior to the constituents (see chapter 5). Therefore, it is hoped that the screening will reveal new improved mixed materials.

It is expected that including multiple phases will make the search more complex, due to a more advanced phase space. For this reason the population size is increased to contain the 20 best individuals, to ensure not ending up in a pre-converged state. Due to the increased population size the convergence criteria were also harshened, requiring the top population to be stable for longer time. This is necessary because a larger population will make the search broader, and therefore it is expected that the convergence will be slowed down. Summing up these thoughts, we require the top five candidates to be stable for six generations, after which it is not expected that new improved structures, would enter the population.

7.3 Convergence Analysis

As mentioned in the previous section some parameters were changed slightly compared to the hexa study presented in chapter 6, which was proven to be able to find the global optimum. Therefore it is important to perform an analysis of the chosen convergence criteria, to check that the robustness of the algorithm is sustained. Again the search was started from three random and thereby different populations. Figure 7.1 shows that the different runs end up finding the same high fitness structures, but using different routes in the phase space. The first run quickly finds high-fitness structures, and converges after only 20 generations using building blocks with relatively high fitness which were found quite early. The second and third run are similar and have slower convergence due to a more slowly changing top five population.

To further test if the chosen convergence criteria were adequate, two extra generations were generated for the three runs, to check if new improved structures entered the populations. The original chosen criteria was top 5 stable for 6 generations. In Figure 7.2 the effect of increasing the requirements is analysed. Run #1-3 show the success compared to the ten best found structures if the individual run had been converged to top 5 stable in 8 generations. Again it is evident that the first run was special, converging very quickly, with the original convergence criteria. As will be discussed in details in section 7.5, the first run is missing two of the candidates found by the two other runs. Only judging from the analysis of the first run, the criteria should have been harsher, as new structures enters in both of the two extra generations (Figure 7.2). However, as mentioned this run was extremely fast, and should not be considered as a representative run. Comparing the two last runs, they are more similar, and do find the same structures, and do not find new structures in the two extra generations.

From all the runs it is clear that the number of generations is the most important part of the criteria, significantly increasing the success by requiring that no new structures enters for 6 generations. It is especially clear from the third run, which would have been stopped halfway after 24 generations, if the convergence criteria for instance had been five stable structures for five generations, only identifying one of the top ten structures. This proves that the chosen convergence criteria are adequate, but comparing top three would actually be enough in this search space – this would however not have lowered the number of structures to test, and requiring stable top five is therefore still recommended.

In Figure 7.2 the Global Success is also included, averaging over the three runs comparing to the best top ten structures found in all runs (similar to final top ten for run #2-3, see Table 7.1). Averaging over the three runs, it is evident that the global success rate is very high, proving the robustness of the algorithm. Therefore one run should in general be enough to find the best candidates, however one should take care if the run converges very fast testing only a small fraction of the total combinations. The last two runs, both testing more than 4 %, identifies exactly the same structures in top ten, indicating that testing around 5 % would be adequate, to identify the ten best candidates.

51
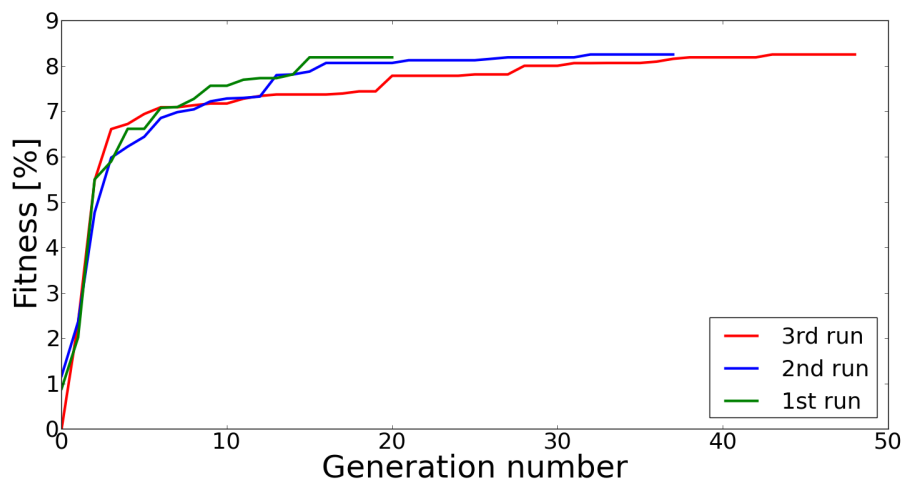
Figure 7.1: Genetic algorithm convergence for three different runs. It shows the evolution of the average fitness of the top five best stable structures as the algorithm runs evolve.
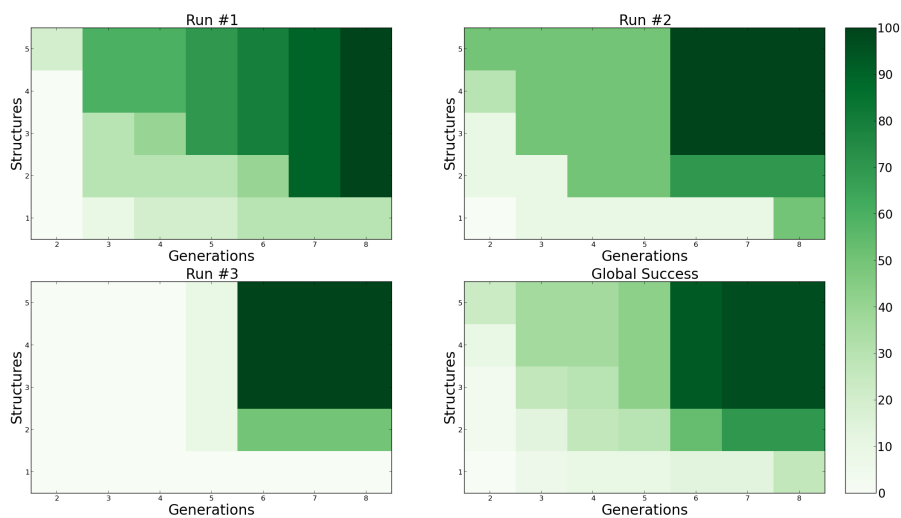
Figure 7.2: Success of algorithm with changed convergence criteria, showing which fraction (in percent) of the top ten structures, that would have been found with different convergence criteria. See section 7.3 for a detailed description.

From the presented analysis, it has been verified that the chosen convergence criteria, were well suited for the investigated search space, with the implemented algorithm and the chosen parameters. As discussed in subsection 3.3.3, the choice of operators for offspring generation are very important for a successful algorithm. From the hexa study presented in paper III it was evident that especially the crossover and neighbor mutation operators were very important for the success of the algorithm - however, the random mutation, cannot be omitted, as it is responsible for the initial guiding of the algorithm. However, as mentioned, it is expected that the current search space is more complex due to the allowance of multiple phases, and therefore the importance of the different operators is again analysed.

Studying Figure 7.3 it is evident, that the multiphase search is different from the hexa study which only checked one ammoniated phase. The mutation operator behaves similar, and is important initially, but of very limited importance in later stages of the runs. In contrast to the hexa study the crossover operator has a relatively low success rate, but nonetheless producing improved offspring throughout the runs. The lower success rate might be due to the increased system size, and corresponding increase of the size of the atom list defining the elements in a given mixture; if bigger building blocks are taken from each parent there will be an increased risk of picking non-compatible blocks, resulting in unstable mixtures. Again it is evident that the neighbor mutation based on chemical intuition is very important and crucial for the success of the algorithm. From the analysis it might be suggested that the neighbor mutation operator should be used more often than the crossover, as both of them should be able to locate a local minimum, but apparently the neighbor mutation is much more effective. Furthermore it might be relevant to lower the number of random mutations, in later generations, when a relative big population size is used.
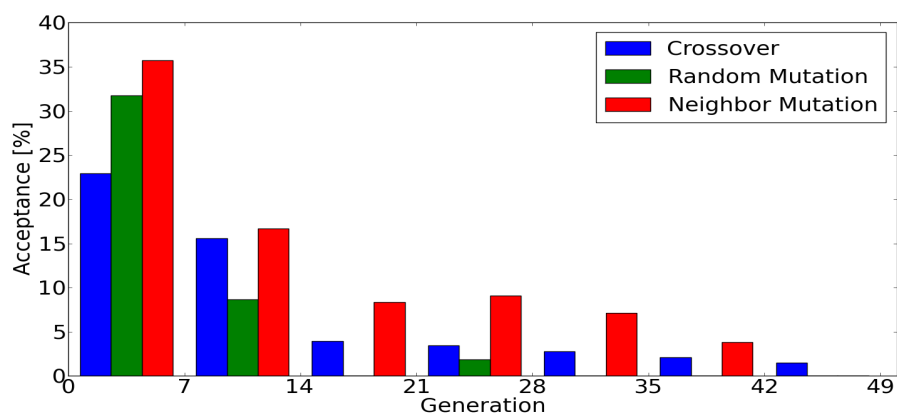
Figure 7.3: Operator success averaged over the three algorithm runs as the algorithm runs evolve. Success is defined as generating an individual with higher fitness, which furthermore obeys the additional rule regarding decomposition stability, for all observed phases.

7.4 Phase Space Analysis

As shown in the previous section it is evident that the phase space is relatively complex. To get a better understanding of the actual properties of all the investigated structures, the fitness and the weighted average of the predicted release enthalpies and the corresponding approximated release temperatures for all stable structures from the three different runs are plotted in Figure 7.4. It is confirmed that the phase space is more complex and different, apparently decoupled structure types exist. In the figure it is also indicated, that a very limited number of structures have a predicted multi-step release occurring in the narrow temperature interval; interestingly, the two best candidates, do however show a two-step release.

The correlations were investigated in details, and as shown in Figure 7.5 the different decoupled groups, are formed as a result of different releases. Clearly, the algorithm have identified the most stable materials giving a release from the octa ammine to a di ammine in the interval. By mutation and crossover these mixtures have created 'a tail' of offspring giving a full release from the octa ammine to the salt, again proving the success of the chosen operators. Again it is evident that the hexa ammines with a one step release, do generally bind the ammonia very hard (similar to Figure 6.5), resulting in releases at relatively high temperatures, often outside the defined temperature interval (and therefore not shown in Figure 7.4 and Figure 7.5).
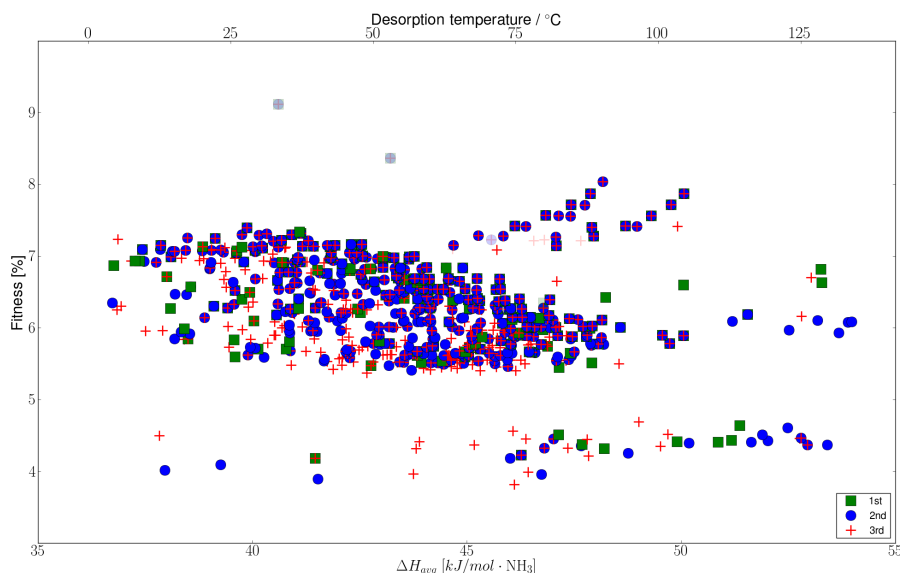
Figure 7.4: Visited parts of the search space defined by the weighted average release enthalpy, is shown for the mixtures found in three different runs. Multi-step releases are marked with faded symbols. Only stable structures which fulfil the decomposition criteria are shown.
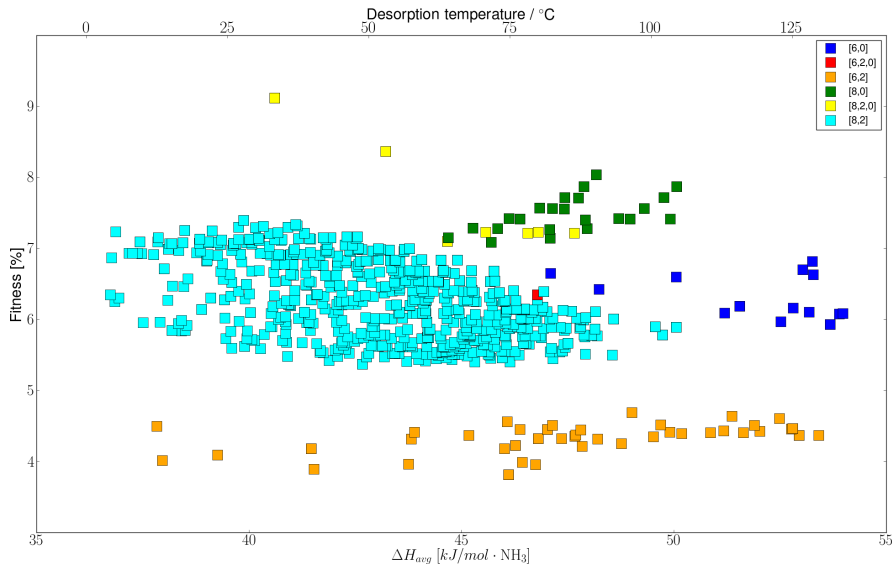
Figure 7.5: Visited parts of the search space, showing that different reactions are grouped in bands. The legends and colouring show the predicted observed phases, where 8 signifies octa ammine, 6 hexa ammine, 2 di ammine and 0 the empty salt. Only stable structures which fulfil the decomposition criteria are shown.

7.5 Optimal Identified Mixtures

Studying the overlap between the three different runs in Figure 7.4, it is again proven that the algorithm has the ability to identify the same high-fitness structures, starting from different populations. This is also reflected in the ten best candidates identified in the three different runs, presented in Table 7.1. It is impressive to see that the three different runs find many of the same structures, and the two last runs find exactly the same top ten.

1st run			2nd run			3rd run		
Structure	Fitness	Reaction	Structure	Fitness	Reaction	Structure	Fitness	Reaction
Ca4Cu2Y2Cl16	9.12%	[8,2,0]	**Ca4Cu2Y2Cl16**	9.12%	[8,2,0]	**Ca4Cu2Y2Cl16**	9.12%	[8,2,0]
Cu2Sr4Y2Cl16	8.37%	[8,2,0]	**Cu2Sr4Y2Cl16**	8.37%	[8,2,0]	**Cu2Sr4Y2Cl16**	8.37%	[8,2,0]
Ba2Sr6Cl16	7.87%	[8,0]	BaSr7Cl16	8.04%	[8,0]	BaSr7Cl16	8.04%	[8,0]
Ba2Sr5YCl16	7.87%	[8,0]	**Ba2Sr6Cl16**	7.87%	[8,0]	**Ba2Sr6Cl16**	7.87%	[8,0]
Ba3Sr5Cl16	7.72%	[8,0]	**Ba2Sr5YCl16**	7.87%	[8,0]	**Ba2Sr5YCl16**	7.87%	[8,0]
Ba3Sr4YCl16	7.71%	[8,0]	**Ba3Sr5Cl16**	7.72%	[8,0]	**Ba3Sr5Cl16**	7.72%	[8,0]
Ba4Sr4Cl16	7.57%	[8,0]	**Ba3Sr4YCl16**	7.71%	[8,0]	**Ba3Sr4YCl16**	7.71%	[8,0]
Ba4Sr3YCl16	7.56%	[8,0]	Ba4CaSr3Cl16	7.71%	[8,0]	Ba4CaSr3Cl16	7.71%	[8,0]
Ba5Sr3Cl16	7.42%	[8,0]	**Ba4Sr4Cl16**	7.57%	[8,0]	**Ba4Sr4Cl16**	7.57%	[8,0]
Ba5Sr2YCl16	7.42%	[8,0]	**Ba4Sr3YCl16**	7.56%	[8,0]	**Ba4Sr3YCl16**	7.56%	[8,0]

Table 7.1: Optimal structures with the highest fitness, from three different runs, starting from random initial populations. The Reaction column shows the predicted observed phases in the temperature interval. The structures in bold are found by all three runs using the original convergence criteria.

Again it is evident, that the first run is special, missing two structures, namely $BaSr_7Cl_{16}$ and $Ba_4CaSr_3Cl_{16}$. From the convergence tests presented in section 7.3, it is actually known that $Ba_4CaSr_3Cl_{16}$ enters in the first of the extra generations tested for the first run. It is also very likely that $BaSr_7Cl_{16}$ would be found, if the algorithm was continued, as all the other Ba/Sr mixtures exist and are in the population used for offspring generation. This confirms that the algorithm is very robust finding identical structures starting from different random populations, testing less than five percent of the structures in the search space.

If the algorithm should find all the Ba/Sr mixtures, and in general have a higher probability of locating local minima and the surroundings, a new concentration operator could be implemented. As described in subsection 3.3.3 this operator is changing the ratio between two of the elements in a parent structure, and might be helpful to address the problem. The already present crossover operator should also have this feature - however, it requires many similar elements in the population used for offspring creation, and furthermore the ordering of the atoms in the structure might result in low probability of changing the ratio between two elements. It should be noted that this concentration operator probably would be useless in the initial focussing of the searches, and it might only be turned on at later stages. Together with the suggested improvements regarding the ratio between the already implemented operators discussed in section 7.3 it might therefore be relevant to dynamically change the use of the operators, which was also implemented, in the original version of the algorithm [101].

All of the identified candidates presented in Table 7.1 are based on releases from octa ammines. This is also expected when studying the constituent metals, which all, except copper are expected to form octa ammines (see Figure 6.3). It is interesting to observe, that it is exactly the copper containing mixtures, which have the highest fitness, and a predicted two-step release in the interval. Based on chemical intuition these mixtures would not have been suggested, as copper would be regarded too small to coordinate eight ammonia molecules. This confirms that the designed algorithm is well suited for this kind of searches, revealing a new pioneering class of ammonia storage materials.

In conclusion many new materials with high fitness have been identified. Again, the fitness function is relative simple, making it possible to determine which structures could potentially show an increased ammonia release in the temperature interval. However, there are still 4736 structures with higher hydrogen weight percent, than the best identified candidates. Therefore it cannot be guaranteed that the identified structures are the best in the defined search space. However, as analysed in section 7.3 the algorithm gave almost identical results starting from different random populations. Even if the optimal mixtures have not been identified, the found candidates do indeed show promising release and storage properties.

7.6   Testing the Alkaline Earth Mixtures

Many of the best identified structures (Table 7.1), are mixtures of strontium and barium chloride, which have been discussed in great details in chapter 5 and paper II. It is therefore already known that most of the mixtures result in a one-step release, as shown in Figure 7.6. $BaSr_7Cl_{16}$ is the only material, which do not show the predicted one-step release from the octa ammine. Despite of this, the material is still interesting, as all the ammonia is released in the defined temperature interval.

In addition to the binary metallic mixtures, a ternary mixture of barium, calcium and strontium, showed up as the eighth best candidate. This candidate was synthesised, and the the ammonia storage properties were analysed. As can be seen in Figure 7.6, $Ba_4CaSr_3Cl_{16}$ do show a one-step release, which however is occurring over a broader temperature interval. A large fraction of the stored ammonia (>95 %) is however released in the predicted interval. Comparing the release to the pure metal halides also shown in the figure, one explanation for the extended release could be that a perfect solid solution has not been formed, and the material has a part behaving like pure calcium chloride, which is known to release the ammonia at higher temperatures.
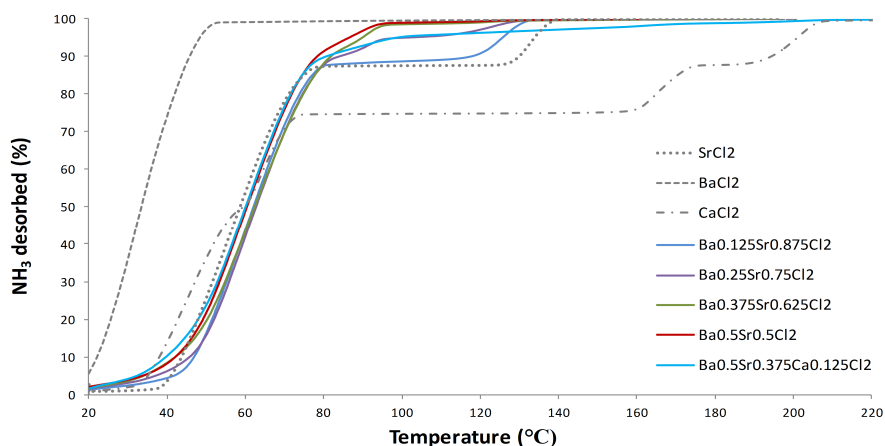
Figure 7.6: Experimental testing of the most promising alkaline earth mixtures identified in the screening study (see Table 7.1). The pure metal halides are also shown for reference.

The stability during cycling has also been tested, as this might be expected to be a problem with three different metals, with relatively different atomic radii [119]. Similar to other metal halide ammines, a small change is observed after the first cycle, most probably due to the formation of pores in the material [19], but the 2nd-5th cycles show no changes. In summary it has been shown, that the algorithm correctly predicted different mixtures of alkaline earth metal halides, which are superior to their constituents. This results in mixtures showing relatively high hydrogen weight percents, and the ability to release the stored ammonia in the defined temperature interval.

7.7 Mixtures Containing Yttrium and Copper

The best candidate, $Ca_4Cu_2Y_2Cl_{16}$, was also tested experimentally. As discussed earlier the template based screening assume that the metals are in oxidation state +2, which is natural for the alkaline earth metals, but more challenging for the d-block metals, which in general exist in multiple oxidation states [138]. One of the constituents, yttrium is normally not found in this oxidation state, as it would normally give up all its valence electrons, reaching an oxidation state of +3. As already discussed in section 6.6 copper is found in multiple oxidation states including +1. A synthesis of the ternary mixture, was therefore started from a mixture of $CaCl_2$, YCl_3 and $CuCl$, hopefully resulting in the correct average oxidation state.

The standard synthesis method employed so far, using spray drying to mix the elements was not applicable, due to the very limited solubility of CuCl [143]. Instead, attempts to synthesise the mixed salt were performed using ball milling (see section 5.2). At first sight the results seemed more promising, as the precursors, could not be identified in the XRD pattern of the freshly milled sample. However, the mixing was not completed as expected as metallic copper was clearly visible. Apart from the peaks associated with metallic copper, the analysis did not reveal any known compounds in a database search, which might be an indication of partial mixing of the material.

Despite the uncertainties regarding the constituent phases in the mixture, the ammonia storage properties of the synthesised material was tested - however, due to the uncertainties, the quantitative storage capacity cannot be trusted. Initially a relatively fast heating ramp of 2 °C/min was employed testing the mixture in four cycles. Interestingly, as shown in Figure 7.7 an increased storage capacity was observed during the first cycles. However, after four cycles it seemed like the release properties were stable, indicating some initial restructuring in the previous cycles. The changes during the first cycles are more pronounced than normally observed for the metal ammines (see for instance Figure 5.3). This might indicate major restructuring, not solely a result of the normally observed formation of pores [19].

A fifth cycle was employed with a significantly lowered heating ramp, revealing details of the multi-step release, as shown in Figure 7.7. Comparing to the two previous cycles the total released amount is constant. However, with the lowered heating ramp, it is clear the the release is occurring in multiple steps. As discussed earlier, a two-step release is predicted from the calculations, initially releasing six out of eight ammonia molecules at ~6 °C and the last two at ~99 °C. This prediction does not fit completely with the observations, probably due to incomplete mixing. Furthermore some of the release temperatures, seems to fit quite well with the pure calcium chloride [19], further indicating limited mixing.

As discussed, there are many indications suggesting that we have not only formed $Ca_4Cu_2Y_2Cl_{16}$. However, from the experiments, it is observed that a large fraction of the ammonia is released in the expected temperature interval. Therefore the system is still interesting, and will be studied further,

together with $Sr_4Cu_2Y_2Cl_{16}$, which might be easier to synthesise. The main problem seems to be the incomplete mixing, which might be due to the synthesis methods, and other methods might be performing better; one example could be co-melting of the salts at high temperatures, possibly resulting in more homogeneous mixtures. The identified materials containing a mixture of alkaline earth metals and yttrium, have not been tested yet, as the synthesis is expected to be even more difficult, due to the challenges regarding oxidation states. However, as discussed in this section, the mixtures are still promising, and the predictions are expected to be correct - the challenge is to synthesise the mixtures.
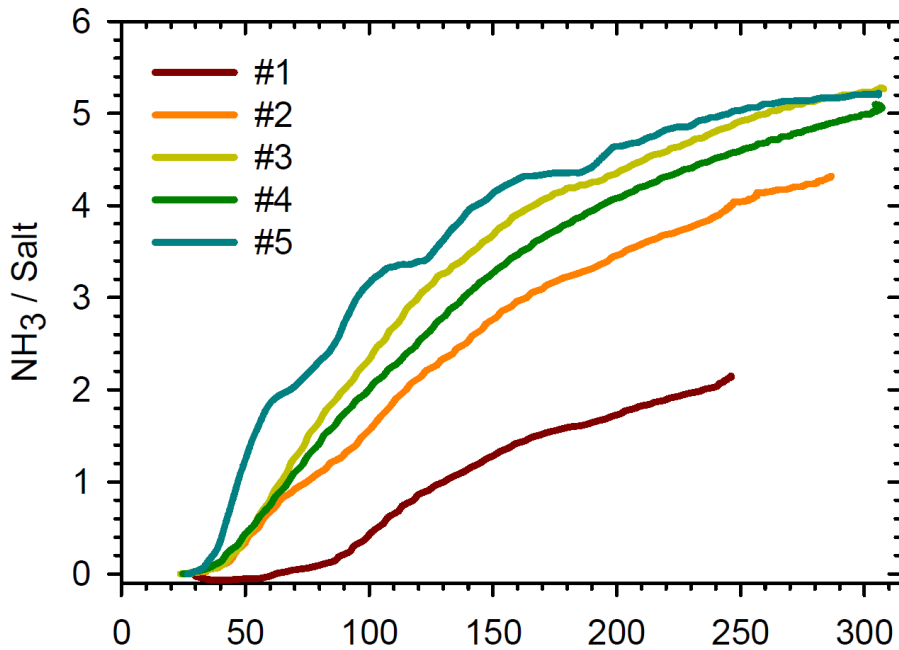
Figure 7.7: Experimental testing of $Ca_4Y_2Cu_2Cl_{16}$ prepared by ball milling. As described in the text, the mixing is not fully understood, and therefore the quantitative release cannot be trusted. Desorption against 1 bar NH_3 with a heating ramp of 2 °C/min for #1-4 and 0.5 °C/min for #5.

Reliability of the Screening Results

8.1   Template Based Screening

In the two screening studies presented in the previous chapters, various assumptions and approximations have been used, even though it is known from chapter 2 how to describe the investigated systems with high accuracy. The primary reason for this, is the enormous amount of computational resources needed to treat all systems in great details. As described in section 3.1, different properties regarding similar systems, have been successfully described by using the template based approach, but we cannot be sure that this is true for the investigated systems. In this chapter, the reliability of the different approximations are studied, from a computational point of view; however the most important verification of the approach is of course the experimental validation of the properties of the proposed materials. As demonstrated in the earlier chapters the predictions have been met to a certain extent for the different tested systems.

8.2   Permutation Tests

One of the most important approximations enforced in the presented screening studies, is the assumption that permuting the positions of the elements in the template structures would result in similar reaction enthalpies (ΔH), because of the cancellation of possible introduced inaccuracies (see section 3.3). This assumption has been crucial for the screening, because it lowers the phase spaces from millions of combinations, to thousands of combinations, which still is on the verge of what can be tackled with the current available computational power.

8.2.1   Smaller System

We start out by analysing the variations in ΔH observed when permuting the relative small systems investigated in the initial screening study presented in chapter 6, and depicted in Figure 6.2. In Table 8.1 the calculated desorption enthalpies for the 12 possible permutations of the best found candidate, $Ti_2CuMgCl_8$ are presented. As shown, the observed variations in the desorption enthalpies for the full step releases are very small, and for this system the

approximation disregarding permutations is applicable.

Atoms String	ΔH	Atoms String	ΔH
MgTiCuTi	54.96	TiTiCuMg	54.95
CuTiMgTi	54.96	TiTiMgCu	54.94
TiMgTiCu	54.96	CuTiTiMg	54.92
TiCuTiMg	54.96	MgTiTiCu	54.92
CuMgTiTi	54.95	TiMgCuTi	54.92
MgCuTiTi	54.95	TiCuMgTi	54.92

Table 8.1: Release enthalpies for the full one stop release from the hexa ammine to the salt, for all 12 permutations of $Ti_2CuMgCl_8$ [kJ/(mol $\cdot$ NH$_3$)].

As discussed in section 6.4, it is important to include the check of intermediate ammine phases, which was not included in the initial test of the algorithm. However, for a selection of the best candidates the stabilities of mono and di ammines were also studied. In relation to this it was checked what effect the permutations had on the stability of the mono ammine of $Ti_2CuMgCl_8$. From the analysis, it was evident that most of the structures showed small variations in the energies, similar to what was observed for the hexa ammine and the salt. However, two out of 12 of the permutations, showed significantly higher energies for the mono ammines (~10 kJ/mol per formula unit containing one metal atom). The two high energy structures were the structures with two titanium atoms as close neighbors.

To get an understanding of the increased energy, an internal relaxation of one of the high energy structures was performed (Figure 8.1). During the relaxation the distance between the titanium atoms was shortened by 0.6 Å, whereas the distance between copper and magnesium was only decreased by 0.02 Å. The distance from titanium to the coordinating ammonia molecules were increased by 0.08 Å, whereas the other ammonia molecules were practically not moved. Furthermore the energy was lowered significantly, resulting in a structure being more stable than the other permutations. The reasons for not observing similar effects for the hexa ammine an the salt, is probably due to the higher symmetry of these structures.
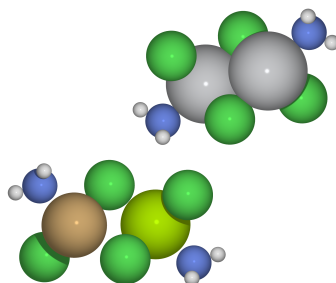
Figure 8.1: High energy version of $Ti_2CuMg(NH_3)_4Cl_8$, after internal relaxation. Mg is depicted light green, Cu brown, Ti grey, N blue, H white and Cl green.

8.2.2   Doubled System

In the bigger screening study presented in chapter 7 the complexity was further increased, by doubling the system size, resulting in octa ammine structures with 280 atoms (Figure 8.2). Due to the increased number of metals, 420 permutations of the metals are possible for the best identified structure $Ca_4Cu_2Y_2Cl_{16}$. It is therefore not feasible to test all structures, and therefore 20 randomly chosen permutations have been studied. As is evident from the results presented in Table 8.2, the accuracy regarding the full one-step release is also very convincing, with a variation of a few $kJ/(mol \cdot NH_3)$. A quaternary metal halide, $Ca_2Sr_2Cu_2Y_2Cl_{16}$, was also tested in the same template, and resulted in similar uncertainties.

Atoms String	ΔH	Atoms String	ΔH
YCuCaCaCaYCuCa	43.54	YYCaCaCuCaCaCu	42.34
CaCaCuYYCaCaCu	43.53	CaCuCaCaYCuCaY	42.29
CaCaCaCaYCuYCu	43.04	CaYCaCuCuYCaCa	42.21
CaCuCuYCaCaYCa	42.92	YCaCuCaCaCaYCu	42.13
CaCaCuCaCaYYCu	42.92	CuYYCuCaCaCaCa	42.07
CuCaYCaCaCuYCa	42.89	YCaCuCuCaCaCaY	41.37
CaYCuCaCaYCaCu	42.87	CaCaYCaCaYCuCu	41.37
CaCuCuCaCaYYCa	42.72	CuCaCaYCaYCaCu	40.97
CaCaCuCaYYCaCu	42.61	CuCaYYCaCaCuCa	40.67
CaCuYCuCaCaYCa	42.52	YCaCuCuCaCaYCa	40.65

Table 8.2: Release enthalpies for the full one stop release from the octa ammine to the salt, for 20 randomly generated permutations of $Ca_4Y_2Cu_2Cl_{16}$. The observed standard deviation is 0.87 $kJ/(mol \cdot NH_3)$.
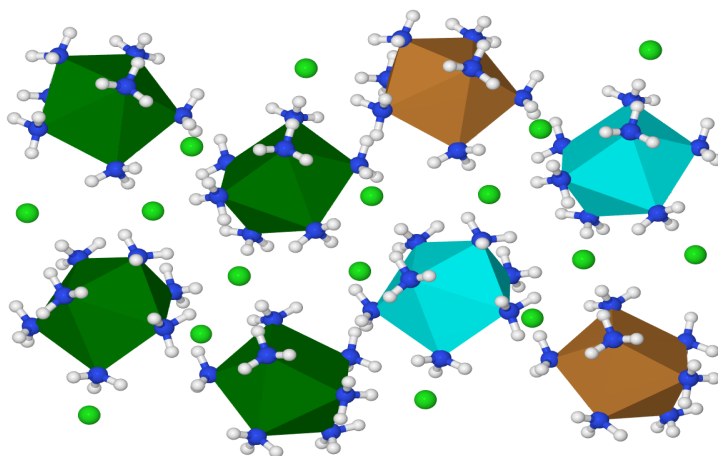
Figure 8.2:   Example of one of the tested permutations of $Ca_4Cu_2Y_2(NH_3)_{64}Cl_{16}$.   Ca is in the centre of the green polyhedra, Cu in the brown polyhedra, Y in the cyan polyhedra, N is depicted blue, H white and Cl light green.

For the intermediate ammonia phases higher uncertainties were observed, similar to what was observed for the mono ammine in the previous section. In general the release enthalpies are reported as per ammonia molecule - therefore there will be an higher inaccuracy on the small releases if the absolute uncertainties in the different phases are comparable. For $Ca_4Cu_2Y_2Cl_{16}$ this results in maximum differences between the highest and lowest predicted release enthalpies from e.g. the di ammine to the salt of ~12 kJ/(mol $\cdot$ NH$_3$), whereas the uncertainty from the octa ammine to either the di ammine, the mono ammine or the salt is 5.8, 3.1 and 2.9 kJ/(mol $\cdot$ NH$_3$) respectively.

For $Ca_4Cu_2Y_2Cl_{16}$ these variations do unfortunately result in huge variations in the predicted amount of ammonia released in the defined temperature interval. This is because the predicted release is a two-step reaction, where the first six ammonia molecules are released on the boarder of the lower limit of the temperature interval, and the last two at the higher boarder. Therefore most of the 20 random structures do actually have a predicted fitness of zero, and the algorithm has just been lucky to use the correct ordering, when the structure was created. Because of this it might in general be suggested to allow a broader interval, if the predicted release is a multi-step reaction, and in general it is always important to choose a sufficiently broad interval to ensure not de-selecting any possibly interesting structures.

Another way of improving the template based screening might be to allow a limited relaxation of each structure, to determine if the chosen ordering of the atoms is a very high energy structure, which can easily be relaxed. Furthermore the initial setup of the structures might be improved to set more important parameters correctly. In addition to the volume scaling and the correction of the distance from the ammonia molecule to the coordinating metal, it might be useful to optimize the distance between the metals, if the average volume scaling is not accurate, as was observed for the mono ammine in the previous section (Figure 8.1). Despite of the observed inaccuracies, the current template based approach do still offer a relatively high accuracy for the full one-step releases, which is most important, as the optimal ammonia storage material should have a one-step release.

8.3 Full vdW Relaxation

As discussed in section 7.6, many of the best candidates identified in the larger screening were already known from the barium-strontium system studied in great details in chapter 5 and paper II. This opens up for a unique opportunity to verify the inaccuracy imposed by using templates instead of fully relaxed structures, which was shown to accurately describe the experimental observations. As is evident from Figure 8.3 the accuracy of using the template based screening is very convincing. The estimated release enthalpies have an error less than two $kJ/(mol \cdot NH_3)$ compared to the full vdW relaxed structures, using significantly lower computation time.

From the figure it is also clear that the largest error is observed for the intermediate concentrations, which results in structures deviating more from the templates; however, the error is still very low. The observed error is however primary a result of the use of the calcium salt as template in the GA screening (as described in paper IV), instead of the cubic strontium salt which is primarily observed for the fully relaxed barium-strontium systems (see Figure 5.1). The energy variations for the octa templates are significantly lower than for the mixed salts.

The comparison using the barium-strontium system is not a complete verification of the template based screening approach, as it is expected that the two metals would show very similar chemistry. To make a more fair comparison the full vdW relaxation should be performed on more 'exotic' metal mixtures. Therefore, before making any final conclusions, additional systems have to be tested - until that has been done it is suggested to perform a full relaxation of selected candidates, after an initial screening. In the end, the most important success criteria is how the mixtures behave in real experiments. However, it should be remembered, that just because a material cannot be synthesised, it does not necessarily mean the calculations are wrong - the synthesis might be complicated or a polymorph with similar energy might be formed.
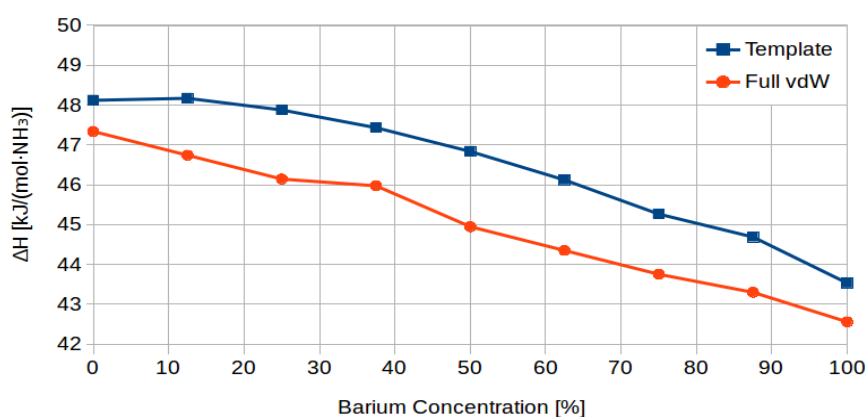
Figure 8.3: Difference in calculated full one-step release enthalpies, for different barium concentrations, using template based screening versus full vdW relaxation. The markers are only connected for clarity.

Summary and Outlook

9.1 Summary

The recurring theme of the work presented in this thesis has been the study and design of optimized ammonia storage materials in the form of metal halide ammines. The studies have been carried out primarily using computational methods, but several materials have also been tested experimentally by collaborators. These collaborations have been very fruitful, both to confirm the computational predictions, but also to give further insight in to details not fully explained from the experiments.

The first material studied in chapter 4 and paper I, is the state-of-the-art material, $Sr(NH_3)_8Cl_2$, used for solid state ammonia storage without the need of chemically transforming the ammonia. Through a combination of experiments and calculations, the experimentally observed anisotropic thermal expansion was explained. It was a result of one of the bonds from strontium to an ammonia molecule being significantly longer and easier to distort than the others. The detailed description of the local structure was very important, and the gained insight has been used to set up new mixed materials.

In chapter 5 and paper II the mixture of strontium and barium chloride was investigated. Again, by combining experiments and theory it was possible to identify mixtures superior to their constituents, releasing all the stored ammonia in one step at intermediate temperatures. Prior to the study, the crystal structures of the ammoniated barium phases were not known. By fully relaxing the mixed structures based on the known strontium structures, it was possible to give an accurate description capable of predicting the observed changes in the release patterns and temperatures.

Inspired by the successful mixing of barium and strontium, a large screening study was initiated. Because of the enormous number of combinations of different metal and halides, an optimized search method was needed. Therefore a genetic algorithm (GA) was implemented to guide the search more effectively. Initially, the algorithm was used to search for the best hexa ammine releasing the stored ammonia in one step (chapter 6 and paper III). The size of the search space and the chosen fitness function made it possible to verify that the found

candidates were the best possible candidates in the search space, proving that the GA implementation is ideal for this kind of computational materials design, requiring calculations on less than two percent of the candidates to identify the global optimum.

In chapter 7 and paper IV the algorithm was applied to a more complicated problem trying to identify the best metal halide ammines to be used as energy carriers for transportation. This study included investigation of many intermediate phases to determine the practical available ammonia release in a relatively narrow temperature interval. Again it was possible to show that the algorithm is very robust in finding the same structures, starting from different random populations. The investigated phase space was however more complicated, and it was therefore not as straightforward to show that the identified structures were the best in the phase space. Interestingly, the algorithm correctly identified all the Ba/Sr mixtures which were already known to exist from paper II. Furthermore a ternary alkaline-earth mixture, $Ba_4CaSr_3Cl_{16}$ was identified, and the predicted release was verified experimentally. The two best candidates, $Ca_4Cu_2Y_2Cl_{16}$ and $Sr_4Cu_2Y_2Cl_{16}$, are examples of materials, one would not suggest using chemical intuition. This shows that the algorithm is able to suggest new materials, by using the available operators, based on a combination of chemical knowledge and random events.

In the two screening studies, various assumptions and approximations were used to reduce the need of computational resources. One of the most important approximations enforced in the screening is the assumption that permuting the positions of the elements in the template structures would result in similar reaction enthalpies. An analysis of the variations in the predicted release enthalpies for selected materials revealed that the approximations result in acceptable uncertainties for the full one-step releases. However, larger variations were observed for the intermediate releases, leaving room for improvements.

Since the barium-strontium mixtures investigated in details in paper II were also found by the GA, a verification of the template based screening was possible. Comparing the results obtained using the fixed templates in the algorithm, to the fully vdW relaxed structures, it was found that the template based screening offers an acceptable accuracy, predicting the correct release patterns with an average error of only l.4 kJ/(mol · NH$_3$).

In conclusion, new record-breaking solid ammonia storage materials have been identified with the use of computational methods. Some of the identified mixtures do only consist of alkaline-earth metals, which are expected to have similar chemistries. Nonetheless, it is important that these mixtures can also be predicted correctly with the used methodology. In addition to these mixtures, which could have been predicted using chemical intuition, new ternary metals consisting of yttrium, copper and either strontium or barium, were predicted to have great storage capacities. The initial experimental tests of the identified candidates show promising results, but do also reveal that the materials can be challenging to synthesize, and might be degraded during ammonia desorption due to unwanted side reactions.

9.2 Outlook

The studies presented in this thesis have shown that it is possible to use the computer as a virtual laboratory and accurately design new materials with improved properties. This can reduce the number of experimental screening tests, facilitating environmentally friendly and cost-saving computational materials design and optimization. Furthermore, as the methods and the available computational power is further improved, even bigger phase spaces can be investigated. This would for example allow the study of lower dopant concentrations or allow a larger variety of template structures to be used, to enhance the chances of identifying new materials.

Instead of increasing the phase spaces, the individual systems could also be studied in greater details. As discussed in subsection 8.2.1 the template based approach might result in high-energy structures, which would initially be disregarded by the algorithm. Therefore, it is highly desirable to allow some degree of relaxation of the identified candidates. This local relaxation might also identify any possible destructible side reactions, which have been observed for some of the tested materials. However, the template based approach is still highly recommended, as the calculation time is significantly lowered, when starting from a good initial guess.

The kinetics should also be considered for the optimal material to be found. The kinetics can in practice only be studied for very small model systems using DFT. To understand real systems using kilograms of salts for ammonia storage, more coarse-grained models are needed to accurately describe the observed phenomena. However, the parameters to be used in the coarse-grained models might be obtained from DFT calculations of the local barriers. This has e.g. been shown to be a plausible approach, to describe the observed surface desorption for the strontium chloride ammine [64].

In the future, computers will probably be used increasingly to optimize existing materials and search for new. As the time passes we will get faster computers, and develop new methods allowing us to perform calculations even faster, which would result in systems capable of solving the present problems extremely fast. However, this would not mean that there will be no jobs for scientists in the future, as we would just study even bigger systems, in even greater details, to get a more complete understanding of the world.

Bibliography

[1]   S. Chu and A. Majumdar. Opportunities and challenges for a sustainable energy future. *Nature*, **488**:294–303, 2012.

[2]   BP Statistical Review of World Energy. Technical Report June, 2014.

[3]   L. Schlapbach and A. Züttel. Hydrogen-storage materials for mobile applications. *Nature*, **414**:353–8, 2001.

[4]   N. Lewis and D. Nocera. Powering the planet: Chemical challenges in solar energy utilization. *PNAS*, **103**:15729–15735, 2006.

[5]   F. Schüth. Chemical Compounds for Energy Storage. *Chemie Ingenieur Technik*, **83**:1984–1993, 2011.

[6]   G. W. Crabtree, M. S. Dresselhaus, and M. V. Buchanan. The hydrogen economy. *Physics Today*, **57**:39–44, 2004.

[7]   H. T. Hwang and A. Varma. Hydrogen storage for fuel cell vehicles. *Current Opinion in Chemical Engineering*, **5**:42–48, 2014.

[8]   B. Sakintuna, F. Lamari-Darkrim, and M. Hirscher. Metal hydride materials for solid hydrogen storage: A review. *International Journal of Hydrogen Energy*, **32**:1121–1140, 2007.

[9]   L. Murray, M. Dincă, and J. Long. Hydrogen storage in metal–organic frameworks. *Chemical Society Reviews*, **38**:1294–1314, 2009.

[10] S.-I. Orimo, Y. Nakamori, J. R. Eliseo, A. Züttel, and C. M. Jensen. Complex hydrides for hydrogen storage. *Chemical reviews*, **107**:4111–32, 2007.

[11] V. Smil. Detonator of the population explosion. *Nature*, **400**:415, 1999.

[12] R. Schlögl. Catalytic synthesis of ammonia-a "never-ending story"? *Angewandte Chemie (International ed. in English)*, **42**:2004–8, 2003.

[13] M. Kitano, Y. Inoue, Y. Yamazaki, F. Hayashi, S. Kanbara, S. Matsuishi, T. Yokoyama, S.-W. Kim, M. Hara, and H. Hosono. Ammonia synthesis using a stable electride as an electron donor and reversible hydrogen store. *Nature chemistry*, **4**:934–40, 2012.

[14] T. Vegge, R. Z. Sørensen, A. Klerke, J. S. Hummelshøj, T. Johannessen, J. K. Nørskov, and C. H. Christensen. *Indirect hydrogen storage in metal ammines*, pages 533–568. British Welding Research Association, 2008.

[15] G. Thomas and G. Parks. *Potential roles of ammonia in a hydrogen economy.* U.S. Department of Energy (DOE), 2006.

[16] C. H. Christensen, R. Z. Sørensen, T. Johannessen, U. J. Quaade, K. Honkala, T. D. Elmøe, R. Køhler, and J. K. Nørskov. Metal ammine complexes for hydrogen storage. *Journal of Materials Chemistry*, **15**:4106–4108, 2005.

[17] C. H. Christensen, T. Johannessen, R. Z. Sørensen, and J. K. Nørskov. Towards an ammonia-mediated hydrogen economy? *Catalysis Today*, **111**:140–144, 2006.

[18] A. Klerke, C. H. Christensen, J. K. Nørskov, and T. Vegge. Ammonia for hydrogen storage: challenges and opportunities. *Journal of Materials Chemistry*, **18**:2304–2310, 2008.

[19] R. Z. Sørensen, J. S. Hummelshøj, A. Klerke, J. B. Reves, T. Vegge, J. K. Nørskov, and C. H. Christensen. Indirect, reversible high-density hydrogen storage in compact metal ammine salts. *Journal of the American Chemical Society*, **130**:8660–8, 2008.

[20] D. Chakraborty, H. N. Petersen, C. Elkjær, A. Cagulada, and T. Johannessen. Solid ammonia as energy carrier: Current status and future prospects. *Fuel Cells Bulletin*, **2009**:12–15, 2009.

[21] R. Lan, J. T. Irvine, and S. Tao. Ammonia and related chemicals as potential indirect hydrogen storage materials. *International Journal of Hydrogen Energy*, **37**:1482–1494, 2012.

[22] F. Schüth, R. Palkovits, R. Schlögl, and D. S. Su. Ammonia as a possible element in an energy infrastructure: catalysts for ammonia decomposition. *Energy & Environmental Science*, **5**:6278–6289, 2012.

[23] R. Lan and S. Tao. Ammonia as a Suitable Fuel for Fuel Cells. *Frontiers in Energy Research*, **2**:3–6, 2014.

[24] W. Biltz. Beiträge zur systematischen Verwandtschaftslehre XXIV. Über das Vermögen kristallisierter Salze, Ammoniak zu binden. *Zeitschrift für anorganische und allgemeine Chemie*, **130**:93–139, 1923.

[25] E. Lepinasse and B. Spinner. Production de froid par couplage de réacteurs solide-gaz I: Analyse des performances de tels systèmes. *International Journal of Refrigeration*, **17**:309–322, 1994.

[26] C. Zamfirescu and I. Dincer. Ammonia as a green fuel and hydrogen source for vehicular applications. *Fuel Processing Technology*, **90**:729–737, 2009.

[27] G. Fournier, I. Cumming, and K. Hellgardt. High performance direct ammonia solid oxide fuel cell. *Journal of Power Sources*, **162**:198–206, 2006.

[28] W. I. F. David, J. W. Makepeace, S. K. Callear, H. M. a. Hunter, J. D. Taylor, T. J. Wood, and M. O. Jones. Hydrogen production from ammonia using sodium amide. *Journal of the American Chemical Society*, **136**:13082–5, 2014.

[29] Y. Wang, K. S. Chen, J. Mishler, S. C. Cho, and X. C. Adroher. A review of polymer electrolyte membrane fuel cells: Technology, applications, and needs on fundamental research. *Applied Energy*, **88**:981–1007, 2011.

[30] B. McNicol, D. Rand, and K. Williams. Fuel cells for road transportation purposes—yes or no? *Journal of Power Sources*, **100**:47–59, 2001.

[31] Q. Li, R. He, J. O. Jensen, and N. J. Bjerrum. Approaches and Recent Development of Polymer Electrolyte Membranes for Fuel Cells Operating above 100 °C. *Chemistry of Materials*, **15**:4896–4915, 2003.

[32] N. Rajalakshmi, T. Jayanth, and K. Dhathathreyan. Effect of Carbon Dioxide and Ammonia on Polymer Electrolyte Membrane Fuel Cell Stack Performance. *Fuel Cells*, **3**:177–180, 2003.

[33] R. Halseid, P. J. Vie, and R. Tunold. Effect of ammonia on the performance of polymer electrolyte membrane fuel cells. *Journal of Power Sources*, **154**:343–350, 2006.

[34] Chemicool Periodic Table, http://chemicool.com, 2013.

[35] G. Jóhannesson, T. Bligaard, A. Ruban, H. Skriver, K. Jacobsen, and J. Nørskov. Combined Electronic Structure and Evolutionary Search Approach to Materials Design. *Physical Review Letters*, **88**:255506, 2002.

[36] T. Bligaard, G. H. Jóhannesson, A. V. Ruban, H. L. Skriver, K. W. Jacobsen, and J. K. Nørskov. Pareto-optimal alloys. *Applied Physics Letters*, **83**:4527–4529, 2003.

[37] T. Bligaard and M. Andersson. Electronic-structure-based design of ordered alloys. *MRS Bulletin*, **31**:986–990, 2006.

[38] M. Andersson, T. Bligaard, A. Kustov, K. Larsen, J. Greeley, T. Johannessen, C. Christensen, and J. Norskov. Toward computational screening in heterogeneous catalysis: Pareto-optimal methanation catalysts. *Journal of Catalysis*, **239**:501–506, 2006.

[39] P. Haas, F. Tran, and P. Blaha. Calculation of the lattice constant of solids with semilocal functionals. *Physical Review B*, **79**:085104–1–10, 2009.

[40] C. J. Cramer and D. G. Truhlar. Density functional theory for transition metals and transition metal chemistry. *Physical Chemistry Chemical Physics*, **11**:10757–816, 2009.

[41] J. Klimeš, D. Bowler, and A. Michaelides. Van der Waals density functionals applied to solids. *Physical Review B*, **83**:1–13, 2011.

[42] A. J. Cohen, P. Mori-Sánchez, and W. Yang. Challenges for density functional theory. *Chemical reviews*, **112**:289–320, 2012.

[43] K. Burke. Perspective on density functional theory. *The Journal of chemical physics*, **136**:150901, 2012.

[44] E. Skúlason, T. Bligaard, S. Gudmundsdóttir, F. Studt, J. Rossmeisl, F. Abild-Pedersen, T. Vegge, H. Jónsson, and J. K. Nørskov. A theoretical evaluation of possible transition metal electro-catalysts for N2 reduction. *Physical chemistry chemical physics : PCCP*, **14**:1235–45, 2012.

[45] J. G. Howalt, T. Bligaard, J. Rossmeisl, and T. Vegge. DFT based study of transition metal nano-clusters for electrochemical NH3 production. *Physical chemistry chemical physics : PCCP*, **15**:7785–95, 2013.

[46] Z. Zeng, F. Calle-Vallejo, M. B. Mogensen, and J. Rossmeisl. Generalized trends in the formation energies of perovskite oxides. *Physical chemistry chemical physics : PCCP*, **15**:7526–33, 2013.

[47] J. K. Nørskov and T. Bligaard. The catalyst genome. *Angew. Chem. Int. Ed.*, **52**:776–7, 2013.

[48] S. Curtarolo, G. L. W. Hart, M. B. Nardelli, N. Mingo, S. Sanvito, and O. Levy. The high-throughput highway to computational materials design. *Nature materials*, **12**:191–201, 2013.

[49] J. Neugebauer and T. Hickel. Density functional theory in materials science. *Wiley interdisciplinary reviews. Computational molecular science*, **3**:438–448, 2013.

[50] P. J. Hasnip, K. Refson, M. I. J. Probert, J. R. Yates, S. J. Clark, and C. J. Pickard. Density functional theory in the solid state. *Philosophical transactions. Series A, Mathematical, physical, and engineering sciences*, **372**:20130270, 2014.

[51] K. Lejaeghere, V. Van Speybroeck, G. Van Oost, and S. Cottenier. Error Estimates for Solid-State Density-Functional Theory Predictions: An Overview by Means of the Ground-State Elemental Crystals. *Critical Reviews in Solid State and Materials Sciences*, **39**:1–24, 2014.

[52] A. Verdaguer-Casadevall, D. Deiana, M. Karamad, S. Siahrostami, P. Malacrida, T. W. Hansen, J. Rossmeisl, I. Chorkendorff, and I. E. L. Stephens. Trends in the electrochemical synthesis of H2O2: enhancing activity and selectivity by electrocatalytic site engineering. *Nano letters*, **14**:1603–8, 2014.

[53] E. Schrödinger. An Undulatory Theory of the Mechanics of Atoms and Molecules. *Physical Review*, **28**:1049–1070, 1926.

[54] M. Born and R. Oppenheimer. Zur Quantentheorie der Molekeln. *Annalen der Physik*, **389**:457–484, 1927.

[55] P. Hohenberg and W. Kohn. Inhomogeneous Electron Gas. *Physical Review*, **136**:B864–B871, 1964.

[56] W. Kohn and L. J. Sham. Self-Consistent Equations Including Exchange and Correlation Effects. *Physical Review*, **140**:A1133–A1138, 1965.

[57] R. Jones and O. Gunnarsson. The density functional formalism, its applications and prospects. *Reviews of Modern Physics*, **61**:689–746, 1989.

[58] J. P. Perdew, K. Burke, and M. Ernzerhof. Generalized Gradient Approximation Made Simple. *Physical Review Letters*, **77**:3865–3868, 1996.

[59] T. Björkman, A. Gulans, A. V. Krasheninnikov, and R. M. Nieminen. Are we van der Waals ready? *Journal of physics. Condensed matter : an Institute of Physics journal*, **24**:424218, 2012.

[60] J. Klimeš and A. Michaelides. Perspective: Advances and challenges in treating van der Waals dispersion forces in density functional theory. *The Journal of chemical physics*, **137**:120901, 2012.

[61] M. Dion, H. Rydberg, E. Schröder, D. C. Langreth, and B. I. Lundqvist. Van der Waals Density Functional for General Geometries. *Physical Review Letters*, **92**:246401, 2004.

[62] Y. Zhang and W. Yang. Comment on "Generalized Gradient Approximation Made Simple". *Physical Review Letters*, **80**:890, 1998.

[63] S. Lysgaard, A. L. Ammitzbøll, R. E. Johnsen, P. Norby, U. J. Quaade, and T. Vegge. Resolving the stability and structure of strontium chloride amines from equilibrium pressures, XRD and DFT. *International Journal of Hydrogen Energy*, **37**:18927–18936, 2012.

[64] A. L. Ammitzbøll, S. Lysgaard, A. Klukowska, T. Vegge, and U. J. Quaade. Surface adsorption in strontium chloride ammines. *The Journal of chemical physics*, **138**:164701, 2013.

[65] J. Wellendorff, K. T. Lundgaard, A. Møgelhøj, V. Petzold, D. D. Landis, J. K. Nørskov, T. Bligaard, and K. W. Jacobsen. Density functionals for surface science: Exchange-correlation model development with Bayesian error estimation. *Physical Review B*, **85**:235149, 2012.

[66] Y. Zhao and D. G. Truhlar. A new local density functional for main-group thermochemistry, transition metal bonding, thermochemical kinetics, and noncovalent interactions. *The Journal of chemical physics*, **125**:194101, 2006.

[67] J. Wellendorff, K. T. Lundgaard, K. W. Jacobsen, and T. Bligaard. mBEEF: an accurate semi-local Bayesian error estimation density functional. *The Journal of chemical physics*, **140**:144107, 2014.

[68] F. Furche. Molecular tests of the random phase approximation to the exchange-correlation energy functional. *Physical Review B*, **64**:195120, 2001.

[69] J. G. Ángyán, R.-F. Liu, J. Toulouse, and G. Jansen. Correlation Energy Expressions from the Adiabatic-Connection Fluctuation–Dissipation Theorem Approach. *Journal of Chemical Theory and Computation*, **7**:3116–3130, 2011.

[70] S. Bahn and K. Jacobsen. An object-oriented scripting interface to a legacy electronic structure code. *Computing in Science & Engineering*, **4**:56–66, 2002.

[71] J. J. Mortensen, L. B. Hansen, and K. W. Jacobsen. Real-space grid implementation of the projector augmented wave method. *Physical Review B*, **71**:035109, 2005.

[72] J. Enkovaara, C. Rostgaard, J. J. Mortensen, J. Chen, M. Dułak, L. Ferrighi, J. Gavnholt, C. Glinsvad, V. Haikola, H. A. Hansen, H. H. Kristoffersen, M. Kuisma, A. H. Larsen, L. Lehtovaara, M. Ljungberg, O. Lopez-Acevedo, P. G. Moses, J. Ojanen, T. Olsen, V. Petzold, N. A. Romero, J. Stausholm-Møller, M. Strange, G. A. Tritsaris, M. Vanin, M. Walter, B. Hammer, H. Häkkinen, G. K. H. Madsen, R. M. Nieminen, J. K. Nørskov, M. Puska, T. T. Rantala, J. Schiøtz, K. S. Thygesen, and K. W. Jacobsen. Electronic structure calculations with GPAW: a real-space implementation of the projector augmented-wave method. *Journal of physics. Condensed matter : an Institute of Physics journal*, **22**:253202, 2010.

[73] P. E. Blöchl. Projector augmented-wave method. *Physical Review B*, **50**:17953–17979, 1994.

[74] H. J. Monkhorst and J. D. Pack. Special points for Brillouin-zone integrations. *Physical Review B*, **13**:5188–5192, 1976.

[75] P. Maragakis, S. A. Andreev, Y. Brumer, D. R. Reichman, and E. Kaxiras. Adaptive nudged elastic band approach for transition state calculation. *The Journal of Chemical Physics*, **117**:4651–4658, 2002.

[76] C. J. Cramer. *Essentials of Computational Chemistry*. Wiley, 2nd edition, 2004.

[77] F. Jensen. *Introduction to Computational Chemistry*. Wiley, 2nd edition, 2007.

[78] S. Heiles and R. L. Johnston. Global optimization of clusters using electronic structure methods. *International Journal of Quantum Chemistry*, **113**:2091–2109, 2013.

[79] E. A. Carter. Challenges in modeling materials properties without experimental input. *Science*, **321**:800–3, 2008.

[80] S.-C. Chung and H. Morioka. Thermochemistry and crystal structures of lithium, sodium and potassium alanates as determined by ab initio simulations. *Journal of Alloys and Compounds*, **372**:92–96, 2004.

[81] J. Voss, J. S. Hummelshøj, Z. Lodziana, and T. Vegge. Structural stability and decomposition of Mg(BH(4))(2) isomorphs-an ab initio free energy study. *Journal of physics. Condensed matter : an Institute of Physics journal*, **21**:012203, 2009.

[82] J. S. Hummelshøj, D. D. Landis, J. Voss, T. Jiang, A. Tekin, N. Bork, M. Dułak, J. J. Mortensen, L. Adamska, J. Andersin, J. D. Baran, G. D. Barmparis, F. Bell, A. L. Bezanilla, J. Bjork, M. E. Björketun, F. Bleken, F. Buchter, M. Bürkle, P. D. Burton, B. B. Buus, A. Calborean, F. Calle-Vallejo, S. Casolo, B. D. Chandler, D. H. Chi, I. Czekaj, S. Datta, A. Datye, A. DeLaRiva, V. Despoja, S. Dobrin, M. Engelund, L. Ferrighi, P. Frondelius, Q. Fu, A. Fuentes, J. Fürst, A. García-Fuente, J. Gavnholt, R. Goeke, S. Gudmundsdottir, K. D. Hammond, H. A. Hansen, D. Hibbitts, E. Hobi, J. G. Howalt, S. L. Hruby, A. Huth, L. Isaeva, J. Jelic, I. J. T. Jensen, K. A. Kacprzak, A. Kelkkanen, D. Kelsey, D. S. Kesanakurthi, J. Kleis, P. J. Klüpfel, I. Konstantinov, R. Korytar, P. Koskinen, C. Krishna, E. Kunkes, A. H. Larsen, J. M. G. Lastra, H. Lin, O. Lopez-Acevedo, M. Mantega, J. I. Martínez, I. N. Mesa, D. J. Mowbray, J. S. G. Mýrdal, Y. Natanzon, A. Nistor, T. Olsen, H. Park, L. S. Pedroza, V. Petzold, C. Plaisance, J. A. Rasmussen, H. Ren, M. Rizzi, A. S. Ronco, C. Rostgaard, S. Saadi, L. A. Salguero, E. J. G. Santos, A. L. Schoenhalz, J. Shen, M. Smedemand, O. J. Stausholm-Møller, M. Stibius, M. Strange, H. B. Su, B. Temel, A. Toftelund, V. Tripkovic, M. Vanin, V. Viswanathan, A. Vojvodic, S. Wang, J. Wellendorff, K. S. Thygesen, J. Rossmeisl, T. Bligaard, K. W. Jacobsen, J. K. Nørskov, and T. Vegge. Density functional theory based screening of ternary alkali-transition metal borohydrides: a computational material design project. *The Journal of chemical physics*, **131**:014101, 2009.

[83] A. Tekin, J. S. Hummelshøj, H. S. Jacobsen, D. Sveinbjörnsson, D. Blanchard, J. K. Nørskov, and T. Vegge. Ammonia dynamics in magnesium ammine from DFT and neutron scattering. *Energy & Environmental Science*, **3**:448–456, 2010.

[84] A. Tekin, R. Caputo, and A. Züttel. First-Principles Determination of the Ground-State Structure of LiBH_{4}. *Physical Review Letters*, **104**:215501, 2010.

[85] R. Caputo and A. Tekin. Ab-initio crystal structure prediction. A case study: NaBH4. *Journal of Solid State Chemistry*, **184**:1622–1630, 2011.

[86] X.-F. Zhou, A. Oganov, G.-R. Qian, and Q. Zhu. First-Principles Determination of the Structure of Magnesium Borohydride. *Physical Review Letters*, **109**:245503, 2012.

[87] T. Vegge, J. G. Howalt, S. Lysgaard, J. Steinar G. Mýrdal, N. Bork, and J. Strabo Hummelshøj. Computational Design of Catalysts, Electrolytes, and Materials for Energy Storage. In *New and Future Developments in Catalysis*, pages 499–521. 2013.

[88] A. J. Medford, J. Wellendorff, A. Vojvodic, F. Studt, F. Abild-Pedersen, K. W. Jacobsen, T. Bligaard, and J. K. Norskov. Assessing the reliability of calculated catalytic ammonia synthesis rates. *Science*, **345**:197–200, 2014.

[89] C. Darwin. *On the Origin of Species by Means of Natural Selection, or the Preservation of Favoured Races in the Struggle for Life.* J. Murray, 1859.

[90] J. H. Holland. *Adaptation in Natural and Artificial Systems*, volume Ann Arbor. University of Michigan Press, 1975.

[91] D. E. Goldberg. *Genetic Algorithms in Search, Optimization, and Machine Learning*. Addison-Wesley, 1989.

[92] S. Forrest. Genetic algorithms: principles of natural selection applied to computation. *Science*, **261**:872–878, 1993.

[93] F. Koskowski and B. Hartke. Towards protein folding with evolutionary techniques. *Journal of computational chemistry*, 2005.

[94] N. Abraham and M. Probert. A periodic genetic algorithm with real-space representation for crystal structure and polymorph prediction. *Physical Review B*, **73**:1–6, 2006.

[95] G. Trimarchi and A. Zunger. Global space-group optimization problem: Finding the stablest crystal structure without constraints. *Physical Review B*, **75**:1–8, 2007.

[96] A. R. Oganov, A. O. Lyakhov, and M. Valle. How evolutionary crystal structure prediction works–and why. *Accounts of chemical research*, **44**:227–237, 2011.

[97] Z. Fang, J. Lin, R. Liu, P. Liu, Y. Li, X. Huang, K. Ding, L. Ning, and Y. Zhang. Computational Design of the Inorganic Nonlinear Optical Crystals Based on the Genetic Algorithm. *CrystEngComm*, 2014.

[98] G. Trimarchi, A. Freeman, and A. Zunger. Predicting stable stoichiometries of compounds via evolutionary global space-group optimization. *Physical Review B*, **80**:092101, 2009.

[99] R. L. Johnston. Evolving better nanoparticles: Genetic algorithms for optimising cluster geometries. *Dalton Trans.*, pages 4193–4207, 2003.

[100] V. A. Froltsov and K. Reuter. Robustness of 'cut and splice' genetic algorithms in the structural optimization of atomic clusters. *Chemical Physics Letters*, **473**:363–366, 2009.

[101] S. Lysgaard, D. D. Landis, T. Bligaard, and T. Vegge. Genetic Algorithm Procreation Operators for Alloy Nanoparticle Catalysts. *Topics in Catalysis*, **57**:33–39, 2014.

[102] P. Jennings and R. Johnston. Structures of small Ti- and V-doped Pt clusters: A GA-DFT study. *Computational and Theoretical Chemistry*, **1021**:91–100, 2013.

[103] S. Q. Wu, M. Ji, C. Z. Wang, M. C. Nguyen, X. Zhao, K. Umemoto, R. M. Wentzcovitch, and K. M. Ho. An adaptive genetic algorithm for crystal structure prediction. *Journal of physics. Condensed matter : an Institute of Physics journal*, **26**:035402, 2014.

[104] L. Vilhelmsen and B. Hammer. Systematic Study of Au_{6} to Au_{12} Gold Clusters on MgO(100) F Centers Using Density-Functional Theory. *Physical Review Letters*, **108**:1–5, 2012.

78

[105] L. B. Vilhelmsen and B. Hammer. Interfacial oxygen under TiO2 supported Au clusters revealed by a genetic algorithm search. *The Journal of chemical physics*, **139**:204701, 2013.

[106] D. Teng, L. B. Vilhelmsen, and D. S. Sholl. Investigating energetics of Au8 on graphene/Ru(0001) using a genetic algorithm and density functional theory. *Surface Science*, **628**:98–103, 2014.

[107] L. B. Vilhelmsen and B. Hammer. Identification of the Catalytic Site at the Interface Perimeter of Au Clusters on Rutile TiO 2 (110). *ACS Catalysis*, **4**:1626–1631, 2014.

[108] L. B. Vilhelmsen and B. Hammer. A genetic algorithm for first principles global structure optimization of supported nano structures. *The Journal of chemical physics*, **141**:044711, 2014.

[109] C. J. Heard, S. Heiles, S. Vajda, and R. L. Johnston. PdnAg(4-n) and PdnPt(4-n) clusters on MgO (100): a density functional surface genetic algorithm investigation. *Nanoscale*, **6**:11777–88, 2014.

[110] L. B. Vilhelmsen and D. S. Sholl. Thermodynamics of Pore Filling Metal Clusters in Metal Organic Frameworks: Pd in UiO-66. *The Journal of Physical Chemistry Letters*, **3**:3702–3706, 2012.

[111] L. B. Vilhelmsen, K. S. Walton, and D. S. Sholl. Structure and mobility of metal clusters in MOFs: Au, Pd, and AuPd clusters in MOF-74. *Journal of the American Chemical Society*, **134**:12807–16, 2012.

[112] S. Goedecker. Minima hopping: an efficient search method for the global minimum of the potential energy surface of complex molecular systems. *The Journal of chemical physics*, **120**:9911–7, 2004.

[113] S. Lysgaard. *Computational analysis of gas-solid interactions in materials for energy storage and conversion.* PhD thesis, Technical university of Denmark, 2012.

[114] P.-C. Chang and S.-H. Chen. The development of a sub-population genetic algorithm II (SPGA II) for multi-objective combinatorial problems. *Applied Soft Computing*, **9**:173–181, 2009.

[115] T. Hiroyasu, M. Miki, and S. Watanabe. The new model of parallel genetic algorithm in multi-objective optimization problems - divided range multi-objective genetic algorithm. In *Proceedings of the 2000 Congress on Evolutionary Computation. CEC00 (Cat. No.00TH8512)*, volume 1, pages 333–340. IEEE, 2000.

[116] J. Alander. On optimal population size of genetic algorithms. In *Proceedings Computer Systems and Software Engineering*, pages 65–70. IEEE Comput. Soc. Press, 1992.

[117] D. D. Landis, J. S. Hummelshoj, S. Nestorov, J. Greeley, M. Dulak, T. Bligaard, J. K. Norskov, and K. W. Jacobsen. The Computational Materials Repository. *Computing in Science & Engineering*, **14**:51–57, 2012.

[118] A. Werner. Nobel Lecture: On the constitution and configuration of higher-order compounds, 1913.

[119] R. Shannon. Revised effective ionic radii and systematic studies of interatomic distances in halides and chalcogenides. *Acta Crystallographica Section A*, **32**:751–767, 1976.

[120] S. Westman, P. Werner, and T. Schuler. X-ray investigation of ammines of alkaline earth metals halides. I. The structures of CaCl2 (NH3) 8, CaCl2 (NH3) 2 and the decomposition product CaClOH. *Acta Chem. Scand. A*, **35**:467–472, 1981.

[121] A. Bialy, P. B. Jensen, D. Blanchard, T. Vegge, and U. J. Quaade. Solid solution barium–strontium chlorides with tunable ammonia desorption properties and superior storage capacity. *Journal of Solid State Chemistry*, **221**:32–36, 2015.

[122] I. Olovsson. Packing principles in the structures of metal ammine salts. *Acta Crystallographica*, **18**:889–893, 1965.

[123] R. Essmann, G. Kreiner, A. Niemann, D. Rechenbach, A. Schmieding, T. Sichla, U. Zachwieja, and H. Jacobs. Isotype Strukturen einiger Hexaamminmetall(II)-halogenide von 3d-Metallen: [V(NH3)6]I2, [Cr(NH3)6]I2, [Mn(NH3)6]Cl2, [Fe(NH3)6]Cl2, [Fe(NH3)6]Br2, [Co(NH3)6]Br2 und [Ni(NH3)6]Cl2. *Zeitschrift für anorganische und allgemeine Chemie*, **622**:1161–1166, 1996.

[124] M. O. Jones, D. M. Royse, P. P. Edwards, and W. I. David. The structure and desorption properties of the ammines of the group II halides. *Chemical Physics*, **427**:38–43, 2013.

[125] C. Y. Liu and K.-i. Aika. Ammonia Absorption on Alkaline Earth Halides as Ammonia Separation and Storage Procedure. *Bulletin of the Chemical Society of Japan*, **77**:123–131, 2004.

[126] N. A. Zarkevich, E. H. Majzoub, and D. D. Johnson. Anisotropic thermal expansion in molecular solids: Theory and experiment on LiBH4. *Physical Review B*, **89**:134308, 2014.

[127] C. Y. Liu and K. Aika. Ammonia Absorption into Alkaline Earth Metal Halide Mixtures as an Ammonia Storage Material. *Industrial & Engineering Chemistry Research*, **43**:7484–7491, 2004.

[128] C. Y. Liu and K. Aika. Effect of the Cl/Br molar ratio of a CaCl2-CaBr2 mixture used as an ammonia storage material. *Industrial & Engineering Chemistry Research*, **3**:6994–7000, 2004.

[129] M. Llugany, C. Poschenrieder, and J. Barceló. Assessment of barium toxicity in bush beans. *Archives of environmental contamination and toxicology*, **39**:440–4, 2000.

[130] G. Brauer and O. Müller. Zur kristallchemie des strontiumchlorids. *Zeitschrift für anorganische und allgemeine Chemie*, **295**:218–226, 1958.

[131] S. Hull, S. T. Norberg, I. Ahmed, S. G. Eriksson, and C. E. Mohn. High temperature crystal structures and superionic properties of SrCl2, SrBr2, BaCl2 and BaBr2. *Journal of Solid State Chemistry*, **184**:2925–2935, 2011.

[132] L. H. Brixner. Orthorhombic srcl2. *Mat. Res. Bull.*, **11**:1453–1456, 1976.

[133] A. Haase and G. Brauer. Hydratstufen und Kristallstrukturen von Bariumchlorid. *Zeitschrift für anorganische und allgemeine Chemie*, **195**:181–195, 1978.

[134] B. Frit, M. Moakil-Chbany, and P. Hagenmuller. Étude isotherme des systèmes pseudo-quaternaires BaCl2-BaBr2-SrCl2-SrBr2 et BaBr2-BaI2-SrBr2-SrI2. *C. R. Acad. Sc. Paris*, **267**:1046–1049, 1968.

[135] C. Kieler. *Synthesis and characterization of mixed metal chloride amines for ammonia storage.* Bachelor thesis, Technical University of Denmark, 2014.

[136] J. S. Hummelshøj. *Computational investigation and design of coordination compounds for hydrogen storage.* PhD thesis, Technical University of Denmark, 2009.

[137] L. Schimka, R. Gaudoin, J. Klimeš, M. Marsman, and G. Kresse. Lattice constants and cohesive energies of alkali, alkaline-earth, and transition metals: Random phase approximation and density functional theory results. *Physical Review B*, **87**:214102, 2013.

[138] C. E. Housecroft and A. G. Sharpe. *Inorganic Chemistry.* Pearson, 2nd edition, 2005.

[139] W. C. Schumb and R. F. Sundström. Ammines of the Lower Chlorides of Titanium. *Journal of the American Chemical Society*, **55**:596–604, 1933.

[140] A. Fuwa and S. Takaya. Producing titanium by reducing TiCl2-MgCl2 mixed salt with magnesium in the molten state. *JOM*, pages 56–60, 2005.

[141] G. Meyer, T. Gloger, and J. Beekhuizen. Halides of Titanium in Lower Oxidation States. *Zeitschrift für anorganische und allgemeine Chemie*, **635**:1497–1509, 2009.

[142] O. Ruff and F. Neumann. Reduktion anorganischer Halogenide II. Die Reduktion des Titantetrachlorids. *Zeitschrift für anorganische und allgemeine Chemie*, **128**:81–95, 1923.

[143] R. M. Keefer and L. J. Andrews. The Solubility of Cuprous Chloride in Aqueous Alcohol Solutions. *Journal of the American Chemical Society*, **71**:1723–1724, 1949.

Paper I

**Temperature- and Pressure-Induced Changes in the Crystal Structure of Sr(NH$_3$)$_8$Cl$_2$**

Rune E. Johnsen, Peter Bjerre Jensen, Poul Norby and Tejs Vegge

Temperature- and Pressure-Induced Changes in the Crystal Structure of Sr(NH₃)₈Cl₂

Rune E. Johnsen,[†] Peter B. Jensen,[†,‡] Poul Norby,[†] and Tejs Vegge*,[†]

[†]Department of Energy Conversion and Storage, Technical University of Denmark, Frederiksborgvej 399, P.O. Box 49, Roskilde, DK-4000, Denmark

[‡]Center for Atomic-scale Materials Design, Technical University of Denmark, Fysikvej 311, DK-2800 Kongens Lyngby, Denmark

🅢 Supporting Information

ABSTRACT: The structural transformations occurring in the crystal structure of strontium chloride octamine, Sr(NH₃)₈Cl₂, as a function of temperature and pressure of ammonia gas were studied by detailed in situ X-ray powder diffraction (XRPD) and supported by density functional theory (DFT) calculations. Rietveld refinements were used to study the crystal structure of Sr(NH₃)₈Cl₂ in details, and the potential presence of super symmetry is discussed. The Rietveld refinements show that the interatomic distance from the strontium ion to one of the ammonia molecules (Sr−N1) increases from 2.950(7) Å at 275 K to 3.50(6) Å at 322 K at P(NH₃) = 2.0 bar. DFT calculations show that only half the energy is required to elongate the Sr−N1 bond from its equilibrium distance compared to the standard Sr−N bonds. The in situ XRPD data show that the *a* parameter of the unit cell increases relatively more than the *b* and *c* parameters during the heating, which is correlated to the crystallographic transformation. The in situ XRPD data show that increasing the heating rate pushes the structural transformation in the crystal structure to higher temperatures by a few kelvin. The in situ XRPD data show that the Sr(NH₃)₈Cl₂ → Sr(NH₃)₂Cl₂ + 6NH₃(g) reaction has the lowest transformation temperature for all the studied ammonia pressures. The Sr(NH₃)₈Cl₂ → Sr(NH₃)Cl₂ + 7NH₃(g) reaction also plays a significant role at lower ammonia pressure. For the absorption of ammonia, Sr(NH₃)Cl₂ + 7NH₃(g) → Sr(NH₃)₈Cl₂ was the only observed reaction.
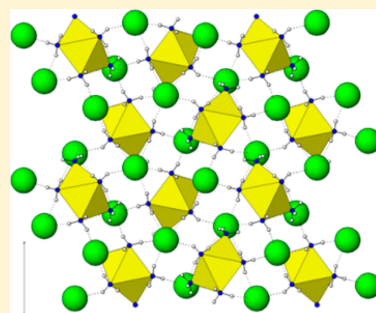
1. INTRODUCTION

Metal halides are highly applicable materials for absorption and storage of ammonia.[1] The theoretical volumetric ammonia densities of some of the metal halides are comparable to that of liquid ammonia, and the solid storage of ammonia in metal halides alleviates the problems of handling the liquid ammonia.[2−4] Thus, absorbing ammonia in metal halides may be a safe and inexpensive method for ammonia storage. Ammonia storage for fuel cells and selective catalytic reduction (SCR) of NO$_x$ gases from combustion processes are among the applications of the materials.[5−7] The metal halide amines may also be used for ammonia separation and thermochemical heat pumps.[8−10] The metal halide salts form various complexes with ammonia with different binding energies and ammonia capacities.[1,11] Mg(NH₃)₆Cl₂ is one of the most studied members of the metal-halide amine family due to its high theoretical volumetric and gravimetric ammonia and hydrogen capacity.[12−18] However, the binding energies are relatively high. Thus, high temperatures are needed to release the first four ammonia molecules (around 445 K with a heating rate of 1 K·min⁻¹), and even higher to release the last two (around 580 and 675 K, respectively).[17] Both SrCl₂ and CaCl₂ can absorb not only six but eight ammonia molecules per formula unit, which gives theoretical volumetric ammonia densities of 642 kg(NH₃)·m⁻³ and 678 kg(NH₃)·m⁻³ for the dense materials at room temperature, respectively, whereas the volumetric ammonia density of liquid ammonia at room temperature is 609 kg(NH₃)·m⁻³. However, one of the eight ammonia molecules in Sr(NH₃)₈Cl₂ is strongly bonded and therefore too energetically expensive to desorb for many practical applications. Thus, the accessible volumetric ammonia density of the Sr(NH₃)₈Cl₂ is only 562 kg(NH₃)·m⁻³. For Ca(NH₃)₈Cl₂, two of the eight ammonia molecules are bonded strongly, giving an accessible volumetric ammonia density of 509 kg(NH₃)·m⁻³. Among others, due to these reasons SrCl₂ is used commercially for SCR of NO$_x$ gases in vehicular exhaust.[19] The stable amines of SrCl₂ are the monoamine phase Sr(NH₃)Cl₂, the diamine phase Sr(NH₃)₂Cl₂, and the octamine Sr(NH₃)₈Cl₂ phase. The octamine phase displays different desorption steps dependent on the temperature and partial pressure of ammonia.[20,21] At some temperatures and ammonia pressures, the diamine phase is found to have marginally higher stability than the monoamine phase and vice versa at others.[22]

In the present study, we focus on the structural transformation occurring in the strontium chloride octamine phase before the initial release of ammonia molecules begins when the
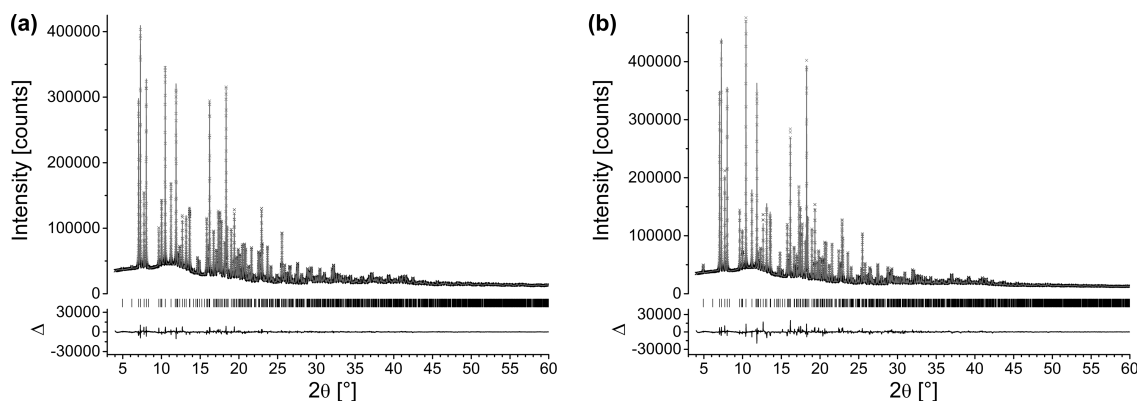
Figure 1. Rietveld refinement plots of strontium chloride octamine at (a) 275 K and (b) 322 K showing the experimental (black crosses), calculated (solid gray line) and difference (solid black line) XRPD patterns. The vertical black bars show the position of the Bragg reflections of the octamine phase.

material is being heated with different heating rates at different ammonia pressures. In situ X-ray powder diffraction (XRPD) has been used to study the transformations in the crystal structure of the $Sr(NH_3)_8Cl_2$ phase. Rietveld refinements based on the XRPD data have provided valuable information about among other things significant temperature-induced changes in the bonding distances between the strontium ions and ammonia molecules. Density functional theory (DFT) calculations have given information about the energy required to change the Sr–N bond lengths.

2. EXPERIMENTAL DETAILS

2.1. In Situ X-ray Powder Diffraction. In situ XRPD was used to study the structural changes in $Sr(NH_3)_8Cl_2$ as a function of temperature and ammonia pressure. The XRPD experiments were performed at beamline I11 at Diamond Light Source in Didcot, United Kingdom. The powder diffraction data were collected using a position sensitive MYTHEN2 microstrip detector from DECTRIS Ltd., focusing optics, a wavelength of 0.827132(2) Å, and a slit size of 0.7 × 2.5 mm. Approximately 6 mm of sample material was placed in the tip of a 0.5 mm quartz glass capillary. Approximately 10 mm of quartz glass wool was placed next to the sample to ensure that the sample was kept in place when vacuum was applied to the capillary. The capillary was mounted in a modified Swagelok fitting, which was connected via tubing to a gas control system. The system allowed the sample cell to be evacuated before a given pressure of ammonia gas was applied to the sample. The actual pressure of the ammonia gas was measured using a pressure transducer. The temperature of the sample was controlled by a Cryostream Plus from Oxford Cryosystems Ltd. The sample material was initially activated by heating the sample to approximately 430 K with a heating rate of 360 K·h^{-1} under an active vacuum in order to ensure the removal of all the water and ammonia present in the sample material and from the tubings before a given pressure of ammonia gas (grade 4.8) was applied to the sample. XRPD patterns of the fully loaded strontium chloride octamine were then acquired during heating and cooling at different pressures. The MYTHEN2 microstrip detector is build-up by a sequence of individual modules separated by approximately 0.2° 2θ. Thus, in order to overcome the gaps in the diffraction patters, each diffraction

pattern is a linear combination of two individual patterns separated by approximately 0.25° 2θ.

2.1.1. Data Analysis. Rietveld refinements were performed based on the acquired in situ data using TOPAS Academic 4.1 (Coelho Software, Brisbane, Australia; http://www.topas-academic.net/). The structure of the octamine phases reported by Westman et al.[23] and Lysgaard et al.[22] in space group *Pnma* was used as the starting point for the Rietveld refinements; a potential different symmetry of the strontium chloride octamine will be discussed later. A split pseudo-Voigt profile function with two half-width parameters and two peak-shape parameters, combined with six *hkl*-dependent Lorentzen parameters, was used for the refinements in a 2θ range of 4–60°. The patterns were corrected for the Lorentz-polarization factor and cylinder absorption for a parallel beam. A total of 24 Chebyshev background parameters were used to describe the background of the XRPD patterns. The scale factor, the 2θ-zero point, and the unit-cell parameters (*a*, *b*, and *c* axes) were refined for the octamine phase. The ammonia molecules were refined as rigid-bodies with fixed N–H bond distances of 1.017 Å and fixed H–N–H bond angles of 107.8°, with the hydrogen atoms pointing away from the coordinating strontium atom. Two of the five ammonia sites are disordered and only half occupied. The atomic coordinates of the ammonia molecules were refined along with the *x* og *z* coordinates of the Sr site and the two Cl sites. All isotropic displacement parameters (b_{iso} factors) were refined, although the ones of the hydrogen atoms were set to be 1.2 times the isotropic displacement parameter of the corresponding nitrogen atoms.

2.2. Computational Methods. The structure of the octamine was studied with DFT in the generalized gradient approximation (GGA),[24,25] using the vdW-DF functional,[26] which ensures accurate description of the hydrogen bonding, observed in the octamine. The calculations were performed using a real-space grid implementation of the projector augmented wave method, GPAW,[27] executed via the atomic simulation environment (ASE).[28] A Monkhorst–Pack grid[29] with approximately 25 *k*-points per Å^{-1} and a 0.18 Å grid spacing was used, and the structure was relaxed using a quasi-Newton optimization algorithm,[30] until the forces were less than 0.05 eV·Å^{-1}. When studying the energy required to displace an ammonia molecule, the rest of the structure was kept fixed, at the values obtained from the initial full
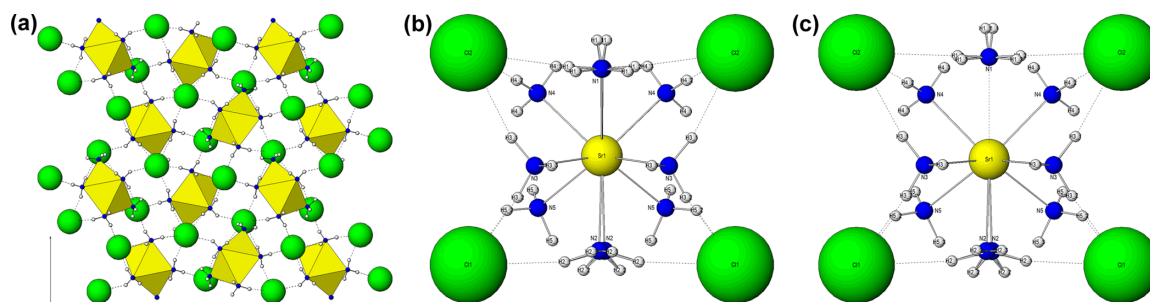
Figure 2. (a) The crystal structure of the strontium chloride octamine at 275 K viewed along the b axis. Sr atoms are located in the center of yellow double capped trigonal prisms or distorted tetragonal antiprisms, Cl atoms depicted as green, N atoms are blue and H atoms are white. The local structure around the Sr atoms at (b) 275 K and (c) 322 K.

optimization of the structure where both the lattice parameters and atomic positions have been optimized iteratively. The linear thermal expansion coefficients were obtained, by compressing and expanding the crystal structure around the minimum in each direction by ±2%, keeping the N−H distances fixed. The thermal expansion coefficients were obtained by fitting the energy versus the distortion to a third-order polynomial as described in a recent paper by Zarkevich et al.[31]

3. RESULTS AND DISCUSSION

3.1. The Crystal Structure of $Sr(NH_3)_8Cl_2$. The crystal structure of $Sr(NH_3)_8Cl_2$ was Rietveld refined in the space group $Pnma$ first reported by Westman et al., 1981,[23] for $Ca(NH_3)_8Cl_2$. Figure 1 shows the Rietveld refinement plot of the octamine at 275 and 322 K based on XRPD collected during heating with a heating rate of 100 K·h^{-1} at $P(NH_3)$ = 2.0 bar. The agreement factors of the Rietveld refinements are as follows: (a) R_p = 1.345%, R_{wp} = 1.756%, R_{exp} = 0.599%, R_B = 1.031% and GoF = 2.932; (b) R_p = 2.105%, R_{wp} = 2.929%, R_{exp} = 0.602%, R_B = 2.114%, and GoF = 4.867. Table S1 and S2 show the atomic coordinates, Wyckoff letters, occupancy factors, isotropic displacement parameters and unit-cell parameters from the Rietveld refinements of the octamine structure at 275 and 322 K, respectively.

The strontium atoms each coordinate to eight ammonia molecules with Sr−N distances in the range from 2.714(2) to 2.950(7) Å at 275 K forming isolated $[Sr(NH_3)_8]$-polyhedra shaped as distorted tetragonal antiprisms or double-capped trigonal prisms (Figure 2a,b). Panthöfer et al., 2004, reported the same shape for the $[Sr(NH_3)_8]$-polyhedra in $[Sr(NH_3)_8]_3(C_{70})_2·19NH_3$ with Sr−N distances in the range from 2.683(5) to 2.800(7) Å.[32] Seven out of the eight Sr−N distances in the $Sr(NH_3)_8Cl_2$ are in the same range [2.714(2) to 2.792(2) Å], whereas the last one is significant longer, 2.950(7) Å. Thus, the $[Sr(NH_3)_8]$-polyhedra have a more symmetric shape in $[Sr(NH_3)_8]_3(C_{70})_2·19NH_3$. The two ammonia molecules forming the caps of the trigonal prisms in $Sr(NH_3)_8Cl_2$ are disordered in the $Pnma$ space group, each with two slightly different oriented ammonia molecules at half occupied sites (Figure 2b,c). Thus, half of the hydrogen atoms (H1_2 and H2_1) of the disordered ammonia molecules have hydrogen bonds to the chloride ions along the b axis in the positive direction and half of them have hydrogen bonds to the chloride ions along the b axis in the negative direction. By lowering the symmetry of the centrosymmetric space group

$Pnma$ to the noncentrosymmetric $Pna2_1$, the number of crystallographically independent ammonia molecules increases from five to eight due to the loss of the mirror plane (the b and c axes are interchanged in the two space groups). The disordered sites of the ammonia molecules forming the caps of the trigonal prisms are thereby converted into single fully occupied sites with a given orientation of the ammonia molecules. Thus, the hydrogen bonding atom of the ammonia molecules only bonds to one of the chloride ions. The six ammonia molecules forming the trigonal prism are coupled two by two by the mirror plane in $Pnma$, whereas they are independent in $Pna2_1$. The octamine structure was attempted refined in the space group $Pna2_1$, but a strong correlation between the positions of ammonia molecules related by the mirror plane in $Pnma$ (and consequently also the Sr−N distances) was observed. The Rietveld refinement in space group $Pna2_1$ gave, besides strong correlations, only slightly (~0.03 percentage point) better agreement factors even though the number of free parameters in the refinement was increased by 17. As the only difference between the $Pnma$ and $Pna2_1$ space groups is the presence of a center of symmetry, they have the same extinction rules. Thus, they cannot be distinguished by systematic extinction of reflections, and no additional nonindexed peaks indicating super symmetry in the crystal structure were observed in the XRPD patterns. However, it is important to bear in mind that hydrogen atoms are scattering the X-ray radiation weakly. Thus, a potential additional symmetry caused by another long-range ordering of the hydrogen atoms of the ammonia molecules is not observable with X-rays. The crystal structures were therefore refined as the average structures in the $Pnma$ space group.

3.2. Structural Changes in $Sr(NH_3)_8Cl_2$ upon Isobaric Heating and Cooling. Figure 3 shows a XRPD plot of $Sr(NH_3)_8Cl_2$ during heating from 275 to 322 K with a heating rate of 100 K·h^{-1} at an ammonia pressure of 2.0 bar. The XRPD plot reveals significant changes in the relative intensities of the diffraction peaks. The intensity of the 221 reflection ($2\theta \sim 15.2°$) is for instance virtually absent at 275 K but clearly visible at 322 K, whereas the opposite is the case for the 002 ($2\theta \sim 6.2°$) and 400 ($2\theta \sim 15.5°$) reflections.

Figure 4a shows the development in the bond distances as a function of temperature during heating of the strontium chloride octamine with a heating rate of 100 K·h^{-1} at an ammonia pressure of 2.0 bar. The bond distances are calculated from the Rietveld refinements and reflect the distance from the strontium atom to the nitrogen atom of the ammonia molecule.
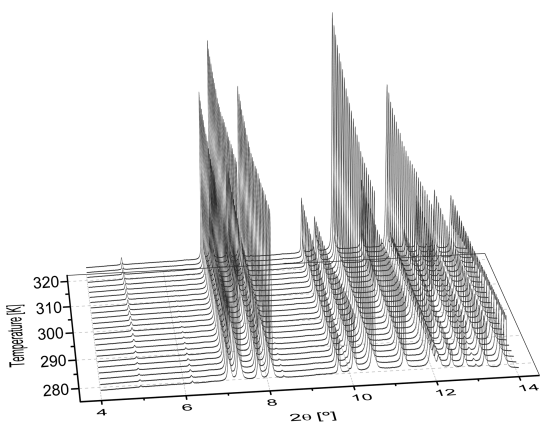
Figure 3. XRPD plot of $Sr(NH_3)_8Cl_2$ during heating with a rate of 100 $K \cdot h^{-1}$ at $P(NH_3) = 2.0$ bar.

The Sr−N2 bond distance does not change significantly during the heating from 275 to 322 K, whereas Sr−N3 increases slightly with temperature, and Sr−N4 and Sr−N5 decrease slightly with temperature. The increased estimated standard deviations of the Sr−N5 bond distance in the temperature range from approximately 296 to 312 K are notable not only for this heating ramp, but also for other isobaric heating experiments with different heating rates and at different ammonia pressures. The continuous decrease in the average Sr−N5 bond distance makes the change in the estimated standard deviations stick, but it seems to correlate somewhat with a change in the increment of the Sr−N1 bond distance. The Sr−N1 bond distance changes more significantly upon heating. It increases nearly linearly until approximately 285 K, where it starts to increase exponentially before it again displays a linear increase from approximately 297 to 322 K, where it reaches a value of to 3.50(6) Å. While the Sr−N1 bond distance increases significantly because the ammonia molecule moves into a void space of the structure at elevated temperature (Figure 2), the Cl2···H1_2 bond distance appears to be virtually unaffected by the increase in temperature (Cl2···H1_2 = 2.85(4) Å at 275 K and Cl2···H1_2 = 2.84(4) Å at 322 K).
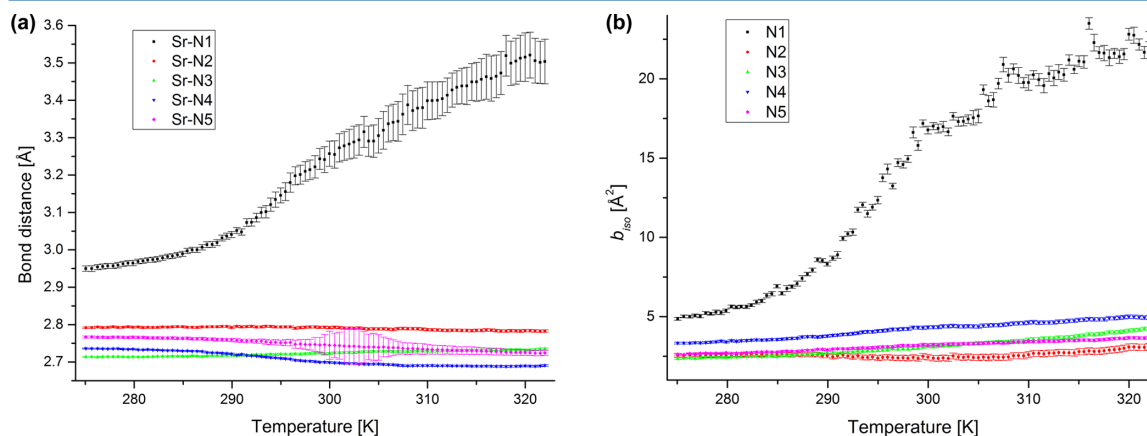
This could suggest that the hydrogen bond Cl2···H1_2 is stronger than the ion-dipole force of the Sr−N1 bond, however it is important to bear in mind that orientation of the ammonia molecules is partly restrained in the refinement (see the description of the rigid bodies in the Experimental Details section). This combined with the fact that the hydrogen atoms are weak X-ray scatterers limit the accuracy of the calculated Cl···H distances.

The isotropic displacement parameter of the N1 site (Figure 4b) also displays a significant increase as the ammonia molecule moves into the void space of the structure and consequently gets more delocalized and almost only kept in place by the hydrogen bond between the chloride ion and the hydrogen atom of ammonia molecule. The isotropic displacement parameters of the three sites forming the trigonal coordination prisms (N3, N4, and N5) are all increasing continuously with a moderate rate reflecting the effect of the temperature. The isotropic displacement parameter of the N2 site has a significantly different temperature dependency. It is nearly constant within the standard deviations and increases only slightly at elevated temperature (starting from around 310 K).

As observed in the XRPD experiment, the Sr−N1 bond is significantly longer than the other Sr−N bonds, also at 275 K. Thus, DFT calculations were used to estimate the energy potential of the different Sr−N bonds by calculating the energy required to change the Sr−N bond length from its equilibrium distance (Figure 5). The energy potential was calculated for the two Sr−N bonds (Sr−N1 and Sr−N2) forming the caps on the trigonal prism and for one of the six Sr−N bonds in the trigonal prism (Sr−NX). From the calculations it is clear that the N1 atom is more loosely bound to the Sr atom than the N2 and NX atoms, as the energy required both to compress and elongate the Sr−N1 bond is significantly lower than that for the other bonds. It only costs approximately 4.6 $kJ \cdot mol^{-1}$ to elongate the Sr−N1 distance by 0.3 Å from its ground state position. The Sr−N2 and Sr-NX bonds behave similar during compression, whereas more energy is required to elongate the Sr-NX bond than the Sr−N2 one. This difference is coupled to the local coordination environment where the N2 ammonia molecule has more open space to move around in. As mentioned, the calculations are deviations from the equilibrium bond lengths, but the three Sr−N bonds are not of equal
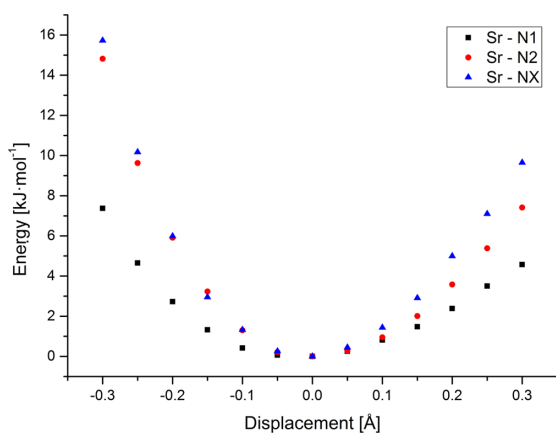

Figure 4. (a) Bond distances as a function of temperature during heating with a rate of 100 $K \cdot h^{-1}$ at $P(NH_3) = 2.0$ bar. (b) Isotropic displacement parameters of the nitrogen atoms of the five ammonia molecules during heating with a rate of 100 $K \cdot h^{-1}$ at $P(NH_3) = 2.0$ bar.

Figure 5. Calculated energy required to change the Sr−N bond length from its equilibrium distance, for three different types of ammonia molecules.

length. The Sr−N1 bond is approximately 0.2 Å longer than the other ones. Thus, the energies required to change the Sr−N bonds from their equilibrium distances are plotted also as a function of bond distance (Figure S1 in the Supporting Information). Figure S1 shows that the N1 atom requires more energy to get close to the Sr than the N2 and NX atoms do. One of the reasons for this is probably coupled to the way the energies are calculated, where all other bond distances are kept fixed. If the other ammonia molecules were allowed to move freely during the relaxation, one or more of them would probably move away from the strontium atom to compensate for the shorter Sr−N1 bond distance.

Figure 6 shows the normalized unit-cell parameters as a function of temperature during heating with a rate of 100 K·h^{-1} at an ammonia pressure of 2.0 bar. The refined unit-cell parameters are $a = 12.22187(4)$ Å, $b = 7.47501(3)$ Å, and $c = 15.34330(8)$ Å at 275 K. It is apparent from the figure that the a unit-cell parameter increases relatively more than b and c. A closer look at the temperature dependency of the a parameter
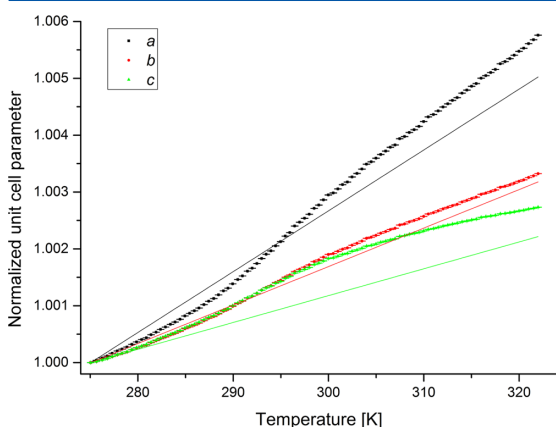

Figure 6. Normalized unit-cell parameters as a function of temperature during heating with a rate of 100 K·h^{-1} at P(NH$_3$) = 2.0 bar (scattered symbols), and the corresponding unit-cell parameters estimated from the calculated expansion coefficients (solid lines).

reveals that the curve has a similar shape as the one of the Sr−N1 bond distance. The Sr−N1 bonds are pointed along the [401] and [$\overline{4}$01] directions. Thus, changing the a parameter has the relatively largest impact on the Sr−N1 bond distance of the three unit-cell parameters. The nonlinear expansion of the unit cell is in others words coupled to the crystallographic transformation in the structure of the strontium chloride octamine mainly caused by the change in the Sr−N1 bond distance. Figure 6 also shows unit-cell parameters calculated from the energies of different degrees of compression and expansion of the unit cell. The absolute values of the calculated unit-cell parameters do not fit the experimental ones perfectly, but this is to be expected from DFT calculations of the ground state properties. The normalized ground state unit-cell parameters do nevertheless predict the anisotropic thermal expansion and the overall magnitude very well, with the a parameter having the highest expansion coefficient and the c parameter having the lowest one, although it should be noted that the inflection point is naturally not captured.

Figure 7 shows the changes in the unit-cell volumes and in the Sr−N1 bond distances during heating with different rates at an ammonia pressure of 2.0 bar. The unit-cell volumes display more or less the same temperature dependency, but shifted by a few kelvin. The unit-cell volumes are shifted by approximately 1 and 2.5 K for the experiment with heating rates of 100 and 300 K·h^{-1} compared to those of the heating experiment with 50 K·h^{-1}. The shift shows that the kinetics of the crystallographic transformation in the Sr(NH$_3$)$_8$Cl$_2$ crystallites is at least slower than 100 K·h^{-1} (at P(NH$_3$) = 2.0 bar). The Sr−N1 bond distances (Figure 7b) also display a shift in the point at which the bond distance starts to increase linearly. The point is shifted upward in temperature by approximately 4 K for the heating experiment with 300 K·h^{-1} compared to that with a rate of 50 K·h^{-1}. As for the unit-cell volume, the shift in the temperature of the Sr−N1 bond distance is correlated with the slow kinetics of the structural transformation. The bond distance of the inflection points also appears to increase with the heating rate.

A comparison of the unit-cell volumes determined during heating and cooling of the octamine phase (Figure S2) show that there is a small but significant difference in the volumes at a given temperature. The unit-cell volumes are bigger during cooling than during heating. The difference decreases generally with temperature and increases with heating/cooling rate. The gap in the temperatures is suggested related to the relatively slow kinetics of the crystallographic transformation in the structure. Figure S2 also shows that unit-cell volumes decrease with increasing ammonia pressure.

3.3. Structural Changes in Sr(NH$_3$)$_8$Cl$_2$ as a Function of Ammonia Pressure. The temperature dependency of the Sr−N1 bond distance is not only affected by changes in the heating rate, but also by changes in the pressure of the ammonia gas surrounding the Sr(NH$_3$)$_8$Cl$_2$ sample, while keeping the heating rate fixed at 100 K·h^{-1} (Figure 8). The inset in Figure 8 reveals that the Sr−N1 bond distance is nearly constant at a value of ∼2.95 Å in the temperature range from approximately 250 to 275 K at an ammonia pressure of 3.4 bar. Thus, whereas all the other seven Sr−N distances are in the range of approximately 2.7−2.8 Å, the Sr−N1 bond distance is approximately 0.15−0.25 Å longer in the temperature range from 250−275 K, which indicates that the ion-dipole forces are weaker for the Sr−N1 bond than for those of the other seven Sr^{2+}−NH$_3$ bonds. The curves with the temperature dependent Sr−N1 bond distances at different ammonia pressures do

(a)

(b)
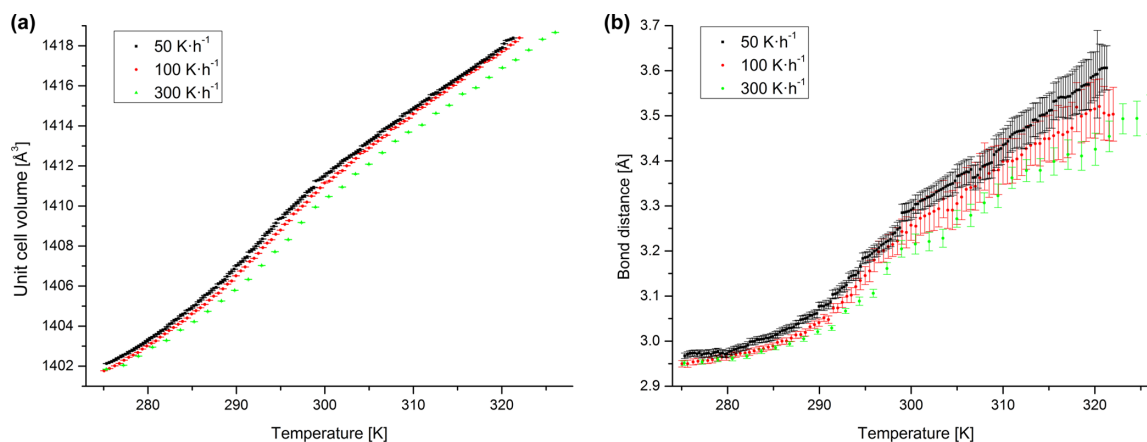
Figure 7. (a) Unit cell volumes and (b) Sr−N1 bond distances as a function of temperature during heating with different rates at $P(NH_3)$ = 2.0 bar.
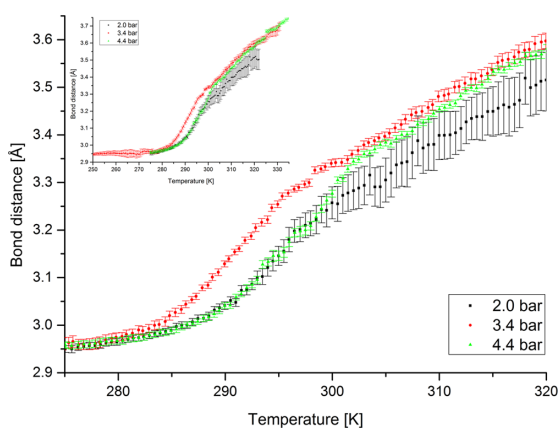

Figure 8. Sr−N1 bond distances as a function of temperature at different ammonia pressures.

display significant similarities. The bond distances increase slightly at lower temperature before they start to increase exponentially until they reach a point at which they increase linearly with temperature. The bond distance at the inflection point is ~3.20 Å at an ammonia pressure of 2.0 bar, ~3.28 Å at 3.4 bar and ~3.34 Å at 4.4 bar, which somewhat remarkably gives a linear relationship between the bond distance and the ammonia pressure. Figure 8 also shows that the linear increment above the inflection point in temperature is identical for the three different pressures. Finally, it is notable that the Sr−N1 bond distance shows a different temperature dependency at an ammonia pressure of 3.4 bar compared to those at 2.0 and 4.4 bar. The significant increase in the bond distance starts at a lower temperature. This difference may be related to the different starting temperatures of the three experiments. The heating of the sample at 3.4 bar started at a temperature of 250 K, whereas it started at a temperature of 275 K for the samples at 2.0 and 4.4 bar. Thus, the different temperature dependency may be partly due to kinetic effects.

3.4. Pressure and Heating Rate Dependent Changes in the Desorption and Absorption Temperature of $Sr(NH_3)_8Cl_2$. The desorption mechanism of ammonia from $Sr(NH_3)_8Cl_2$ upon heating depends on the partial pressure of

the surrounding ammonia gas. It may desorp via the diamine, $Sr(NH_3)_2Cl_2$, or desorp directly to the monoamine, $Sr(NH_3)Cl_2$. For all the three pressures studied herein, the first transformation observed upon heating is the octamine-to-diamine reaction, whereas the monoamine transforms directly into the octamine upon cooling in an atmosphere of ammonia gas. Thus, the diamine phase is not observed during the absorption of ammonia in $SrCl_2$. Figure 9 shows the octamine-
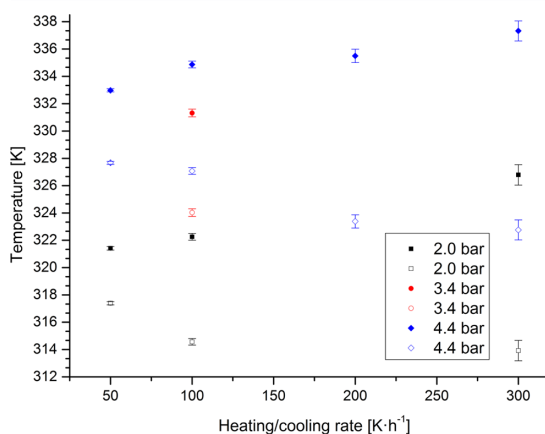
Figure 9. Temperature of the octamine-to-diamine (solid symbols) and monoamine-to-octamine (open symbols) transformations upon heating and cooling, respectively, as a function of heating/cooling rate.

to-diamine and monoamine-to-octamine transformation temperatures upon heating and cooling, respectively. The transformation temperatures are the temperatures where the diamine and octamine phases were observed first during heating and cooling, respectively. The figure reveals that the temperature of the octamine-to-diamine transformation increases with the heating rate, whereas the temperature of the monoamie-to-octamine transformation decreases with increasing the cooling rate. Thus, the increasing gap in the transformation temperatures with heating/cooling rate demonstrates that the kinetics of the desorption and absorption processes plays a limiting role. The transformation temperatures are pushed to higher or lower temperatures during

heating and cooling, respectively, due to the slow desorption and absorption kinetics in the capillary. Huttig,[33] Raldow et al.,[20] and Lysgaard et al.[22] have also observed slow kinetics when approaching true equilibrium pressures. Figure 9 also shows that the transformation temperatures increase with ammonia pressure. The transformation temperatures were investigated at three different ammonia pressures with rates of 100 K·h^{-1}. These temperatures and pressures were used for van 't Hoff plots to roughly estimate the absorption and desorption enthalpies and entropies. For the desorption reaction, Sr-$(NH_3)_8Cl_2 \rightarrow Sr(NH_3)_2Cl_2 + 6NH_3(g)$, it gave ΔH_{desorp} = 56.3(4.0) kJ·mol^{-1} and ΔS_{desorp} = 180(12) J·mol^{-1}·K^{-1}, and the absorption reaction $Sr(NH_3)Cl_2 + 7\ NH_3(g) \rightarrow Sr(NH_3)_8Cl_2$ gave ΔH_{absorb} = 54.3(6.9) kJ·mol^{-1} and ΔS_{absorb} = 178(21) J·mol^{-1}·K^{-1} (Figure S3 in the Supporting Information). The enthalpy of desorption from the octamine to diamine is significant higher than the value, 43.4(0.8) kJ·mol^{-1}, reported by Lysgaard et al.[22] for the same reaction, and much closer to the enthalpy of the diamine-to-monoamine reaction, 58.9(1.9) kJ·mol^{-1}, also reported by Lysgaard et al. However, it is important to note that the monoamines start to appear in the herein studied diffraction patterns at temperatures only a few kelvin higher than the ones where the diamines start to appear at P(NH$_3$) = 2.0 bar. Thus, the desorption enthalpies of the $Sr(NH_3)_8Cl_2 \rightarrow Sr(NH_3)Cl_2 + 7NH_3(g)$ and/or $Sr(NH_3)_2Cl_2 \rightarrow Sr(NH_3)Cl_2 + NH_3(g)$ reactions are expected to be only slightly higher than the one of the $Sr(NH_3)_8Cl_2 \rightarrow Sr(NH_3)_2Cl_2 + 6NH_3(g)$. One should also bear in mind that the kinetics plays an important role for desorption process, and the enthalpies of this study are not determined from equilibrium conditions, but using a heating rate of 100 K·h^{-1}. Thus, the herein calculated enthalpies and entropies are only rough estimates. Figure S4 in the Supporting Information shows normalized peak intensities of the three amine phases (octa-, di-, and mono-) as a function of temperature during isobaric heating with different heating rates and ammonia pressures. The figure reveals that the desorption processes are separated in temperature at ammonia pressures of 3.4 and 4.4 bar. The first desorption process is the octamine-to-diamine reaction where the curve with the normalized peak intensity of the octamine phase crosses the corresponding one for the diamine phase at ∼50%. The same is the case for the diamine-to-monoamine reaction at higher temperatures. The desorption process is different at lower ammonia pressure (P(NH$_3$) = 2.0 bar), where a significant amount of the octamine phase still is present when the monoamine phase starts to be formed. The normalized peak intensities indicate that the direct octamine-to-monoamine transformation starts at temperatures only a few kelvin higher than the octamine-to-diamine transformation starts. The two reactions are then running in parallel until all the octamine is transformed. The formed diamine is then transformed into monoamine at higher temperatures. The normalized peak intensities also show that the kinetics of the diamine-to-monoamine reaction is slower than that of the octamine-to-diamine and octamine-to-monoamine reactions.

4. CONCLUSION

The in situ XRPD study has revealed markedly changes in the crystal structure of the $Sr(NH_3)_8Cl_2$ as a function of temperature and ammonia pressure, and has shown the transformation processes of the strontium chloride amines during absorption and desorption of ammonia gas.

Rietveld refinements showed that the strontium ions each are coordinated to eight ammonia molecules with Sr−N distances in the range from 2.714(2) to 2.950(8) Å at 275 K and P(NH$_3$) = 2.0 bar, forming isolated Sr-(NH$_3$)$_8$ polyhedra shaped as distorted tetragonal antiprisms or double capped trigonal prisms. Seven out of the eight Sr−N distances are in the range of 2.714(2) to 2.792(2) Å, and they only increase slightly during heating to 322 K. The last Sr−N distances increases to 3.50(6) Å at 322 K. DFT calculations showed that only half the energy is required to elongate the Sr−N1 bond from its equilibrium distance compared to the standard Sr−N bonds. The length of the hydrogen bond from the chloride ion to the hydrogen atom of the ammonia molecule appears not to be significantly changed by the temperature. The elongation of the Sr−N1 distance causes the ammonia molecules to move out into a void space of the crystal structure. The isotropic displacement parameter of the ammonia molecule increases consequently by more than a factor of four. The in situ XRPD data showed that the *a* parameter of the unit cell increases relatively more than the *b* and *c* parameters during the heating because changing the *a* parameter has the largest effect on the Sr−N1 distance. DFT calculations confirmed the overall trend for the expansion of the unit-cell parameters. The in situ XRPD data also showed that increasing the heating rate pushes the structural transformation in the crystal structure to higher temperatures by a few kelvin. Increasing the pressure of the surrounding ammonia gas changes the temperature dependency of the Sr−N1 distance. The bond distance at the inflection point where the temperature-dependent Sr−N1 distance starts to increase linearly increases with the ammonia pressure.

The in situ XRPD data showed that the $Sr(NH_3)_8Cl_2 \rightarrow Sr(NH_3)_2Cl_2 + 6NH_3(g)$ reaction has the lowest transformation temperature for all the three studied ammonia pressures (2.0, 3.4, and 4.4 bar). Desorption of ammonia according to the $Sr(NH_3)_8Cl_2 \rightarrow Sr(NH_3)Cl_2 + 7NH_3(g)$ reaction was also observed at P(NH$_3$) = 2.0 bar. For the absorption of ammonia, the $Sr(NH_3)Cl_2 + 7NH_3(g) \rightarrow Sr(NH_3)_8Cl_2$ was the only observed reaction.

■ ASSOCIATED CONTENT

Ⓢ Supporting Information

The Supporting Information contains tables and figures with additional results relevant for this study. This material is available free of charge via the Internet at http://pubs.acs.org.

■ AUTHOR INFORMATION

Corresponding Author

*E-mail: teve@dtu.dk; Phone: +45 51641787; Fax: +45 46775758.

Notes

The authors declare no competing financial interest.

■ REFERENCES

(1) Vegge, T.; Sørensen, R. Z.; Klerke, A.; Hummelshøj, J. S.; Johannessen, T.; Nørskov, J. K. Indirect Hydrogen Storage in Metal Amines. In *Solid-State Hydrogen Storage: Materials and Chemistry*; Woodhead Publishing Ltd: Cambridge, U.K., 2008.

(2) Klerke, A.; Christensen, C. H.; Nørskov, J. K.; Vegge, T. Ammonia for Hydrogen Storage: Challenges and Opportunities. *J. Mater. Chem.* **2008**, *18*, 2304.

(3) Christensen, C. H.; Sørensen, R. Z.; Johannessen, T.; Quaade, U. J.; Honkala, K.; Elmøe, T. D.; Køhler, R.; Nørskov, J. K. Metal Ammine Complexes for Hydrogen Storage. *J. Mater. Chem.* **2005**, *15*, 4106.

(4) Christensen, C. H.; Johannessen, T.; Sørensen, R. Z.; Nørskov, J. K. Towards an Ammonia-Mediated Hydrogen Economy? *Catal. Today* **2006**, *111*, 140−144.

(5) Elmøe, T. D.; Sørensen, R. Z.; Quaade, U.; Christensen, C. H.; Nørskov, J. K.; Johannessen, T. A High-Density Ammonia Storage/Delivery System Based on $Mg(NH_3)_6Cl_2$ for SCR−DeNO$_x$ in Vehicles. *Chem. Eng. Sci.* **2006**, *61*, 2618−2625.

(6) Chakraborty, D.; Petersen, H. N.; Elkjær, C.; Cagulada, A.; Johannessen, T. Solid Ammonia as Energy Carrier: Current Status and Future Prospects. *Fuel Cells Bull.* **2009**, *2009*, 12−15.

(7) Fulks, G.; Fisher, G. B. .; Rahmoeller, K.; Wu, M.-C.; D'Herde, E.; Tan, J. A Review of Solid Materials as Alternative Ammonia Sources for Lean NO$_x$ Reduction with SCR. *SAE [Tech. Pap.]* **2009**, DOI: 10.4271/2009-01-0907.

(8) Lepinasse, E.; Spinner, B. Production de Froid Par Couplage de Réacteurs Solide-Gaz I: Analyse Des Performances de Tels Systèmes. *Int. J. Refrig.* **1994**, *17*.

(9) Liu, C. Y.; Aika, K. Ammonia Absorption on Alkaline Earth Halides as Ammonia Separation and Storage Procedure. *Bull. Chem. Soc. Jpn.* **2004**, *77*, 123−131.

(10) Huang, H.; Wu, G.; Yang, J.; Dai, Y.; Yuan, W.; Lu, H. Modeling of Gas−Solid Chemisorption in Chemical Heat Pumps. *Sep. Purif. Technol.* **2004**, *34*, 191−200.

(11) Jensen, P. B.; Lysgaard, S.; Quaade, U. J.; Vegge, T. Designing Mixed Metal Halide Ammines for Ammonia Storage Using Density Functional Theory and Genetic Algorithms. *Phys. Chem. Chem. Phys.* **2014**, *16*, 19732−19740.

(12) Hwang, I.; Drews, T.; Seppelt, K. $Mg(NH_3)_6Hg_{22}$, a Mercury Intercalation Compound. *J. Am. Chem. Soc.* **2000**, *122*, 8486−8489.

(13) Tekin, A.; Hummelshøj, J. S.; Jacobsen, H. S.; Sveinbjörnsson, D.; Blanchard, D.; Nørskov, J. K.; Vegge, T. Ammonia Dynamics in Magnesium Ammine from DFT and Neutron Scattering. *Energy Environ. Sci.* **2010**, *3*, 448.

(14) Jacobsen, H. S.; Hansen, H. A.; Andreasen, J. W.; Shi, Q.; Andreasen, A.; Feidenhans'l, R.; Nielsen, M. M.; Ståhl, K.; Vegge, T. Nanoscale Structural Characterization of $Mg(NH_3)_6Cl_2$ during NH$_3$ Desorption: An in Situ Small Angle X-ray Scattering Study. *Chem. Phys. Lett.* **2007**, *441*, 255−260.

(15) Song, X.; Liu, G.; Sun, Z.; Yu, J. Comparative Study on the Molecular and Electronic Structure of $MgCl_2 \cdot 6NH_3$ and $MgCl_2 \cdot 6H_2O$. *Asia-Pacific J. Chem.* **2012**, 221−226.

(16) Zhu, H.; Gu, X.; Yao, K.; Gao, L.; Chen, J. Large-Scale Synthesis of $MgCl_2 \cdot 6NH_3$ as an Ammonia Storage Material. *Ind. Eng.* **2009**, 5317−5320.

(17) Sørensen, R. Z.; Hummelshøj, J. S.; Klerke, A.; Reves, J. B.; Vegge, T.; Nørskov, J. K.; Christensen, C. H. Indirect, Reversible High-Density Hydrogen Storage in Compact Metal Ammine Salts. *J. Am. Chem. Soc.* **2008**, *130*, 8660−8668.

(18) Jones, M. O.; Royse, D. M.; Edwards, P. P.; David, W. I. F. The Structure and Desorption Properties of the Ammines of the Group II Halides. *Chem. Phys.* **2013**, *427*, 38−43.

(19) Amminex Home Page. http://www.amminex.com/ (accessed Oct 10, 2014).

(20) Raldow, W. M.; Johnston, D. W.; Wentworth, W. Utilization of Suspensions in a Nonvolatile Inert Solvent to Study Solid-Gas Equilibriums. An Investigation of the Strontium Dichloride-Ammonia System. *J. Phys. Chem.* **1980**, 2599−2601.

(21) Erhard, A.; Spindler, K.; Hahne, E. Test and Simulation of a Solar Powered Solid Sorption Cooling Machine. *Int. J. Refrig.* **1998**, *21*, 133−141.

(22) Lysgaard, S.; Ammitzbøll, A. L.; Johnsen, R. E.; Norby, P.; Quaade, U. J.; Vegge, T. Resolving the Stability and Structure of Strontium Chloride Amines from Equilibrium Pressures, XRD and DFT. *Int. J. Hydrogen Energy* **2012**, *37*, 18927−18936.

(23) Westman, S.; Werner, P. E.; Schuler, T.; Raldow, W. X-ray Investigations of Ammines of Alkaline Earth Metal Halides. I. The Structures of $CaCl_2(NH_3)_8$, $CaCl_2(NH_3)_2$ and the Decomposition Product CaClOH. *Acta Chem. Scandinavica A* **1981**, 467−472.

(24) Kohn, W.; Sham, L. J. Self-Consistent Equation including Exchange and Correlation Effects. *Phys. Rev.* **1965**, *140*.

(25) Hohenberg, P.; Kohn, W. Inhomogeneous Electron Gas. *Phys. Rev. B* **1964**, *136*.

(26) Dion, M.; Rydberg, H.; Schröder, E.; Langreth, D. C.; Lundqvist, B. I. Van Der Waals Density Functional for General Geometries. *Phys. Rev. Lett.* **2004**, *92*, 246401.

(27) Mortensen, J.; Hansen, L.; Jacobsen, K. Real-Space Grid Implementation of the Projector Augmented Wave Method. *Phys. Rev. B* **2005**, *71*, 035109.

(28) Bahn, S. R.; Jacobsen, K. W. An Object-Oriented Scripting Interface to a Legacy Electronic Structure Code. *Comput. Sci. Eng.* **2002**, *4*, 56−66.

(29) Monkhorst, H. J.; Pack, J. D. Special Points for Brillouin-Zone Integrations. *Phys. Rev. B* **1976**, *13*, 5188−5192.

(30) Maragakis, P.; Andreev, S. A.; Brumer, Y.; Reichman, D. R.; Kaxiras, E. Adaptive Nudged Elastic Band Approach for Transition State Calculation. *J. Chem. Phys.* **2002**, *117*, 4651.

(31) Zarkevich, N. A.; Majzoub, E. H.; Johnson, D. D. Anisotropic Thermal Expansion in Molecular Solids: Theory and Experiment on LiBH$_4$. *Phys. Rev. B* **2014**, *89*, 134308.

(32) Panthöfer, M.; Wedig, U.; Brumm, H.; Jansen, M. Geometric and Electronic Structure of Polymeric C$_{70}$-Fullerides: The Case of $_\infty^1[C_{70}{}^{3-}]$. *Solid State Sci.* **2004**, *6*, 619−624.

(33) Huttig, G. Articles on the Systematic in Law Teaching XVIII The Ammoniacate of Strontium Halogenide. *Z. Anorg. Allg. Chem.* **1922**, *124*, 322−332.
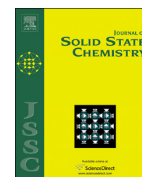
Paper II

Solid solution barium–strontium chlorides with tunable ammonia desorption properties and superior storage capacity
Agata Bialy, Peter Bjerre Jensen, Didier Blanchard, Ulrich J. Quaade and Tejs Vegge
Journal of Solid State Chemistry **221**:32-36, 2015

Solid solution barium–strontium chlorides with tunable ammonia desorption properties and superior storage capacity

Agata Bialy [a], Peter B. Jensen [b,c], Didier Blanchard [b], Tejs Vegge [b,*], Ulrich J. Quaade [a,**]

[a] Amminex Emissions Technology A/S, Gladsaxevej 363, 2860 Soeborg, Denmark
[b] Department of Energy Conversion and Storage, Technical University of Denmark, Frederiksborgvej 399, DK-4000 Roskilde, Denmark
[c] Center for Atomic-scale Materials Design, Department of Physics, Technical University of Denmark, Fysikvej 311, DK-2800 Kgs. Lyngby, Denmark

ARTICLE INFO

ABSTRACT

Metal halide ammines are very attractive materials for ammonia absorption and storage—applications where the practically accessible or usable gravimetric and volumetric storage densities are of critical importance. Here we present, that by combining advanced computational materials prediction with spray drying and in situ thermogravimetric and structural characterization, we synthesize a range of new, stable barium-strontium chloride solid solutions with superior ammonia storage densities. By tuning the barium/strontium ratio, different crystallographic phases and compositions can be obtained with different ammonia ab- and desorption properties. In particular it is shown, that in the molar range of 35–50% barium and 65–50% strontium, stable materials can be produced with a practically usable ammonia density (both volumetric and gravimetric) that is higher than any of the pure metal halides, and with a practically accessible volumetric ammonia densities in excess of 99% of liquid ammonia.

© 2014 Published by Elsevier Inc.

1. Introduction

Metal halide ammines are superior materials for ammonia/hydrogen storage and desorption with a wide range of applications including thermochemical heat pumps, ammonia separation, fuel cells and selective catalytic reduction (SCR) [1–8]. Metal halide ammines in general show ammonia desorption temperatures ranging from below room temperature to above 400 °C [1]. For many applications such as e.g. fuel cells and SCR, however, a temperature range between 20 °C and 100 °C is highly desirable. The lower limit of 20 °C is set for safety reasons to reduce the toxic vapor pressure when the system is not in operation. The higher limit, 100 °C, is advantageous to (i) limit the time and energy needed to release the ammonia, (ii) enable the use of waste heat, often in the form of hot water, for desorption, and (iii) enable use of cheap engineering materials. The ammonia that desorbs between 20 °C and 100 °C at 1 bar is here defined as the usable ammonia content. In this narrow temperature window strontium and calcium chlorides are the most interesting among the pure metal halides. $CaCl_2$ binds 8 ammonia molecules, and has the highest gravimetric ammonia capacity among the metal halides (551 g NH_3/kg). However, the last 2 ammonia molecules require temperatures of 198–242 °C to desorb [1]. If the temperature is

limited to 100 °C, the usable gravimetric ammonia density decreases to 413 g NH_3/kg. In the same way, the gravimetric ammonia density of $SrCl_2$ decreases from 462 g NH_3/kg to a usable gravimetric ammonia density of 404 g NH_3/kg.

Recent studies have shown that ammonia binding energies and material densities depend on the elements and crystal structures of the salts [9]. The determination of the ammonia equilibrium pressures combined with X-ray diffraction (XRD) and density functional theory (DFT) calculations brought a complete understanding of the crystal structures of the strontium chloride ammines and revealed that several different crystal structures exist with energies close to the ground state. Only small modifications are needed to interchange the energies, and thus the stability of these structures. Further, Aika and Liu showed that bromides and chlorides of strontium and calcium spontaneously form mixed solid solutions with ammonia binding properties different from the pure salts [10].

These observations led us to investigate the possibility to design novel ammonia storage materials based on mixed solid solutions of metal halides, with the target of obtaining simultaneous high usable gravimetric and volumetric ammonia density. Strontium chloride is one of the metal halides with the highest usable ammonia storage capacity. And since barium is an abundant impurity of naturally occurring strontium minerals and the only metal halide known with high ammonia density, which releases all the ammonia in one step, we chose to investigate the barium–strontium chloride system.

* Corresponding author. Tel.: +45 46775818.
** Corresponding author. Tel.: +45 20892383.
E-mail addresses: teve@dtu.dk (T. Vegge), ujq@amminex.com (U.J. Quaade).

2. Materials and methods

2.1. Synthesis

Solid solutions of strontium and barium chlorides were prepared by spray drying of the aqueous solutions, a method which is commonly used in production of strontium chloride. Prior to the experiment, strontium chloride and barium chloride (min. purity 99%) were dried in an oven at 200 °C. So obtained anhydrous compounds, in pre-described molar ratios, were dissolved in demineralized water to obtain a 10 wt% aqueous solution. Mixtures with stoichiometries ranging from 99:1 to 25:75, $SrCl_2$:$BaCl_2$ were prepared. A laboratory scale B290 Buchi Mini Spray Dryer was used with the following settings: (a) inlet temperature: 220 °C, (b) feed rate: 10% (0,2 L/h), (c) aspirator rate: 60% (20 m^3/h), (d) spray drying air flow: 40 mm (680 NL/h). Prior to testing all the samples were further dried in an oven at 200 °C for 24 h to reach a water content below 0.05 wt%.

2.2. Characterization

So prepared materials were characterized in regards to their structure, ammonia absorption and desorption properties, and densities. Structures were investigated using Powder diffraction X-ray (PXD) and were recorded on a BRUKER D8 (40 kV, 40 mA, Cu radiation $K\alpha = 1.542$ Å). To avoid contact with air or moisture a polyethylene film covered the samples. The film gives rise to the background in the angular range from 10° to 25° in 2θ, background accompanied by two broad peaks at around 21° and 25° in 2θ. These peaks were excluded from the patterns during the Rietveld refinements. Ammonia absorption and desorption properties were analyzed using thermogravimetric desorption measurements, which were performed on a high pressure thermogravimetric analyzer, HP-TGA ISOSORP Gas LP-flow from Rubotherm. A unique feature of this instrument is the separation of the balance from the sample environment by magnetic coupling, which allows for the use of corrosive gases, such as ammonia. All samples were analyzed with the same method comprising the following steps: (a) annealing of the sample at 200 °C in nitrogen gas atmosphere, (b) cool down to 20 °C and evacuation, (c) saturation with ammonia gas at 5 bar at 20 °C, (d) desorption of ammonia by increasing temperature by 1 °C/min in 1 bar of ammonia gas. The density of ammoniated samples was measured by compacting the material under a mechanical pressure of 740 MPa (7.5 t/cm^2) and measuring the density of the obtained pellets. Samples were kept cold prior to testing to avoid ammonia desorption, measurements were performed in dry nitrogen atmosphere and the ammonia content was verified after each measurement by heating and weighing the samples. Each concentration was tested three times.

2.3. DFT calculations

Density functional theory (DFT) calculations were performed to predict the thermodynamic and structural properties of the mixed metal halide ammines, and for comparison with experimental observations. The calculations were done within the Atomic Simulation Environment (ASE) using the GPAW code; a real space implementation of the Projector Augmented Wave (PAW) method [11–15]. The vdW-DF functional was used to account for dispersion and van der Waals forces [16]. The Brillouin-zone was sampled using a Monkhorst-Pack grid with at least 25 k-points per Å^{-1} in each direction, the grid spacing was 0.18 Å and all structures were allowed to relax the atomic coordinates by a quasi-Newton type optimization algorithm [17,18]. The energy of NH$_3$(g) was calculated by placing a molecule in a cube with a side length of 8 Å, removing the periodic boundary conditions and

using the same grid spacing as above. The enthalpies of desorption were calculated by subtracting the absolute electronic energies of the most stable structures in the desorption step and including the gas-phase energy of the released ammonia molecules. The desorption temperatures were determined by calculating the entropic and finite temperature enthalpy corrections for the strontium and barium systems, and using the weighted averages to calculate the release temperatures using the van't Hoff equation. For the solids, the correction was found by summation of the mean energies of the vibrational frequencies calculated in the harmonic approximation at finite temperatures; the gas phase correction was calculated in the ideal gas approximation, by including the translational, rotational and vibrational degrees of freedom in the NH$_3$ molecule [19].

3. Results and discussion

Examples of ammonia desorption into 1 bar of ammonia when the temperature is ramped 1 °C/min from 20 °C to 160 °C from 3 different mixtures of Ba$_x$Sr$_{(1-x)}$(NH$_3$)$_8$Cl$_2$ ($x=0.125$, $x=0.25$ and $x=0.5$) are shown in Fig. 1a together with Ba(NH$_3$)$_8$Cl$_2$ and Sr(NH$_3$)$_8$Cl$_2$.

For pure Sr(NH$_3$)$_8$Cl$_2$, the ammonia desorption is seen to start close to 40 °C and releases 87.5% in one step. This corresponds to 7 out of the 8 ammonia molecules. The last molecule, however, only desorbs above 125 °C. For pure Ba(NH$_3$)$_8$Cl$_2$, all 8 ammonia molecules are desorbed below 50 °C. When barium is added to Sr(NH$_3$)$_8$Cl$_2$, the desorption of the first 7 molecules resembles desorption from pure Sr(NH$_3$)$_8$Cl$_2$. The effect of the increasing barium concentration is mostly a shift in desorption of the last ammonia molecule to lower temperatures. For the composition Ba$_{0.5}$Sr$_{0.5}$Cl$_2$, essentially all the ammonia desorbs in one step and results in a usable gravimetric ammonia density of 422 g NH$_3$/kg. This excellent behavior is maintained with cycling as seen in Fig. 1b: Ba$_{0.5}$Sr$_{0.5}$Cl$_2$ is saturated with ammonia and degassed 10 times in total. A small change is observed from the first to the second cycle. This is seen in all cycling experiments for pure and mixed salts, and is associated with formation of porosity in the first cycle [8]. Apart from that, the amount of ammonia desorbing below 100 °C remains constant (Fig. 1b) and no degradation is observed. The stability was confirmed by XRD. Fig. 2 presents the diffraction patterns of Ba$_{0.5}$Sr$_{0.5}$Cl$_2$ before and after seven
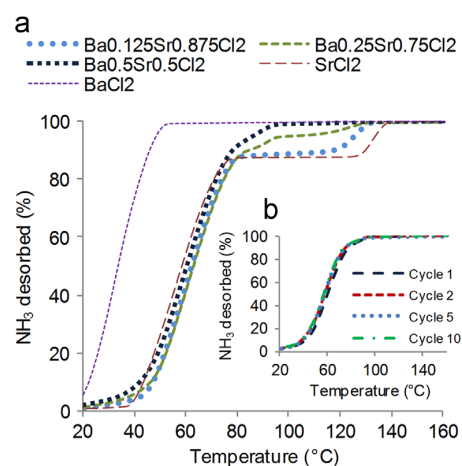

Fig. 1. Ammonia temperature programmed desorption (TPD) curves. (a) Ammonia TPD from Ba$_x$Sr$_{(1-x)}$Cl$_2$ with x equal to 0.125, 0.25 and 0.5. (b) Ammonia TPD from Ba$_{0.5}$Sr$_{0.5}$Cl$_2$ after 1, 2, 5 and 10 saturation cycles. (For interpretation of the references to color in this figure legend, the reader is referred to the web version of this article.)

ammonia cycles (bottom and top curves). It shows the stability of the phase, the only difference being a broadening of the reflections due to the fragmentation of the crystallites because of the lattice strain induced by the volume changes during the first ammonia absorption. On the same figure, the diffraction pattern of the ammoniated phase is shown (middle curve). The peaks can be indexed as a *Pnma* structure similar to those of $Sr(NH_3)_8Cl_2$ or $Ca(NH_3)_8Cl_2$ [9]. However, no Rietveld refinement was performed because of the poor quality of the data. Indeed the ammoniated sample is not stable enough at room temperature, if no ammonia pressure is applied, to perform long time measurement. The XRD pattern shown on Fig. 2 was acquired in 30 min., and the following measurement already showed some differences. In-situ diffraction, varying the ammonia pressure and the temperature applied to the mixed salt is thus require if one want to draw the full phase diagram. This is beyond the scope of the present publication.

In order to obtain the volumetric ammonia density, the material densities of the fully saturated ammines of $Ba_xSr_{(1-x)}(NH_3)_8Cl_2$ are measured (described in Section 2) as a function of barium content as shown in Fig. 3c.

Based on the thermogravimetric desorption results and material densities, the usable gravimetric and volumetric ammonia densities are determined as shown in Fig. 3a and b, respectively. It is seen that both the usable gravimetric and volumetric ammonia density increases from around 10% barium content and reaches a maximum close to 37.5% barium. At the maximum, the usable gravimetric and volumetric ammonia densities are 6% and
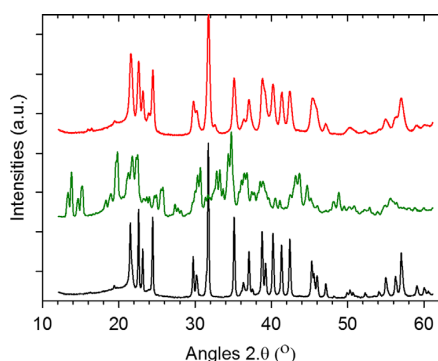
Fig. 2. XRD patterns. Bottom (black line): $Ba_{0.5}Sr_{0.5}Cl_2$. Middle (green line): $Ba_{0.5}Sr_{0.5}(NH_3)_8 Cl_2$. Top (red line): $Ba_{0.5}Sr_{0.5}Cl_2$ after seven ammonia (absorption–desorption) cycles. After spray drying samples were annealed at 500 °C. (For interpretation of the references to color in this figure legend, the reader is referred to the web version of this article.)
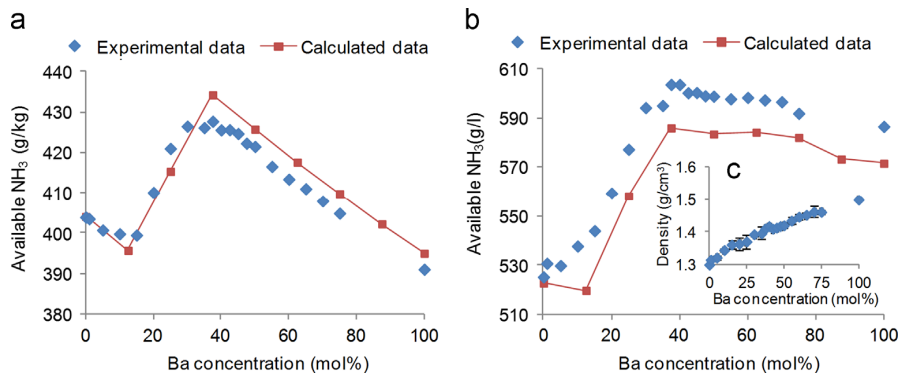
15% higher than for pure $Sr(NH_3)_8Cl_2$ respectively, and 1% and 8% higher than for pure $Ba(NH_3)_8Cl_2$. Thus, the mixed salt exhibits properties superior to both of the individual components. The experimental results are in excellent quantitative agreement with thermodynamic and gravimetric properties predicted from the van der Waals corrected DFT calculations (vdW-DF) as seen in Fig. 3a and b.

The calculated usable ammonia densities in Fig. 3 are based on the DFT calculations: To perform a thermodynamic prediction of changes in the desorption pathway resulting from varying the barium content in the strontium chloride ammines, reliable candidate structures are needed. Since the mixed ammine phases have not previously been characterized, the initial structures are based on the structures determined for pure strontium chloride ammines [9]. The starting structure for e.g. the 12.5% barium octa ammine structure is obtained by substituting one out of the eight strontium atoms by barium. This structure is then relaxed using internal relaxation of all atomic coordinates, followed by a unit cell relaxation, one direction at a time, and a final relaxation of the internal coordinates.

To predict the available amount of ammonia released below 100 °C, we calculate the change in free energy and thus the release temperatures for all possible reaction pathways (see Supplementary Table S1). To determine the amount of barium substitution required to release the residual NH_3 molecule, we determine the change in the release temperature for the reaction going from the mono ammine to the salt, and compare this to the experimentally observed shift. For 25% barium, the release temperature is shifted down by 33 °C compared to the pure strontium system, in excellent agreement with the 30 °C observed experimentally (green curve in Fig. 1a). For higher concentrations, the calculated shifts are larger, and give full release below 100 °C for 37.5% barium. For lower concentrations only 87.5% release is predicted below 100 °C. To account for the heating rate and the width of the desorption steps, an average release of 7.5 molecules is assigned for 25% Ba. Using these release percentages, we see an excellent agreement with the experiments (Fig. 3a, b), both estimating the usable gravimetric and volumetric ammonia densities.

The favorable changes in desorption profiles with increasing amount of barium in the mixed salts can be understood by the examination of the crystal structures of the solid solutions after spray drying. Powder diffraction is used and a summary of the observations is presented on Fig. 4 and Fig. 5 (see also Supplementary Fig. S1 for more details).

The data was collected for mixed salts, $SrCl_2:BaCl_2$, with molar stoichiometry ranging from 99:1 to 45:55. Three different domains of composition are identified. When low molar concentrations of

Fig. 3. Usable ammonia densities of ammoniated $Ba_xSr_{(1-x)}Cl_2$. (a) Experimental and calculated usable gravimetric ammonia density as a function of Ba concentration. (b) Experimental and calculated usable volumetric ammonia density as a function of Ba content. (c) Compacted densities of fully ammoniated $Ba_xSr_{(1-x)}Cl_2$ as a function of Ba content.
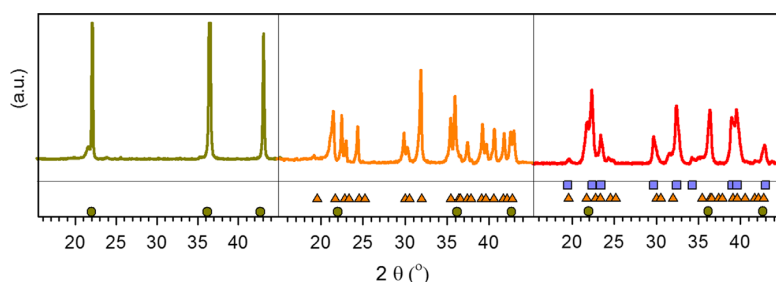
Fig. 4. Examples of three X-ray patterns illustrating the three different regions of composition. Left: $Ba_{0.04}Sr_{0.96}Cl_2$, center of $Ba_{0.25}Sr_{0.75}Cl_2$ and right $Ba_{0.55}Sr_{0.45}Cl_2$. Below the patterns are displayed the positions of the main Bragg peaks for the different phases. (See Supplementary information Section 2 for more details on the diffraction analysis).
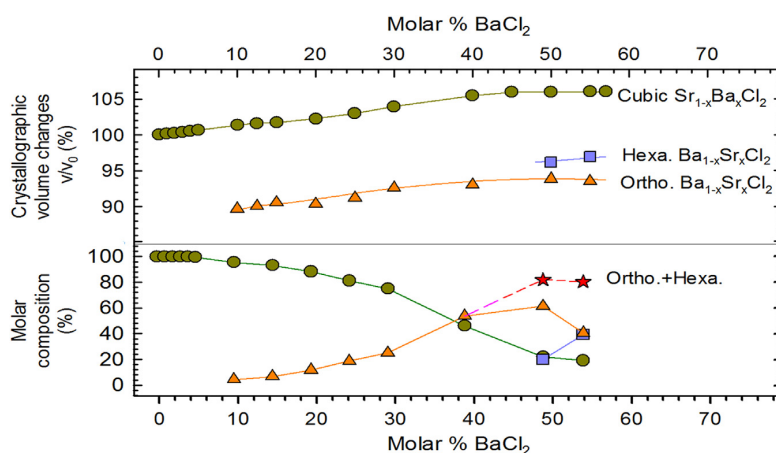
Fig. 5. XRD results. (a) Volume expansion (V/V_0) of the different crystalline phases as function of the $BaCl_2$ content in the $SrCl_2$:$BaCl_2$ spray dried samples—V_0 is the volume of the pure phases, i.e. no solid solution. (b) Molar compositions of the spray dried samples as function of the $BaCl_2$ content.

$BaCl_2$ are used (from 1 to 10%), only a single phase with the cubic structure of $SrCl_2$ is detected (left part, Fig. 5). In the middle concentration range of $BaCl_2$ (10 to 40%, center part, Fig. 5), two crystalline structures are observed, the cubic $SrCl_2$ structure (space group $Fm3m$) and the orthorhombic polymorph (space group $Pnma$) of $BaCl_2$. In the high $BaCl_2$ concentration domain (above 40%, right hand part, Fig. 5), three crystalline phases are present, the cubic $SrCl_2$, as a trace, and the two polymorphs of $BaCl_2$, the orthorhombic and the hexagonal, space groups $Pnma$ and $P62m$, respectively.

It is observed (Fig. 5b) that in the range 10–40% of barium, the two phases cubic $Sr_{1-x}Ba_xCl_2$ and ortho $Ba_{1-x}Sr_xCl_2$ co-exist and especially close to 37.5%, where all the ammonia is desorbed in a single step, they co-exist in comparable amounts. This rules out that the single step desorption is a result of switching from one phase to the other. Instead, it is observed (Fig. 5a) that the lattice of both phases expands systematically with the barium concentration in the range 10% to 40%. Also, Fig. 1a shows that the effect of barium is almost exclusively to destabilize the strongest bound ammonia molecule, and Fig. 3a implies that the release temperature of the strongest bound ammonia molecule decreases with barium concentration exactly in the range 10% to 40%. This supports that the ammonia binding properties of the two phases are similar and that the binding energy of the strongest bound ammonia molecule decreases with the lattice expansion induced by adding barium, as predicted by the DFT calculations.

As a final remark to the experimental results we note, that according to refs. [10,20], metal halide mixtures having common anions, but different cations were not previously observed to

spontaneously form mixed cations solid solutions. Based on the XRD and ammonia desorption results it is shown that, even if they do not form spontaneously, solid solutions can be obtained by spray drying synthesis.

In Table 1 the gravimetric and volumetric ammonia densities of selected mixed strontium–barium chlorides are compared to the ordinary metal halides with highest ammonia content and to liquid ammonia. The usable ammonia densities of the ordinary metal halides are obtained experimentally in the same way as described for the mixed barium strontium chlorides. The substances are ordered by usable volumetric ammonia density.

4. Conclusions

This study has demonstrated the possibility of predicting and synthesizing stable mixed metal halides even if they do not spontaneously form solid solutions. The study focused on designing and optimizing the ammonia storage capacity for a specific temperature regime relevant for multiple applications beyond just picking the best simple metal halide from the periodic table. New materials with the highest usable ammonia capacity in the important 20–100 °C temperature interval are identified. The integrated theoretical and experimental approach is capable of predicting and designing modifications to physical and chemical parameters, e.g. by changing crystal structures and bond lengths, resulting from formation of mixed solid solution metal halide ammines. The developed methodology opens for a general

Table 1
Total and usable gravimetric and volumetric ammonia densities.

Salt	gNH_3/L max	gNH_3(usable)/ L	gNH_3/kg max	gNH_3(usable)/ kg
Anhydrous liquid NH_3	610.0	610.0	1000	1000
$Ba_{0.375}Sr_{0.625}Cl_2$	613.0	604.0	435	428
$Ba_{0.4}Sr_{0.6}Cl_2$	613.0	604.0	433	427
$Ba_{0.5}Sr_{0.5}Cl_2$	605.0	599.0	426	422
$BaCl_2^{\#}$	597.0	597.0	396	396
$SrCl_2$	601.0	526.0	462	404
$CaCl_2$	670.0	502.0	551	413
$FeCl_2^{*}$	678.0	452.0	446	298
$NiCl_2^{*}$	657.0	438.0	441	294
$MgCl_2^{*}$	639.0	426.0	518	345
$MnCl_2$	618.0	412.0	448	299
$ZnCl_2$	608.0	406.0	429	286
$LiCl$	550.0	367.0	547	364

*,#Ammonia desorbs above 100 °C (*) or below 20 °C (#)· but the materials are included for reference. For these materials the usable ammonia densities are based on the amount of ammonia that desorbs in the first desorption step.

characterization and optimization of this important class of materials with a wide range of applications.

Acknowledgments

Appendix A. Supplementary material

Supplementary data associated with this article can be found in the online version at http://dx.doi.org/10.1016/j.jssc.2014.09.014.

References

[1] T. Vegge, R.Z. Sørensen, A. Klerke, J.S. Hummelshøj, T. Johannessen, J.K. Nørskov, Indirect Hydrogen Storage in Metal Amines in Solid-state Hydrogen Storage: Materials and Chemistry, in: G. Walker (Ed.), Woodhead Publishing Ltd, Cambridge, ISBN 978-1-84569-270-4, 2008.
[2] E.S. Lepinasse, B. Spinner, Int. J. Refrig.—Reveu Internationale Du Froid 17 (1994) 309–322.
[3] C. Liu, K. Aika, Bull. Chem. Soc. Jpn. 77 (2004) 123–131.
[4] C.H. Christensen, R.Z. Sørensen, T. Johannessen, U.J. Quaade, K. Honkala, T.D. Elmøe, R. Køhler, J.K. Nørskov, J. Mater. Chem. 15 (2005) 4106–4108.
[5] A. Klerke, C.H. Christensen, J.K. Nørskov, T. Vegge, J. Mater. Chem. 18 (2008) 2304–2310.
[6] D. Chakraborty, H.N. Petersen, C. Elkjær, A. Cagulada, T. Johannessen, Fuel Cells Bull (2009) 12.
[7] T.D. Elmøe, R.Z. Sørensen, U.J. Quaade, C.H. Christensen, J.K. Nørskov, T. Johannessen, Chem. Eng. Sci. 61 (2006) 2618–2625.
[8] R.Z. Sørensen, J.S. Hummelshøj, A. Klerke, J.B. Reves, T. Vegge, J.K. Nørskov, J. Am. Chem. Soc. 130 (2008) 8660–8668.
[9] S. Lysgaard, A.L. Ammitzbøll, R.E. Johnsen, P. Norby, U.J. Quaade, T. Vegge, Int. J. Hydrogen Energy 37 (2012) (2012) 18927–18936.
[10] C. Liu, K. Aika, Ind. Eng. Chem. Res. 43 (2004) 7484–7491.
[11] P. Hohenberg, W. Kohn, Phys. Rev. 136 (1964) B864–B871.
[12] W. Kohn, L. Sham, Phys. Rev. 140 (1965) A1133–A1138.
[13] S. Bahn, K. Jacobsen, Comput. Sci. Eng 4 (2002) 56–66.
[14] J. Mortensen, L. Hansen, K. Jacobsen, Phys. Rev B: Condens. Matter 71 (1-11) (2005) 035109.
[15] P. Blochl, Phys. Rev. B: Condens. Matter 50 (1994) 17953–17979.
[16] M. Dion, H. Rydberg, E. Schroder, D. Langreth, B. Lundqvist, Phys. Rev. Lett. 92 (1-4) (2004) 246401.
[17] H. Monkhorst, J. Pack, Phys. Rev. B: Condens. Matter 13 (1976) 5188–5192.
[18] P. Maragakis, S. Andreev, Y. Brumer, D. Reichman, E. Kaxiras, J. Chem. Phys. 117 (2002) 4651–4658.
[19] C.J. Cramer, Essentials of Computational Chemistry, second ed., 2004, Wiley. ISBN: 978-0-470-09182-1; A.L. Ammitzbøll, S. Lysgaard, A. Klukowska, T. Vegge, U.J. Quaade, J. Chem. Phys. 138 (2013) 164701-1–164701-6.
[20] C. Liu, K. Aika, Ind. Eng. Chem. Res. 43 (2004) 6994–7000.

Paper III

Designing Mixed Metal Halide Ammines for Ammonia Storage Using Density Functional Theory and Genetic Algorithms

Peter Bjerre Jensen, Steen Lysgaard, Ulrich J. Quaade and Tejs Vegge

PAPER

Designing mixed metal halide ammines for ammonia storage using density functional theory and genetic algorithms†

Peter Bjerre Jensen,[ab] Steen Lysgaard,[a] Ulrich J. Quaade[c] and Tejs Vegge*[a]

Metal halide ammines have great potential as a future, high-density energy carrier in vehicles. So far known materials, *e.g.* $Mg(NH_3)_6Cl_2$ and $Sr(NH_3)_8Cl_2$, are not suitable for automotive, fuel cell applications, because the release of ammonia is a multi-step reaction, requiring too much heat to be supplied, making the total efficiency lower. Here, we apply density functional theory (DFT) calculations to predict new mixed metal halide ammines with improved storage capacities and the ability to release the stored ammonia in one step, at temperatures suitable for system integration with polymer electrolyte membrane fuel cells (PEMFC). We use genetic algorithms (GAs) to search for materials containing up to three different metals (alkaline-earth, 3d and 4d) and two different halides (Cl, Br and I) – almost 27 000 combinations, and have identified novel mixtures, with significantly improved storage capacities. The size of the search space and the chosen fitness function make it possible to verify that the found candidates are the best possible candidates in the search space, proving that the GA implementation is ideal for this kind of computational materials design, requiring calculations on less than two percent of the candidates to identify the global optimum.

1. Introduction

Ammonia is one of the most important chemicals produced, making it possible for the world's population to grow dramatically, because of its use in fertilizers.[1] There is, however, also an interest in using ammonia as a future energy carrier in vehicles[2–6] and as an ammonia reservoir for the selective catalytic reduction (SCR) of NO_x gases in diesel cars and trucks;[7] a segment in rapid growth, in *e.g.* Asia that has large, unresolved challenges for urban pollution.[8] The toxicity of ammonia is, however, a major drawback, making handling and storing difficult. It has been shown that storing ammonia in metal halide ammines can be both safe, by lowering the vapor pressure significantly, and inexpensive.[2,9] One of the most studied metal ammines is $Mg(NH_3)_6Cl_2$,[9,10] which has a high hydrogen density, displays good kinetics,[11,12] but has an unpractical multi-step release occurring at too high temperatures (450 K, 585 K and 680 K).[9,10] Also $Sr(NH_3)_8Cl_2$ displays a high energy density, but depending on the reaction conditions a mono- or diammine is generally too stable, making the practically available ammonia density at least 12.5% lower.[13] Because of this, new materials with high storage capacities, releasing all ammonia, preferably in one step, are needed.

For energy storage for transportation usage, it is possible to burn the stored ammonia in an internal combustion engine,[14] but this will not reduce the pollution and climate challenges. The energy should therefore be extracted using a fuel cell, which can either run directly on ammonia in a high temperature SOFC,[15] in a direct ammonia fuel cell (DAFC) operating at intermediate temperatures,[16] or decomposed, and the hydrogen can then be used in a low-[17] or high temperature PEMFC,[18] which is a much more mature fuel cell technology. If the ammonia is decomposed and used in the PEMFC, there will be energy losses in form of waste heat from both processes – this waste heat can be used to release the stored ammonia making the total system efficiency higher.[2] Ultimately the success of energy storage materials depends on the usable energy density, therefore we search for materials releasing all the stored ammonia in one step, with the highest possible weight percent.

Here, we use computational methods to search for new materials because the potential phase space of mixed metal halide ammines is very large, thus experimentally testing all compounds is not practically feasible. We use van der Waal's corrected density functional theory (DFT) calculations (vdW-DF)[19–21] to obtain predictive accuracy on the formation enthalpies. DFT is

a Department of Energy Conversion and Storage, Technical University of Denmark, Frederiksborgvej 399, DK-4000 Roskilde, Denmark. E-mail: teve@dtu.dk; Fax: +45 4677 5858; Tel: +45 4677 5818

b Center for Atomic-scale Materials Design, Technical University of Denmark, Fysikvej 311, DK-2800 Kgs. Lyngby, Denmark. E-mail: pbjen@dtu.dk

c Amminex Emmisions Technology A/S, Gladsaxevej 363, DK-2860 Søborg, Denmark. E-mail: ujq@amminex.com

† Electronic supplementary information (ESI) available. See DOI: 10.1039/c4cp03133d

19732 | *Phys. Chem. Chem. Phys.*, 2014, **16**, 19732–19740

This journal is © the Owner Societies 2014

however still a relatively computationally expensive method, which sets a limit on how many structures can be studied, and in how great detail each structure can be studied. Therefore, we are employing a template based screening, where the calculations are performed on structures in known crystal symmetries, which will allow us to investigate electronic trends, selecting materials with improved characteristics, which can then undergo a more detailed computational and experimental investigation. The applied structural templates for the DFT calculations must capture the local coordination well in order to be able describe relative energy differences in the range of only a few kJ mol^{-1}, as discussed previously for related coordination complexes.[22,23]

It has been shown that it is possible to form multiple stable mixtures, *e.g.* of alkaline-earth chlorides and bromides, both mixing the halides and the metals, resulting in new stable materials with changed ab- and desorption characteristics, which are *not* simply the average of the pure metal ammines in the mixture.[24] In this work, we identify a number of new, promising mixed metal halide ammines combining a range of different metals and halides for applications as energy carrier in the transportation sector, which first of all requires that the ammonia/energy density is high to be competitive with existing liquid fuels. Furthermore, the elements used should be earth abundant, and thereby also cheaper, and the possible toxicity should be manageable – both during normal operation and in case of traffic accidents. From a practical point of view, a material releasing all stored ammonia in one step is preferred in order to be able to release the stored ammonia fast and in a steady stream when needed. A one-step release in a predefined temperature interval is thus the target of the screening and an analysis of possible intermediate phases is therefore also performed before selecting the most promising candidates. We use the magnesium chloride system[9,10] as a model, since a one-step release is more probable in mixed metal halide hexa ammines than octa ammines.

We study materials with a maximum of three different metals in a unit cell containing four metals in total. The allowed metals are alkaline-earth (except Ra) and the 3d and 4d transition metals (except Tc). Because large quantities of materials are needed for automotive applications, earth abundant and non-expensive materials are needed; we have therefore introduced a maximum limit of 25% of expensive metals, defined as Nb, Sc, Ag, Pd, Rh, Ru and Be.[25] On the halide side, we allow a maximum of two different of the halides Cl, Br and I at a time, since it is practically difficult to synthesize compounds with multiple halides.[26] Fluorides are excluded from the search given the very limited commercial interest due to their toxicity.[27]

Since the screening is based on template structures, atomic permutations within a specific stoichiometry are not considered explicitly, and structures with the same composition are treated as identical. For a given crystal structure of a mixed metal halide ammine, this is not necessarily correct, but sufficient to investigate *e.g.* electronic trends systematically. In total, this results in a search space containing almost 27 000 possible mixtures resulting in 54 000 possible structures to test, as both the energy of the hexa ammine and the empty salt have to be calculated.

This large, but not intangible number of combinations of metals and halides, is ideal for testing our genetic algorithm (GA),[28–35] an evolutionary guided search technique, which we have earlier successfully implemented to predict the optimal structure of nano particles,[36] since it enables an absolute validation of the ability of the algorithm to identify the most fit materials combinations. The proposed algorithm implementation is part of the Atomic Simulation Environment (ASE), which is freely available at https://wiki.fysik.dtu.dk/ase/.

2. Methods

2.1 Calculation details

We use DFT calculations[19,20] to determine the thermodynamic properties of the observed mixed metal halide ammines. The calculations are performed within the ASE framework[37] using the Grid-based Projector Augmented Wave method (GPAW);[38] a real space implementation of the PAW method.[39] We use the PBE (Perdew, Burke and Ernzerhof) exchange–correlation functional[40] for structural optimizations of reference structures, which gives good geometries,[41] and use the computationally more expensive vdW-DF functional[21] for single point energy calculations on the optimized structures. The vdW-DF functional accounts for dispersion and van der Waal's forces, which are essential to describe the metal halide ammines, containing a large amount of hydrogen bond donors (N–H) and acceptors (X^{-}). The Brillouin-zone is sampled using a Monkhorst–Pack grid[42] with at least 25 k-points Å^{-1} in each direction, the grid spacing is 0.18 Å and all crystal reference structures are allowed to relax the atomic coordinates by a quasi-Newton type optimization algorithm[43] using the calculated DFT forces. The energy of NH$_3$(g) is calculated by placing a molecule in a cube with a side length of 8 Å and using the same grid spacing as above.

The data set of pure metal halide reference energies is calculated by substituting the metals and halides into the optimized experimental magnesium chloride structures and subsequently the cell is allowed to relax hydrostatically, thereby keeping the symmetry. The enthalpies of desorption for the mixed ammines are calculated as the difference between the absolute electronic energies of the mixed hexa ammines and the salts including the gas-phase energy of the released ammonia molecules. The desorption temperatures are determined using a standard entropy value of 230 J (mol K NH$_3$)$^{-1}$ which is a representative average value observed for the pure metal halide ammines,[44] and the van't Hoff equation to calculate the temperature at which the equilibrium pressure, p_{eq}, reaches 10^5 Pa (1 bar) for a given reaction, *e.g.* a full one step release from a mixed metal halide ammine: Sr$_2$Mg$_2$(NH$_3$)$_{24}$Cl$_8$(s) → Sr$_2$Mg$_2$Cl$_8$(s) + 24NH$_3$(g).

The GA implementation described in the following is closely coupled to the Computational Materials Repository (CMR),[45] an open source database implementation for electronic structure calculations. All structures are stored and retrieved from the database during the genetic algorithm run. This has several advantages including easy monitoring and post-processing of

the data, reuse of already calculated data (both from the current and old GA runs) and easy sharing among colleagues. All of this can be done both from a web interface or locally using scripting.

2.2 Genetic algorithm setup

Genetic algorithms are evolutionary guided searches that work by breeding on a population of individuals to create new and hopefully better offspring; the best, or most 'fit', of these will then be mated with each other. This is parallel to natural evolution, and has been proven to be useful for search and optimization in many different scientific disciplines.[29] Brute force screening is often the only alternative, but for large search spaces it is not possible to calculate the fitness of all individuals. The search space investigated in this work with around 54 000 structures is on the verge of what can be done with the currently available computational power, requiring millions of CPU hours – however, the ultimate goal is to investigate lower dopant concentrations, which require bigger unit cells, thereby increasing both the total number of combinations and the computational time needed to calculate the fitness of each individual. Just doubling the unit cell to eight metal atoms, increases the search space drastically, making it unfeasible to tackle with brute force screening.

The efficiency and success of a GA run depends explicitly on the choice of fitness function and crossover/permutation operators. Multiple aspects can be included in the fitness function, but it is challenging to determine the relative weights of different components. Because of this, a better choice is often to choose a single parameter as the fitness function, and then set up extra rules, which determines if a new trial structure is accepted for further progress. It is important to notice that such rules do not guide the search directly, because the selection of parent structures for a new generation is solely dependent on the fitness where only the individuals with highest fitness are selected; however the rules determines where *not* to search. In addition to these rules determining what is accepted, one can post-process the datasets generated, and rank the evaluated structures according to other criteria, *e.g.* price or expected desorption temperatures, which might be relevant for specific applications. This can be useful for identifying the scientific optimal mixtures, and then afterwards determine which of these would have commercial interest. Here, we apply a simple fitness function, which is simply the weight percent of hydrogen in the material (wH) combined with selection rules setting the relevant formation enthalpy and stabilities (see below), because these are ultimately the most important factors in determining whether a material is interesting for use as an energy carrier in the transportation sector. This wH-fitness also give us the opportunity, to validate the GA predictions and test whether structures potentially could be better than those found by the algorithm, as the maximum wH value can be calculated easily.

We have chosen two criteria for determining whether a structure is accepted in the population – namely that it should be stable against decomposition into the simple metal halides salts and ammines (*e.g.* $Mg_3Be(NH_3)_{4x}Cl_8 \rightarrow 3Mg(NH_3)_xCl_2 + Be(NH_3)_xCl_2$, for $x = 0, 6$) and have an acceptable ammonia desorption temperature. Given the use of predefined template

structures, we also include marginally unstable mixtures (up to 0.5 eV per formula unit containing one metal atom) in order not to exclude candidates that may potentially display stability following full relaxation of all structures. For ΔH, we have chosen an interval from 35 to 55 kJ $(mol\ NH_3)^{-1}$ per released ammonia molecule, which corresponds to a release temperature of approximately 260 to 410 degrees Kelvin, by using the van't Hoff equation and the representative entropy value of 230 J $(mol\ K\ NH_3)^{-1}$. Small variations in the reaction entropies for different metal halides are observed,[44] so the estimated release temperatures have higher uncertainty than the reaction enthalpies. Calculating the reaction entropy changes for all the mixtures is, however, not computationally feasible in a screening study of this size, so one have to remember this uncertainty, which we do by screening a relatively broad temperature interval. The chosen temperature range is suitable for system integration with both low- and high temperature PEMFC[16] and is generally chosen to be sufficiently broad to avoid de-selection of potential candidate materials. For offspring creation, we allow a slightly broader region, by allowing parents with ΔH outside the interval, with an exponentially decreasing probability, since chemically closely related structures can have correlated binding characteristics, and thereby a child of parents on the border of the interval, might likely end up being inside the interval. Parents outside the region are selected with an exponentially decreasing probability fitted to be 25% for being 3 kJ $(mol\ NH_3)^{-1}$ and 1% for being 10 kJ $(mol\ NH_3)^{-1}$ off, respectively.

The initialization of the algorithm is done by generating 15 random mixed metal halide ammines (*individuals*) from the defined phase space. This population size is chosen so that it is large enough to ensure that the algorithm does not end up in a local, pre-converged optimum. On the other hand the population size should not be too large, as this would result in wasting time by testing too many structures. As a general rule of thumb, the population size, S, should be in the range $\log_2(N) < S < 2\log_2(N)$, where N is the total number of combinations in the search space.[46] The following generations are created by selecting some of the best known candidates from the current population, as parents and using the standard operators of GAs, namely crossover and mutation (Fig. 1).[29] The crossover is picking a random point at the atoms list, which is specifying the constituents of the two parents, and taking the part before the cut from the first parent and the last part from the other parent.

We apply the following mutation operators:

(1) *Random mutation*: picking one element and substituting it to another chosen randomly.

(2) *Neighbor mutation*: one random element is exchanged for one of its neighbors in the periodic table (up, down, left or right).

(3) *Complete mutation*: to prevent the algorithm from getting stuck in local minima, we also use a complete mutation random operator, which generates a new structure without using any information from the current population (similar to creating the structures in the initial population).

As a further precaution, to ensure not ending up in a pre-converged state, parents are not only selected from the current
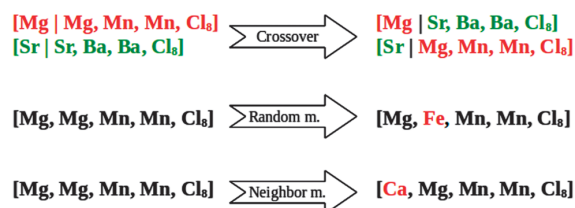
Fig. 1 Illustration of the different operators acting on random input strings.

population, but a small number of parents are selected with a probability dependent on their fitness, no matter if they are part of the current population or not. More specifically, three out of 15 individuals are selected from all tested structures with a probability equal to

$$\frac{\exp\left(\dfrac{\text{fitness}}{\text{best}_{\text{fitness}}}\right) - 1}{e - 1} \qquad (1)$$

where $\text{best}_{\text{fitness}}$ is the fitness of the best structure seen so far.

This type of coordination compounds often display correlations between different mixtures and local operators (crossover and the neighbor mutation) are therefore expected to be more important for the efficiency of the search than random operators. We therefore employ a $3:1$ ratio between them, indicating that local operators are used three times more frequently than random operators. Within the local operators, twice as many crossovers as neighbor mutations, and within the random operators we use the random mutation three times more than the complete mutation operator. To determine when the algorithm is converged, *i.e.* when it is not expected that further progress would create better offspring, the algorithm keeps track of whether new stable individuals, with ΔH in the specified interval, are entering the population; more specifically the convergence criteria is set to be that the five best structures remain unchanged for five generations.

2.3 Template based screening

As mentioned in the introduction, magnesium chloride can store six ammonia molecules per metal atom, corresponding to 9.2% stored hydrogen by weight (wH). Here, we focus on the metal halide hexa ammines although certain metal halides are known to form octa ammines.[13,44] This is done because metal halides forming octa ammines are generally heavier and more prone to multi-step release, and multiple metal halides are known to form hexa ammines and share simple crystal symmetries, *e.g.* $MgCl_2$, $NiCl_2$, $FeBr_2$ and CrI_2,[10,47] with potential of having a high weight percent. Since all the stored ammonia in $Mg(NH_3)_6Cl_2$ is not accessible at relevant temperatures, we direct the search towards a one step release at an acceptable temperature between 260 and 410 degrees Kelvin. Using the template structure for all candidates provides an estimate of how the mixed systems will behave and especially the relative stabilities and desorption enthalpies are expected to be correctly determined. A range of the generated structures will exist in other crystal structures, but we expect that

the error would be comparable in the salt and the hexa ammine, resulting in an unchanged ΔH, which is one of the important selection criteria.

All single metal halides, *i.e.* consisting of only one metal atom and one halide in the ratio $1:2$, are calculated as reference structures for the GA search. This is done for completeness although it is known that not all can form stable hexa ammines, *e.g.* $TiCl_2$, where only a tetra ammine has been observed[48] and $SrCl_2$ since strontium is big enough to coordinate eight ammonia molecules.[13] The last fact is taken into account in our screening, when determining the stability of the mixed hexa ammine, where it is possible that mixtures split up to a mixture of single metal hexa and octa ammines. To determine whether it would split up to some octa ammine, we have also calculated all pure reference structures in the strontium octa ammine structure, and thereby determined whether the system prefers to be an octa ammine or a hexa ammine and two free ammonia molecules in the gas phase (Fig. 2). The octa ammine is actually only preferred for a small number of the investigated metals, where mainly alkaline-earth metals containing *e.g.* Ca, Sr or Ba would split up to some octa ammine and some pure salt, resulting in that the stability of *e.g.* $SrMg(NH_3)_{12}Cl_4$ would be calculated relative to $(3Sr(NH_3)_8Cl_2 + SrCl_2)/4$ and $Mg(NH_3)_6Cl_2$. The decomposition energy is always calculated relative to the most favorable way of splitting up the constituents, which especially is relevant when the mixture contains both different anions and cations.

Another advantage of using the magnesium system is that the hexa ammine crystallizes in the relatively simple K_2PtCl_6 cubic structure, containing four metal atoms per unit cell,[49,50] which makes it ideal for this screening. The magnesium chloride salt crystallizes in the trigonal $P\bar{3}m1$ space group (# 164), normally referred to as the layered $CdCl_2$ structure.[51] After the GA run, a stability check is also performed on the mono- and diammines of the best compounds to determine whether the release of ammonia is a one step reaction. Here, we define that the mono ammine is observed if the desorption enthalpy for going from the hexa ammine to the mono ammine is more than 2 kJ $(\text{mol } NH_3)^{-1}$ lower than for going directly to the salt; the same considerations holds for determining the existence of a diammine. The presence of intermediate ammine phases lower the amount of available hydrogen and the fitness is lowered accordingly. The structure used in order to determine the existence of the mono ammine phase is similar to the one proposed in ref. 10, which, when minimized, has orthorhombic *Pbnm* symmetry (space group # 62). The diammine is based on the magnesium structure,[52] which when relaxed has an orthorhombic *Ccme* symmetry (space group # 64).

To set up a new mixed structure (example shown in Fig. 3), the atoms are substituted into the template structures, and the following parameters are set: the volume is set as the average volume of the constituents, and the metal to nitrogen distances are set for each metal, using the values calculated for the pure reference structures (for details, see Section 2.1). The chosen structures are therefore not necessarily the thermodynamic
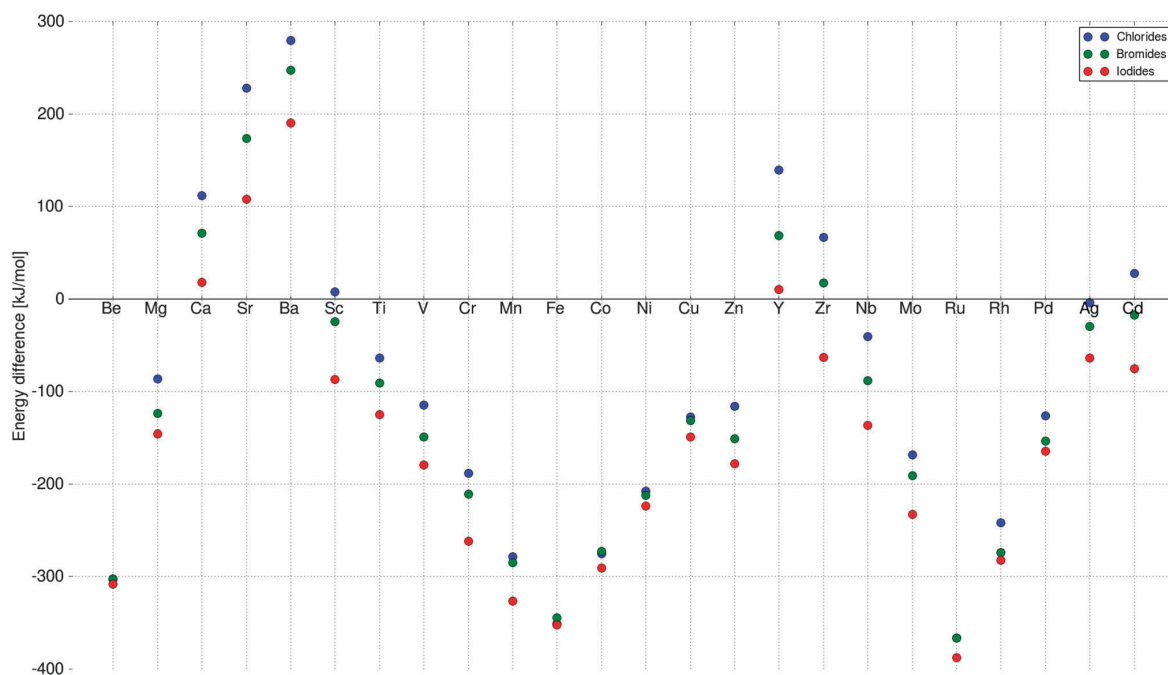
This journal is © the Owner Societies 2014

Phys. Chem. Chem. Phys., 2014, **16**, 19732–19740 | **19735**

Fig. 2 Stability of octa *vs.* hexa + $2NH_3(g)$. If energy > 0 octa is preferred.
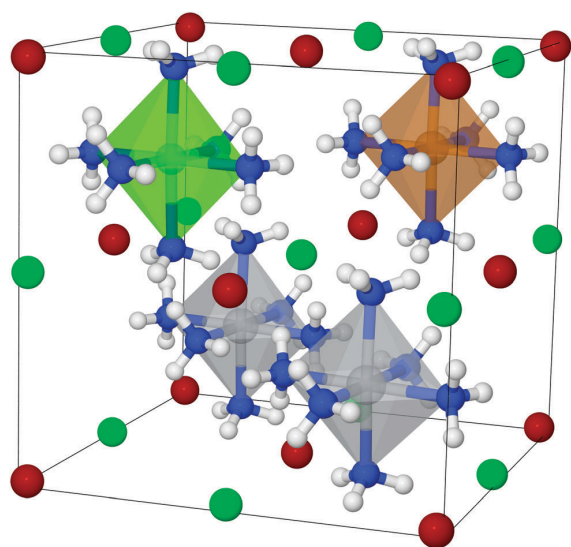
Fig. 3 Example of a mixed hexa ammine, $Ti_2CuMgCl_4Br_4$, in the cubic structure. Metals are centered in the polyhedra surrounded by ammonia molecules, Ti is depicted gray, Mg light green, Cu brown, Cl green, Br dark red, N blue and H white.

ground state structures, since it is simply not feasible to make computationally intense structural optimizations of all the structures during a GA run, and as explained previously, it is expected that the template structures will give reasonable estimates of desorption enthalpies.

3. Results and discussion

3.1 Visiting relevant parts of the search space

To test the efficiency of the GA search, the algorithm was started three times with the specified parameters, starting from three randomly chosen and thereby different initial populations (for details, see Table S1, ESI†). The algorithm progresses very similarly for the three different runs and ends up finding optimal mixtures with similar fitness and composition (Fig. 4). In Fig. 5, the fitness (wH) for all the potentially stable mixtures that are tested by the algorithm are plotted against the desorption enthalpies. As can be seen from the figure, the full interval of allowed desorption enthalpies does not appear to be sampled equally, which might be due to

Fig. 4 Fitness (hydrogen weight percent, wH) of the best individual as a function of generation number. As indicated by a dotted line, the 1st run was continued for a longer time to test the convergence, as described in the performance section.

19736 | *Phys. Chem. Chem. Phys.*, 2014, **16**, 19732–19740

This journal is © the Owner Societies 2014

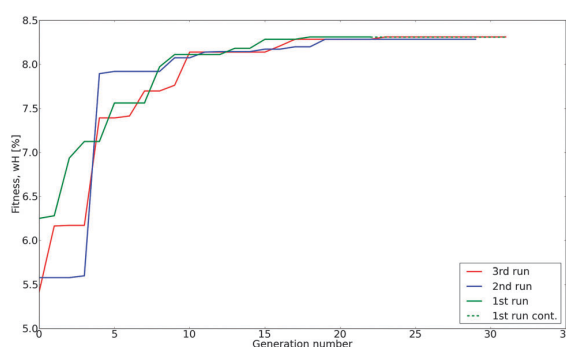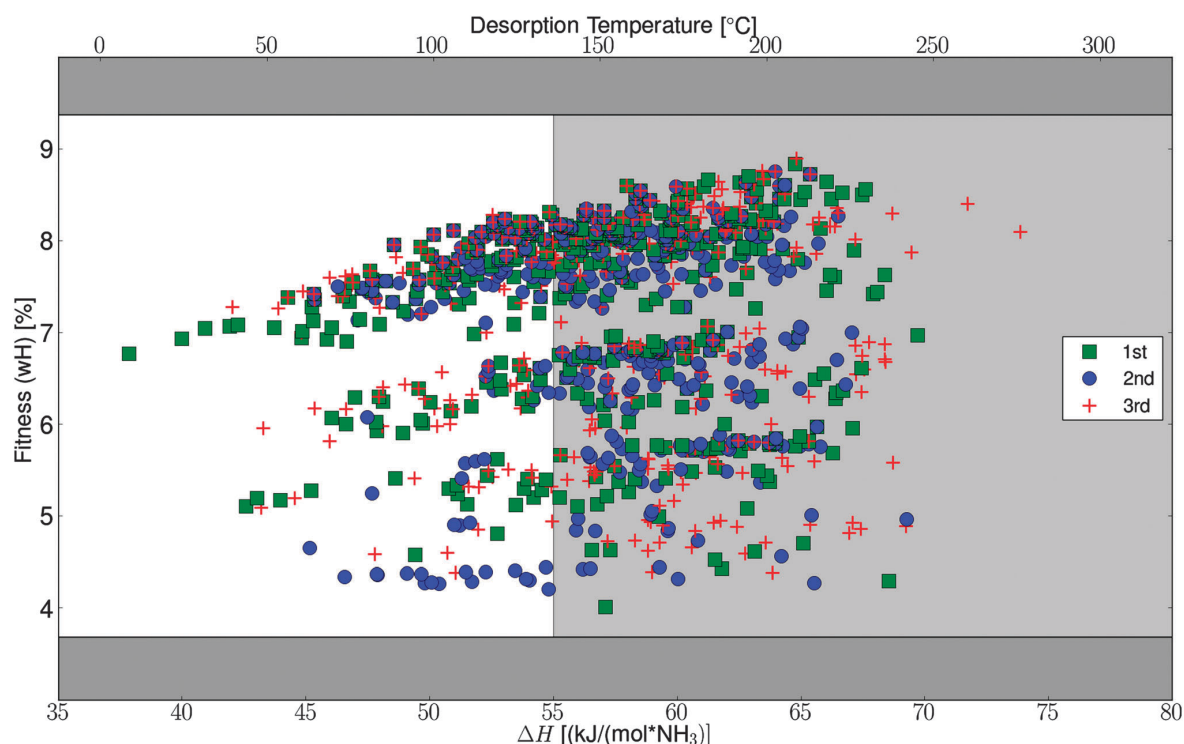**Fig. 5** Visited parts of search space, for all the three runs. The dark gray area indicates wH not accessible within the defined search space. The white window indicates structures with acceptable release temperatures. Only structures which fulfill the decomposition stability criteria are shown.

the fact that light mixtures, with high fitness, simply bind the ammonia harder. It should be stressed that the full interval is allowed in the algorithm runs, it is simply an observation that the generated mixtures have ΔH values in the high end of the interval.

3.2 Optimal identified structures

Several materials have been found with a high fitness (hydrogen weight percent, wH) as can be seen in Table 1 showing the top ten structures for the three different runs. As explained in Section 2.2, the structures allowed in the population all satisfy the requirements of having acceptable desorption enthalpies and being stable or marginally unstable against decomposition. The structures

which are strictly stable against all decomposition reactions are highlighted in the table, as they naturally are the most interesting structures. As can be seen, the algorithm is able to find the same relevant structures, from three random start populations, with the selected parameters proving that the concept, in this case can be used without rerunning the algorithm, however for other systems this should be tested (pure $TiCl_2$, which was found only the 2nd run, does not form hexa ammines as described earlier).

As can be seen in Table 1, there is a high dominance of titanium rich structures, which is not surprising because it is one of the lightest elements in the search space, and apparently the mixtures have a relatively low ΔH resulting in acceptable

Table 1 Optimal structures with the highest fitness (hydrogen weight percent, wH), from three different runs, starting from random initial populations. The structures in bold are structures that are strictly stable against decomposition in both phases

1st run		2nd run		3rd run	
Structure	Fitness (wH)	Structure	Fitness (wH)	Structure	Fitness (wH)
TiScTiCaCl8	8.31	**TiTiCuMgCl8**	**8.28**	CaTiTiScCl8	8.31
TiTiCuMgCl8	**8.28**	ScTiTiTiCl8	8.24	**CuTiTiMgCl8**	**8.28**
TiTiTiScCl8	8.24	**TiTiTiTiCl8**	**8.21**	ScNiCaCaCl8	8.28
TiScTiVCl8	**8.21**	**ScTiTiVCl8**	**8.21**	TiTiTiScCl8	8.24
TiScTiCrCl8	8.20	ScTiTiCrCl8	8.20	CaTiCuCaCl8	8.21
TiTiTiVCl8	**8.18**	**TiTiVTiCl8**	**8.18**	**TiTiVScCl8**	**8.21**
TiTiTiCrCl8	8.17	TiTiTiCrCl8	8.17	CrTiTiScCl8	8.20
ScCuCuMgCl8	**8.17**	**ScCuCuMgCl8**	**8.17**	**VTiTiTiCl8**	**8.18**
VTiTiVCl8	8.15	TiVVTiCl8	8.15	CrTiTiTiCl8	8.17
VTiTiCrCl8	8.14	TiVTiCrCl8	8.14	**ScCuCuMgCl8**	**8.17**

This journal is © the Owner Societies 2014

Phys. Chem. Chem. Phys., 2014, **16**, 19732–19740 | **19737**

release temperatures. The top four stable candidates, $Ti_2CuMgCl_8$, Ti_2ScVCl_8, Ti_3VCl_8 and $ScCu_2MgCl_8$, have predicted release temperatures of 136, 130, 130 and 130 °C respectively, and furthermore both the ammines and the salts are stable against decomposition. Especially $Ti_2CuMgCl_8$ and $ScCu_2MgCl_8$ are predicted to be very stable compared to having the pure metal halide ammines and salts separated (for details, see Table S2, ESI†).

3.3 Genetic algorithm performance

We have made a more detailed analysis of the convergence of the algorithm, which will be described in this section. In general it is found that the chosen convergence criteria and suggested operators are ideal for this kind of template based screening. The general suggestion from the analysis is that rerunning the algorithm multiple times, to ensure finding the global optimum, is preferred over changing the convergence criteria or increasing the populations size – this is further favored in our setup where we reuse data from earlier algorithm runs as described in Section 2.1. The importance of reusing data has been observed already from the 2nd run where 21% of the calculations are skipped, and for the 3rd run 34% was reused; these numbers is only counting reuse from the original part of the first run, not including the extra convergence test. These numbers support the general suggestion about rerunning instead of changing the convergence criteria or increasing the populations size.

As mentioned, the algorithm succeeds in finding the same optimal structures, from three random start populations, which is very interesting. In general, the algorithm needs approximately ten generations before it ends up in the area with the optimal elements and high fitness, no matter where it starts (Fig. 4). After this initial narrowing, the algorithm only makes slight improvements from generation to generation, where more and more optimal candidates are seen, but the maximum is not changing much. The observed jumps in the fitness function in the first part of the search, can also be seen in Fig. 5, where the searched parts of space are organized in almost horizontal bands, in between which not much have been tested. These bands represent use of different halides or mixtures thereof.

To test the chosen convergence criteria, *i.e.* that the five best structures are constant for five generations, the first run was continued until a new structure entered the population (Fig. 4). The original run fulfilled the convergence criteria after generation number 22, and almost 50% longer run time was necessary to find a new candidate in generation 31. As a result, we conclude that our convergence criteria are well chosen, and it is generally better to rerun the algorithm for different starting populations, to ensure that the algorithm searches in a different parts of the search space. The extra candidate found in the extension of the first run was $TiCaCuCaCl_8$ which entered as the 4th best structure with fitness, wH = 8.21, however the hexa ammine is slightly unstable with a decomposition energy of 27 kJ mol^{-1} per formula unit containing one metal atom. A possible explanation for not observing the calcium containing structures in all the different runs, is that calcium structures in general have too high ΔH values, and therefore have a very low probability of being selected
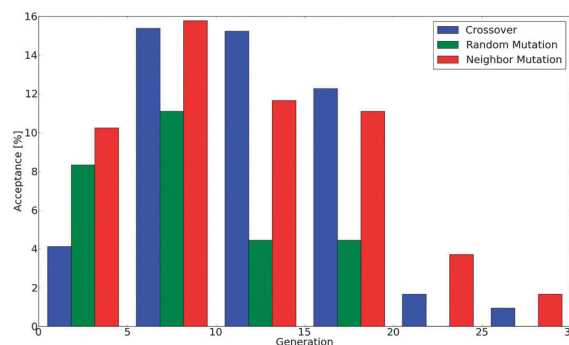

Fig. 6 Operator success during the three algorithm runs. Success is defined as generating an individual with higher fitness, which furthermore obeys the additional rules on ΔH and stability.

for offspring creation. Furthermore, the decomposition energy is calculated relative to the calcium chloride octa ammine, which is known to be more stable than a hexa ammine (Fig. 2), requiring the mixed hexa ammine to be very stable.

Different kinds of operators are available for generating new offspring and we tested whether all the used operators are relevant and equally important for finding the optimal solution (Fig. 6). The crossover operator behaves as expected, where it initially has a relatively low success rate, because the components it mixes are not the optimal one; in the middle it has a maximum, where it directs the search by combining better and better building blocks, and later on the success rate drops again. The chemical neighbor operator does generally have a high success rate and seems to be very important, to guide the search. The mutation operator has the lowest success rate, which probably is because the fitness function is the weight percent, which gets harder and harder to optimize, when substituting in a random element. If one would continue with this fitness function it might be suggested to lower the rate of random mutations as a function of time, however, if other fitness functions are used this is probably not advisable. In our earlier work with use of GAs[36] we argued that dynamically operators are more efficient for optimization of nano particles, but this does not seem to be important for the template based screening performed here.

3.4 Global optimum

A validation of the method and the results can be performed because the weight percent is chosen as the fitness, since it is possible to determine which structures in the search space have a higher weight percent and could potentially have acceptable stabilities and release temperatures. It turns out that only 253 structures in the search space would have a higher weight percent than the best candidate, $Ti_2CuMgCl_8$, found by all of the three runs, and 83 of these have already been tested by the three runs, leaving us with 170 candidates. Because it is this very limited number of structures, we manually tested all of these candidates. None of these structures were found to have acceptable ΔH and fulfill the stability criteria. This demonstrates that

the global optimum structure was found by the algorithm in all three GA runs, thereby proving that the suggested algorithm is very efficient.

Only ~ 400 out of the $\sim 27\,000$ structures were tested on average for a genetic algorithm run in this search space. The top-down validation approach is naturally only possible in this special case because of the simple fitness function. The goal of a screening is often to find multiple candidates, which would favor the use of the genetic algorithm; in this specific example it would require 253 calculations to get the best, 337 to get top two, 372 to get top three and 401 to get top four, which is more than the average length of one run, which in all cases find the top four candidates. Furthermore, the GA would also find stable structures, with lower, but still high wH, which is a lot better than the top-down approach leaving us with only one to four stable structures.

3.5   Check on possible intermediate ammine phases

For the best candidates in Table 1, we also tested whether a mono- or diammine would be observed, as this might result in a multi-step release, possibly lowering the available energy density (details in Table S2, ESI†). As a result of this analysis some of the suggested candidates are found not to be interesting, due to slightly unstable mixed phases. However, intermediate ammine phases are not expected for the three out of the four best materials, Ti_2ScVCl_8, Ti_3VCl_8 and $ScCu_2MgCl_8$, further verifying, that they are indeed interesting candidates for new improved materials. From these extra checks it was found that $Ti_2CuMgCl_8$, would have a stable diammine, lowering the practical amount of ammonia, and releasing the last two ammonia molecules at high temperatures ($>200\ ^\circ C$). Again, it must be stressed that we are doing template based screening and it could still be interesting to test all compounds for completeness. When disregarding the unstable mixtures, we are left with compounds which are titanium-rich. It has been shown that similar mixtures are synthesizable, *e.g.* $TiMgCl_4$,[53] and pure titanium(II) chloride has been observed in the $MgCl_2$ structure,[54] which indicates that the suggested materials can be synthesized, and the templates used should give accurate energies.

4.   Conclusion

By using genetic algorithms combined with vdW-DF density functional theory calculations, we have identified a number of new, mixed metal hexa ammines with hydrogen storage capacities in excess of 8 wt% and excellent desorption characteristics, releasing all the ammonia in one step at temperatures relevant for HT-PEMFC applications. The most promising candidates are currently investigated further, both computationally and experimentally. The developed methods, which have been shown to be able to find the global optimum, testing a very limited number of structures (less than two percent of the total number of combinations), are easy transferable to other searches, with different search parameters, possibly including more intermediate phases, which we are currently investigating.

Acknowledgements

References

1 V. Smil, *Nature*, 1999, **400**, 415.
2 A. Klerke, C. H. Christensen, J. K. Nørskov and T. Vegge, *J. Mater. Chem.*, 2008, **18**, 2304–2310.
3 C. H. Christensen, T. Johannessen, R. Z. Sørensen and J. K. Nørskov, *Catal. Today*, 2006, **111**, 140–144.
4 D. Chakraborty, H. N. Petersen, C. Elkjær, A. Cagulada and T. Johannessen, *Fuel Cells Bull.*, 2009, **2009**, 12–15.
5 R. Lan, J. T. S. Irvine and S. Tao, *Int. J. Hydrogen Energy*, 2012, **37**, 1482–1494.
6 F. Schüth, R. Palkovits, R. Schlögl and D. S. Su, *Energy Environ. Sci.*, 2012, **5**, 6278–6289.
7 T. D. Elmøe, R. Z. Sørensen, U. Quaade, C. H. Christensen, J. K. Nørskov and T. Johannessen, *Chem. Eng. Sci.*, 2006, **61**, 2618–2625.
8 U. S. Energy Information Administration, *International Energy Outlook 2013*, 2013.
9 C. H. Christensen, R. Z. Sørensen, T. Johannessen, U. J. Quaade, K. Honkala, T. D. Elmøe, R. Køhler and J. K. Nørskov, *J. Mater. Chem.*, 2005, **15**, 4106–4108.
10 R. Z. Sorensen, J. S. Hummelshoj, A. Klerke, J. B. Reves, T. Vegge, J. K. Norskov, C. H. Christensen, R. Z. Sørensen, J. S. Hummelshøj and J. K. Nørskov, *J. Am. Chem. Soc.*, 2008, **130**, 8660–8668.
11 H. S. Jacobsen, H. A. Hansen, J. W. Andreasen, Q. Shi, A. Andreasen, R. Feidenhans'l, M. M. Nielsen, K. Ståhl and T. Vegge, *Chem. Phys. Lett.*, 2007, **441**, 255–260.
12 A. Tekin, J. S. Hummelshøj, H. S. Jacobsen, D. Sveinbjörnsson, D. Blanchard, J. K. Nørskov and T. Vegge, *Energy Environ. Sci.*, 2010, **3**, 448.
13 S. Lysgaard, A. L. Ammitzbøll, R. E. Johnsen, P. Norby, U. J. Quaade and T. Vegge, *Int. J. Hydrogen Energy*, 2012, **37**, 18927–18936.
14 C. Zamfirescu and I. Dincer, *Fuel Process. Technol.*, 2009, **90**, 729–737.
15 G. G. M. Fournier, I. W. Cumming and K. Hellgardt, *J. Power Sources*, 2006, **162**, 198–206.
16 T. Vegge, R. Z. Sørensen, A. Klerke, J. S. Hummelshøj, T. Johannessen, J. K. Nørskov and C. H. Christensen, in *Solid state hydrogen storage: Materials and chemistry*, ed. G. Walker, British Welding Research Association, 2008, pp. 533–568.
17 B. McNicol, D. Rand and K. Williams, *J. Power Sources*, 2001, **100**, 47–59.
18 Q. Li, R. He, J. O. Jensen and N. J. Bjerrum, *Chem. Mater.*, 2003, **15**, 4896–4915.

This journal is © the Owner Societies 2014

Phys. Chem. Chem. Phys., 2014, **16**, 19732–19740 | **19739**

19 P. Hohenberg and W. Kohn, *Phys. Rev.*, 1964, **136**, B864–B871.
20 W. Kohn and L. J. Sham, *Phys. Rev.*, 1965, **140**, A1133–A1138.
21 M. Dion, H. Rydberg, E. Schröder, D. C. Langreth and B. I. Lundqvist, *Phys. Rev. Lett.*, 2004, **92**, 246401.
22 J. Voss, J. S. Hummelshøj, Z. Lodziana and T. Vegge, *J. Phys.: Condens. Matter*, 2009, **21**, 012203.
23 J. S. Hummelshøj, D. D. Landis, J. Voss, T. Jiang, A. Tekin, N. Bork, M. Dułak, J. J. Mortensen, L. Adamska, J. Andersin, J. D. Baran, G. D. Barmparis, F. Bell, a. L. Bezanilla, J. Bjork, M. E. Björketun, F. Bleken, F. Buchter, M. Bürkle, P. D. Burton, B. B. Buus, A. Calborean, F. Calle-Vallejo, S. Casolo, B. D. Chandler, D. H. Chi, I. Czekaj, S. Datta, A. Datye, A. DeLaRiva, V. Despoja, S. Dobrin, M. Engelund, L. Ferrighi, P. Frondelius, Q. Fu, A. Fuentes, J. Fürst, A. García-Fuente, J. Gavnholt, R. Goeke, S. Gudmundsdottir, K. D. Hammond, H. a. Hansen, D. Hibbitts, E. Hobi, J. G. Howalt, S. L. Hruby, A. Huth, L. Isaeva, L. Jelic, I. J. T. Jensen, K. a. Kacprzak, A. Kelkkanen, D. Kelsey, D. S. Kesanakurthi, J. Kleis, P. J. Klüpfel, I. Konstantinov, R. Korytar, P. Koskinen, C. Krishna, E. Kunkes, a. H. Larsen, J. M. G. Lastra, H. Lin, O. Lopez-Acevedo, M. Mantega, J. I. Martínez, I. N. Mesa, D. J. Mowbray, J. S. G. Mýrdal, Y. Natanzon, A. Nistor, T. Olsen, H. Park, L. S. Pedroza, V. Petzold, C. Plaisance, J. a. Rasmussen, H. Ren, M. Rizzi, a. S. Ronco, C. Rostgaard, S. Saadi, L. a. Salguero, E. J. G. Santos, a. L. Schoenhalz, J. Shen, M. Smedemand, O. J. Stausholm-Møller, M. Stibius, M. Strange, H. B. Su, B. Temel, A. Toftelund, V. Tripkovic, M. Vanin, V. Viswanathan, A. Vojvodic, S. Wang, J. Wellendorff, K. S. Thygesen, J. Rossmeisl, T. Bligaard, K. W. Jacobsen, J. K. Nørskov and T. Vegge, *J. Chem. Phys.*, 2009, **131**, 014101.
24 C. Y. Liu and K. I. Aika, *Ind. Eng. Chem. Res.*, 2004, **43**, 7484–7491.
25 www.chemicool.com, 2013.
26 S. Hodorowicz, E. Hodorowicz and H. Eick, *J. Solid State Chem.*, 1983, **50**, 180–188.
27 O. Barbier, L. Arreola-Mendoza and L. M. Del Razo, *Chem.-Biol. Interact.*, 2010, **188**, 319–333.
28 J. H. Holland, *Adaptation in Natural and Artificial Systems*, University of Michigan Press, Ann Arbor, 1975.
29 S. Forrest, *Science*, 1993, **261**, 872–878.
30 G. Jóhannesson, T. Bligaard, A. Ruban, H. Skriver, K. Jacobsen and J. Nørskov, *Phys. Rev. Lett.*, 2002, **88**, 255506.
31 T. Bligaard, G. H. Jóhannesson, A. V. Ruban, H. L. Skriver, K. W. Jacobsen and J. K. Nørskov, *Appl. Phys. Lett.*, 2003, **83**, 4527–4529.

32 L. B. Vilhelmsen, K. S. Walton and D. S. Sholl, *J. Am. Chem. Soc.*, 2012, **134**, 12807–12816.
33 L. B. Vilhelmsen and D. S. Sholl, *J. Phys. Chem. Lett.*, 2012, **3**, 3702–3706.
34 D. Teng, L. B. Vilhelmsen and D. S. Sholl, *Surf. Sci.*, 2014, **628**, 98–103.
35 L. B. Vilhelmsen and B. Hammer, *J. Chem. Phys.*, 2014, **141**, 044711.
36 S. Lysgaard, D. D. Landis, T. Bligaard and T. Vegge, *Top. Catal.*, 2014, **57**, 33–39.
37 S. R. Bahn and K. W. Jacobsen, *Comput. Sci. Eng.*, 2002, **4**, 56–66.
38 J. J. Mortensen, L. B. Hansen and K. W. Jacobsen, *Phys. Rev. B: Condens. Matter Mater. Phys.*, 2005, **71**, 035109.
39 P. E. Blöchl, *Phys. Rev. B: Condens. Matter Mater. Phys.*, 1994, **50**, 17953–17979.
40 J. P. Perdew, K. Burke and M. Ernzerhof, *Phys. Rev. Lett.*, 1996, **77**, 3865–3868.
41 P. Haas, F. Tran and P. Blaha, *Phys. Rev. B: Condens. Matter Mater. Phys.*, 2009, **79**, 085104.
42 H. J. Monkhorst and J. D. Pack, *Phys. Rev. B: Solid State*, 1976, **13**, 5188–5192.
43 P. Maragakis, S. A. Andreev, Y. Brumer, D. R. Reichman and E. Kaxiras, *J. Chem. Phys.*, 2002, **117**, 4651–4658.
44 E. Lepinasse and B. Spinner, *Int. J. Refrig.*, 1994, **17**, 309–322.
45 D. D. Landis, J. S. Hummelshoj, S. Nestorov, J. Greeley, M. Dulak, T. Bligaard, J. K. Norskov and K. W. Jacobsen, *Comput. Sci. Eng.*, 2012, **14**, 51–57.
46 J. T. Alander, *Proceedings Computer Systems and Software Engineering*, IEEE Comput. Soc. Press, 1992, pp. 65–70.
47 R. Essmann, G. Kreiner, A. Niemann, D. Rechenbach, A. Schmieding, T. Sichla, U. Zachwieja and H. Jacobs, *Z. Anorg. Allg. Chem.*, 1996, **622**, 1161–1166.
48 W. C. Schumb and R. F. Sundström, *J. Am. Chem. Soc.*, 1933, **55**, 596–604.
49 I. Olovsson, *Acta Crystallogr.*, 1965, **18**, 889–893.
50 I. Hwang and T. Drews, *J. Am. Chem. Soc.*, 2000, 8486–8489.
51 I. Bassi, F. Polato, M. Calcaterra and J. Bart, *Z. Kristallogr.*, 1982, **159**, 297–302.
52 A. Leineweber, M. W. Friedriszik and H. Jacobs, *J. Solid State Chem.*, 1999, **147**, 229–234.
53 A. Fuwa and S. Takaya, *JOM*, 2005, 56–60.
54 G. Meyer, T. Gloger and J. Beekhuizen, *Z. Anorg. Allg. Chem.*, 2009, **635**, 1497–1509.

Paper IV

Accelerated DFT-based Design of Materials for Ammonia Storage
Peter Bjerre Jensen, Agata Bialy, Didier Blanchard, Steen Lysgaard, Ulrich J. Quaade and Tejs Vegge

Accelerated DFT-Based Design of Materials for Ammonia Storage

Peter Bjerre Jensen[a,b], Agata Bialy[c], Didier Blanchard[a], Steen Lysgaard[a], Ulrich J. Quaade[c] and Tejs Vegge*[a]

Future energy carriers are needed in order to lower the CO_2 emissions resulting from the burning of fossil fuels. One possible energy carrier is ammonia, which can be stored safely in metal halide ammines; however, the release often occurs in multiple steps at too high temperatures. Therefore, there is a need for new materials, releasing the ammonia in a narrow temperature interval, determined by the specific application. To search for new mixed metal halide chlorides, with superior storage properties we use DFT calculations guided by a genetic algorithm (GA) to expedite the search, as the defined search space allowing up to three different metals (alkaline-earth, 3d and 4d) is very large containing more than 100.000 different structures. Here, we search for materials releasing the ammonia between 0 and 100 °C, a temperature range suitable for system integration with low-temperature polymer electrolyte membrane fuel cells (PEMFC). In this temperature range, waste heat from the PEMFC can be used to release the stored ammonia to improve the system efficiency. The success of the implemented algorithm is verified by three trial runs capable of finding the same optimal mixtures starting from different random populations, testing < 5 % of the candidates. Some of the best candidates are already confirmed experimentally and others offer a record high, accessible hydrogen capacity exceeding 9 wt%. Three of the best materials were synthesised using spray drying and mechano-chemical synthesis, characterized structurally with X-ray diffraction and their ammonia storage properties were confirmed using temperature programmed desorption (TPD).

Introduction

Ammonia is a widely used chemical with many different applications, most importantly as the main component in fertilizers, sustaining the growth of the world's population[1]. A major drawback of ammonia is however its toxicity, requiring careful handling and storage[2]. It is well-known that pure metal halide ammines have the ability to store ammonia, and release it when heat is supplied[3,4]. These solid storage materials have been proposed as energy carriers for transportation usage[5–12] and for on-board reduction of NO_X gases from combustion processes[13]. The ammines often display good kinetics[14,15], but most of the pure metal halides release the ammonia at high temperatures and in multiple steps spread over broad temperature intervals[8,16]. Therefore, new materials with optimized release patterns are needed if ammonia should be used as a future energy carrier for transportation. A number of

mixed metal halide ammines have already been investigated, both mixing the cations and the anions[17–19], resulting in materials performing better than their individual components, encouraging the search for other mixed materials.

The search for new optimized materials described in this paper is based on the use of genetic algorithms (GAs) [20–29] in combination with accurate van der Waal's (vdW-DF) corrected density functional theory (DFT)[30–32] to predict new stable ammonia storage materials with superior storage capacities. In a previous work[20], we have demonstrated that testing less than two percent of the candidates in the search space was sufficient to identify the global optimum in a search among >27.000 structures. Furthermore, the algorithm was rerun to validate that the same candidates were identified, starting from random and thereby different initial populations. The search focused on a one-step release of all the stored ammonia at temperatures relevant for system integration with high-temperature polymer electrolyte membrane fuel cells (HT-PEMFC) using the stored hydrogen, after releasing and decomposing the ammonia.

In general, it is preferred to have a continuous release of ammonia when needed, which can either be achieved by a one-step release or a multiple-step release in a narrow temperature interval. In the present study both are allowed within a narrow temperature interval, to ensure that the release is not over a too broad temperature interval. More specifically, we screen for binary and ternary metal chloride ammines releasing the highest possible amount of ammonia between 0 and 100 °C, a temperature range suitable for low-temperature

[a] Department of Energy Conversion and Storage, Technical University of Denmark, Frederiksborgvej 399, DK-4000 Roskilde, Denmark; E-mail: teve@dtu.dk
[b] Center for Atomic-scale Materials Design, Technical University of Denmark, Fysikvej 311, DK-2800 Kgs. Lyngby, Denmark. E-mail: pbjen@dtu.dk
[c] Amminex Emmisions Technology A/S, Gladsaxevej 363, DK-2860 Søborg, Denmark; E-mail: ujq@amminex.com
* Corresponding author: Phone: +45 4677 5818, Fax: +45 4677 5858
† Electronic Supplementary Information (ESI) available: TGA measurements showing stability during cycling and detailed experimental analysis of the attempts to synthesize further candidates is presented. See DOI: 10.1039/b000000x/

PEMFC[16,33]. To ensure the prediction of the correct release pattern, a range of known pure metal halide ammines structures with different ammonia contents are included. Both octa and hexa ammines are investigated as smaller cations would normally form compact and relatively light hexa ammines, whereas larger cations form structures allowing the uptake of more ammonia to form the octa ammine, possibly resulting in high energy densities[4,12,16,19]. It is therefore expected that either the octa or hexa ammine would be observed, but mixtures thereof passing through both the hexa and octa ammine are also allowed. To determine whether the release is a multi-step reaction, the stability of possible intermediate di- and mono ammines are checked.

In this screening, 24 selected metals, the alkaline-earths (except Ra) and the 3d and 4d transition metals (except Tc), are allowed as constituents of mixtures with maximum three different metals at a time in a mixed metal chloride. Materials properties might be modified by doping with a small amount of another element, but this is computationally difficult to tackle in a screening study, as small dopant concentrations require very big unit cells with many atoms. The lowest dopant levels are therefore not investigated explicitly, and the minimum concentration of one metal is 12.5 %, resulting in a unit cell with eight metal atoms, and up to 280 atoms in total, which is the maximum feasible cell to use in a screening study of this size. Although different types of halides could be included, we are only screening for chlorides, which have been predicted to form mixed hexa ammines[20]. Furthermore, it is the lightest halide, disregarding fluorides due to their limited commercial interest, because of toxicity[34]. Another important requirement for a future energy carrier is the availability and acceptable cost of the precursors; therefore a maximum of 25 % in total of expensive metals[35], defined as Sc, Rh, Be, Ag, Zr, Ru, Nb, V, Pd, Ti and Y, is allowed. Since the screening is based on template structures, atomic permutations within a specific stoichiometry are not considered explicitly, and structures with the same composition are treated as identical. For a given crystal structure of a mixed metal halide ammine, this is not absolutely correct, but sufficient to investigate e.g. electronic trends systematically. In total, this results in more than 100.000 structures, requiring approximately ten million CPU hours if all calculations had to be performed. It is thus necessary to use a more selective approach, e.g. our GA to perform an optimized search, thereby lowering the total number of calculations that have to be performed[20].

Methods

Calculation Details

To ensure predictive accuracy of the desorption temperatures and the release patterns, we use DFT[30,31] as implemented in the Grid-based Projector Augmented Wave method (GPAW)[36], a real-space implementation of the PAW method[37]. The choice of an appropriate exchange-correlation (XC) energy functional in DFT is crucial, and the choice is a balance between wanted accuracy and available computational resources. The metal halide ammines investigated in this screening, are demanding,

in the sense that they contain many hydrogen bonds between the ammonia molecules and the halides. These bonds are not very well described by standard functionals, but require a treatment of the van der Waal's interaction, to get a correct energetic description. However, standard generalized gradient approximation (GGA) functionals, do give a correct description of local coordination[38]. Therefore the PBE functional[39] is used for structural optimization and the more computational demanding vdW-DF functional[32] is used to calculate single point energies of the optimized structures. The Brillouin-zone is sampled using a Monkhorst–Pack grid[40] with at k-point density of approximately 25 k-points per Å^{-1} using a grid spacing of 0.18 Å.

The release patterns are determined by calculation of the enthalpies of desorption (ΔH) from the different mixed ammine phases, starting out by determining the highest observed phase, which is the phase with the highest ammonia content to be observed (e.g. the hexa ammine for $MgCl_2(NH_3)_6$ and octa ammine for $SrCl_2(NH_3)_8$). The phase with the highest stable ammonia content is determined by comparing the energy of having the ammonia molecules absorbed or in the gas phase: $M(NH_3)_xCl_2$ (s) $\leftrightarrow$ $M(NH_3)_{x-y}Cl_2$ (s) + $Y \cdot NH_3$ (g). The expected route from the highest stable content is then determined by calculating the desorption enthalpy towards the lower phases, and ordering the ΔH's; the route taken from the highest content is determined to be to the phase with the lowest ΔH. However, if the ΔH's are too close is energy, the phases cannot be distinguished during experiments, and therefore the release is going to be to that of the low concentration, with similar ΔH. A value of 2 kJ/(mol·NH$_3$) is chosen as the minimum separation, corresponding to a peak separation of approx. 15 degrees. The desorption temperatures are estimated using the van 't Hoff equation to determine when the equilibrium pressure, p_{eq} reaches 1 bar, using a standard entropy value of 230 J/(mol·K·NH$_3$), which is a representative average value observed for the pure metal halide ammines[4], and shown previously to give a reasonable estimate of the temperatures. It should be noted that a higher uncertainty is then expected on the release temperatures than on the enthalpies of desorption.

The stability of a new mixed metal chloride is determined from the decomposition energy, to its constituent pure metal halide ammines (or salts). The dataset of pure metal halide ammines is generated by substituting the new elements into the optimized template crystal structure, obtained from the experimental structures, which are allowed to relax the atomic coordinates by a quasi-Newton type optimization algorithm[41] using the calculated DFT forces. Subsequently, the cell is allowed to relax hydrostatically, thereby keeping the symmetry. The energy of NH$_3$(g) is calculated by placing a molecule in a cube with a side length of 8 Å and using the same grid spacing as above. The decomposition energy is always calculated with reference to the most favourable way of splitting up the constituents, which might include splitting a mixed hexa ammine up to some pure octa ammine and an empty salt, when e.g. strontium is present, because it is known that strontium can coordinate eight ammonia molecules (for a detailed description of the procedure, see Ref. [20]).

The template structures used for the different phases are the computational relaxed versions of known crystal structures, as described above. The octa ammine is based on the $Sr(NH_3)_8Cl_2$ structure[12,42] with orthorhombic *Pnma* symmetry (#62). $Mg(NH_3)_6Cl_2$[43,44] is used for the hexa ammine and has cubic *Fm-3m* symmetry (#225). The di ammine is based on $Ca(NH_3)_2Cl_2$[45], which is known to be isostructural with $Sr(NH_3)_2Cl_2$[42], that upon relaxation ends up with orthorhombic *Ccme* symmetry (#64). The mono ammine is based on $Mg(NH_3)Cl_2$[8] with orthorhombic *Pbnm* symmetry (#62). Different packing and coordination is observed for the simple metal halide salts of the general form MX_2, depending on ratio between the radii of the metal (M) and the halide (X) (rM/rX)[46,47]. The cubic fluorite structure is generally observed for large ratios *e.g.* in the case of $SrCl_2$[47,48]; lowering this ratio, first the $CaCl_2$[49] structure and finally the layered $MgCl_2$[50] structure is observed, when very small cations (or big anions) are present. For the pure metal chlorides only containing one metal, primarily the structures of $MgCl_2$ and $CaCl_2$ are observed, and only a very limited number of materials exist in the cubic $SrCl_2$ structure (e.g. $SrCl_2$ itself and $BaCl_2$); because of this, the new mixed materials are only tested in the two former structures, and the one with the lower energy is selected. The salt structures are $MgCl_2$[50], with trigonal *P-3m1* symmetry (#164) and $CaCl_2$[49], with tetragonal *P4₂/mnm* symmetry (#136).

To set up a new structure, the database of pure metal chlorides is consulted to obtain the important structural parameters, which have to be set to get a correct description of the energy. The starting point is always the reference template structure, which initially is scaled to have the average volume of the pure references. Subsequently the distance between the ammonia molecules, and the coordinating metal is adjusted to represent the observed values for the pure metal ammines. This is done individually for all the eight metal atoms present in the structure, to ensure that the local description of the hydrogen bonds is correct. By using the template-based set-up, the structures are not necessarily the thermodynamic ground state structures, but by keeping the template structures fixed, the systematic variations and stability trends become apparent. The structural uncertainty is expected to be similar in all phases, resulting in a good description of the release enthalpy. Full optimization of all the structures is not practically feasible and will only be performed for selected candidates.

The control of the genetic algorithm and the set-up and execution of the calculations are performed using the atomic simulation environment (ASE)[51] and the Computational Materials Repository (CMR) database[52]. Recently, an internal database have been added to ASE, facilitating easier set-up of the genetic algorithm. Both environments allow the user to store and retrieve data while the algorithm is running, allowing easy monitoring and sharing of results. Furthermore, prior to making a calculation, the algorithm checks if any of the included structures have already been run with the same parameters earlier - if that is the case, the structure and relevant parameters are simply retrieved, significantly lowering the total computing time. All necessary software to use the algorithm and introductory tutorials are freely available at https://wiki.fysik.dtu.dk/ase.
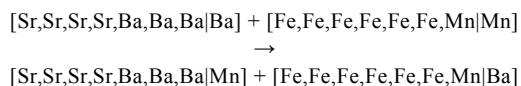
Genetic Algorithm Setup

The present screening approach is an extension of our earlier work using genetic algorithms[20], where the goal was to predict new ammonia storage materials for HT-PEMFC, which successfully located the global optimum in the defined search space. For a discussion of the selection of specific parameters the reader is referred to [20]. We apply a relative simple fitness function and define some selection rules determining where the algorithm should not search further. As mentioned, the goal of the screening is to find the optimal binary or ternary metal chlorides, which have the highest possible uptake and release of ammonia in a specific temperature interval. Because the ammines should be used as future energy carriers, the total system weight is very important, and therefore the ultimate structure has the highest release in the interval relative to the weight of the material. The fitness function is thus defined as the accessible weight percent of hydrogen (wH) released in the specified temperature interval, not taking into account the number of steps, as long as the releases are in the interval (see "Calculation Details", for information about the determination of the temperatures). To ensure that the proposed materials are thermodynamically stable during cycling, only structures which are stable against decomposition are allowed in the population, which defines the "parents" that can be used for offspring creation. We define a material as being stable if all predicted observed phases are stable against decomposition. Because of the use of fixed template structures, mixed phases are allowed to be marginally unstable (up to 0.25 eV per formula unit containing one metal atom), as the structures may be stabilized upon full relaxation.

Because of the more complex phase space with multiple phases, a relatively big population with 20 individuals is chosen, to ensure that different runs will identify the same mixtures. From the general guidelines a population size containing between 14 and 28 structures is suggested[53]. Increasing the population size changes the convergence, and therefore the convergence criteria has also been changed. The algorithm run is defined to be converged if no new individuals enters the top five of the population, containing the best 20 structures seen so far, for six generations. To ensure diversity, three candidates in the population, are chosen from all of the investigated candidates which are stable against decomposition. The parents for offspring creation are selected randomly from the population containing these 3 structures and the 17 best structures seen so far. In the initial generations, a limited number of stable structures with a release in the interval may be observed, but at the same time having unstable structures with a release. If this occurs, the unstable structures with a release in the interval are included, as they are expected to be better building blocks, than compounds having no release in the interval.

Another very important component of a successful genetic algorithm is the operators used to generate offspring. The operators employed in the current implementation are variations of the basic operators of GAs, namely crossover

and mutations[20,22]. The crossover operator takes two parent structures and splice them at a random point in the atoms string representing the metal constituents, and bring together the first part from one parent with the last part from the other parent and vice versa:

[Sr,Sr,Sr,Sr,Ba,Ba,Ba|Ba] + [Fe,Fe,Fe,Fe,Fe,Fe,Mn|Mn]
→
[Sr,Sr,Sr,Sr,Ba,Ba,Ba|Mn] + [Fe,Fe,Fe,Fe,Fe,Fe,Mn|Ba]

Three different mutation operators are available: the random mutation substituting one random chosen metal to another random chosen metal; a neighbour mutation using chemical knowledge and mutating a random chosen metal to one of neighbours in the periodic table (up, down, left, right); and finally a complete mutation making a totally random structure without using any information from the previous generations at all. All the operators are important for different reasons: to ensure not ending up in a pre-converged state, the random operators (random mutation and complete mutation) are important, and to ensure using previous important genetic information, the local operators (crossover and neighbour mutation) are important for the optimization of the found structures in a more local part of the phase space. Most important are the local operators, as they lower the total number of calculations, and they are therefore used three times more than the random operators. Regarding the random operators, the random mutation is obviously more important to generate optimized offspring, and is therefore used three times more than the complete mutation. For the local operators, it is most important to combine genetic information from different parents using the crossover operator, which therefore is used twice as much as the neighbour mutation.

By calculating energies for all the pure metal chlorides in the cubic [SrCl$_2$] structure, it is evident that only SrCl$_2$ and BaCl$_2$ prefer the cubic structure, because of this, only [CaCl$_2$] and [MgCl$_2$] are used as templates as mentioned. This will introduce a small error in candidates containing Sr or Ba, and to ensure that no candidates are missed, the temperature interval has been increased in the high-temperature end, because using a salt with higher energy would result in a higher ΔH value, and a corresponding higher release temperature. More specifically, the allowed interval is set to be [0;130°C], which should be large enough to include the structures with the highest differences.

Experimental

Synthesis by Spray Drying

To prepare the mixed salts by spray drying, the following procedure was followed. The salts (min. purity 99 %) were dried in an oven at 300 °C to obtain anhydrous metal chlorides, in pre-described molar ratios, and dissolved in demineralised water to obtain a 10 wt% aqueous solution. The solid solution was made by spray drying of the aqueous solution. A laboratory scale B290 Buchi Mini Spray Dryer was used for this purpose. After analysing different parameters and their influence on the final properties of the

solid mixture, the following settings were selected: inlet temperature: 220 °C, feed rate: 10 % (0.2 L/h), aspirator rate: 60 % (20 m^3/h), spray drying air flow: 680 L/h. Prior to testing, the sample was further dried in an oven above 300 °C for 24 h to reach a water content below 0.05 wt%.

Thermogravimetric Analysis (TGA)

Thermogravimetric desorption measurements were performed on a high pressure thermogravimetric analyser, HP-TGA ISOSORP Gas LP-flow produced by Rubotherm. The distinctive feature of this instrument is the separation of the balance from the sample environment by magnetic coupling. This enables the sample to be exposed to corrosive gases, such as ammonia, at different pressures without affecting the balance.

All samples were analysed with the following method: 1) annealing of a sample at 200 °C – 400 °C in nitrogen gas atmosphere; the temperature was varied, depending on the sample compositions and temperature required to remove all residual water, 2) cool down to 20 °C and evacuation, 3) saturation with ammonia gas at 4 bars at 20 °C, 4) desorption of ammonia by increasing temperature from 20 °C to 250 °C with a heating rate of 1 °C/min in 1 bar of ammonia gas.

Results and Discussion

Phase Space Analysis

Three different runs from different random populations where started. Figure 1 shows all the investigated structures from the three different runs after complete searches fulfilling the convergence criteria (5 best individuals constant for 6 generations). The fitness and the predicted release enthalpies and the corresponding release temperatures for all stable structures from the three different runs are shown. As can be seen from the figure, the two best structures, which are found by all three runs, seem to be somewhat decoupled from the other investigated structures, proving the algorithms ability to identify structures, in different regions of the phase space. The two best structures are special in the way that they have a multi-step release in the temperature interval, which is only seen for a very limited number of structures in the searches (many materials do have a multi-step release, but with some of the releases at too low or high temperatures). The rest of the structures seem to be more correlated, also proving the algorithms success to find the optimal solution in a small subset. Both features are important for the algorithm to work, and appear to support the choice of operators.

In Figure 2 the different decoupled groups have been characterized by the release pattern. As is evident the groups are formed as a result of different releases. Clearly, the algorithm has tested most materials giving a release from the octa ammine to a di ammine in the interval. By mutation and crossover, these mixtures have created "a tail" of offspring giving a full release from the octa ammine to the salt. It is also evident that the hexa ammines with a one step release, generally bind the ammonia strongly, resulting in releases at relatively high temperatures, often outside the defined temperature interval (and therefore not shown in Figure 1 and 2).
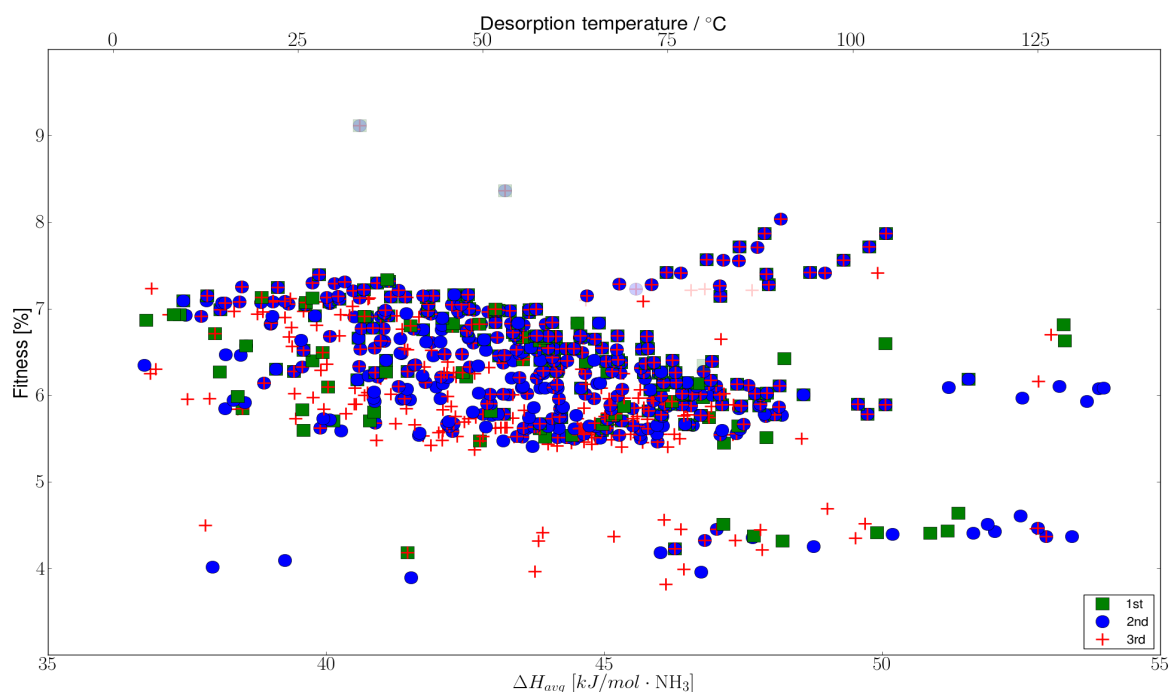
Figure 1: Visited parts of the search space defined by the weighted average release enthalpy, ΔH_{avg}, is shown for the mixtures found in three different runs. Multi-step releases are marked with faded symbols. Only stable structures which fulfil the decomposition criteria are shown.
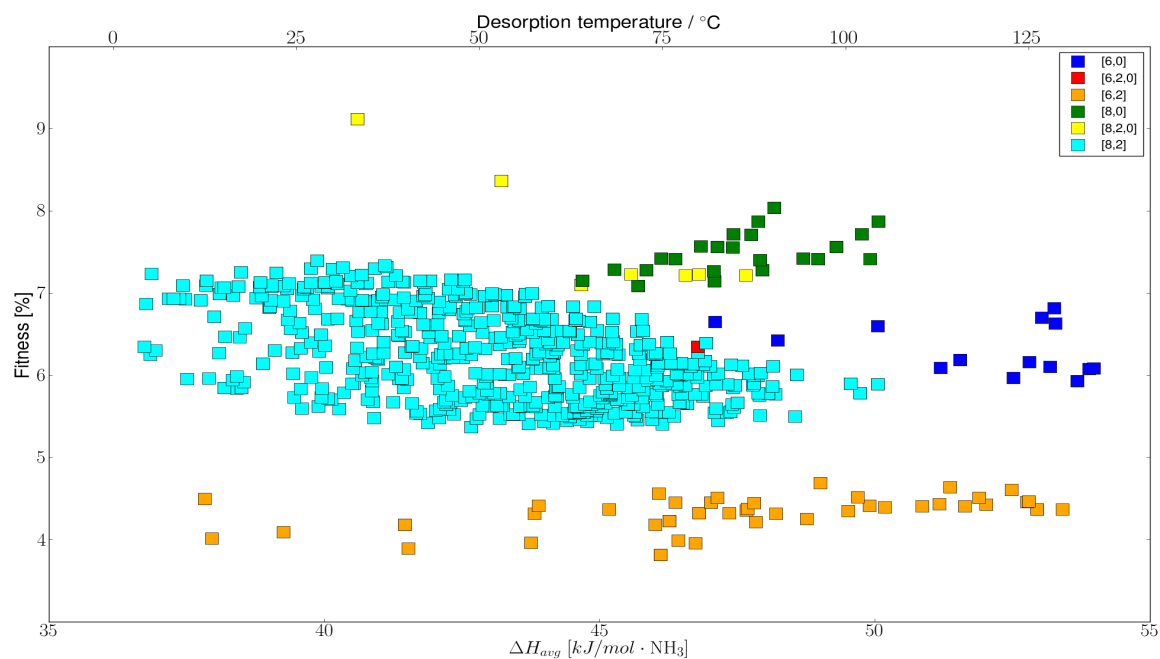

Figure 2: Visited parts of the search space, showing that different reactions are grouped in bands. The legends and colouring show the predicted observed phases, where 8 signifies octa ammine, 6 hexa ammine, 2 di ammine and 0 the empty salt.

Best Identified Structures

As is evident from Figure 1, many similar structures have been tested and found to be stable; this is also the case for the best structures found from the three different runs presented in Table 1. The first fact to notice from the table is that the top ten is identical for the 2nd and 3rd run, and only two of the best 10 structures are missing in the first run, namely $BaSr_7Cl_{16}$ and $Ba_4CaSr_3Cl_{16}$. From the convergence tests highly similar structures are, however, identified and these structures may likely be identified if more strict convergence criteria had been applied (see section "Analysis of Algorithm Robustness").

Several of the best candidates contain a mixture of strontium and barium, which we have studied in details both computationally and experimentally previously[19]. Comparing with the previous study, which included full vdW relaxation of all structures and showed excellent agreement with experiments, it is found that using the template structures in the genetic algorithm predict the correct one-step releases with a mean average error of the estimated desorption enthalpies of only 1.4 kJ/(mol·NH₃). This is an impressive accuracy even using a salt template structure from calcium, which is known not to be the minimum, as described in the methods section.

Common for all the structures containing barium and strontium is the predicted one-step release, as opposed to the two-step release predicted for the two top candidates containing a mixture of copper, yttrium and either strontium or calcium. As discussed in the introduction, a one-step release is genereally preferred, and if a multi-step release is to be used, it is important that the release temperatures for the different steps are in a relatively narrow interval. The two best candidates, have a relatively big gap between the release temperatures, which make them less attractive with a temperature span of the release of almost 100 °C. However, the difference in release enthalpies of going from the octa ammine to the di ammine or directly to the salt is only around 3 kJ/(mol·NH₃), which is only slightly higher than the limit of 2 kJ/(mol·NH₃) that was defined as the minimum gap needed to separate the phases in an experiment. It might therefore be possible to tune the system to give a one-step release, which would have an interesting release temperature (Figure 1).

As mentioned, a relatively simple fitness function was applied, and the maximum possible release in the interval corresponds to the maximum weight percent of hydrogen (wH) in the ammoniated compound. It is therefore possible to determine the number of structures that could in principle have a higher fitness than the best structure found so far – in this case there are 4736 structures, which one have to check to ensure that the global optimum in the defined search space is found. However, in our earlier work[20], we verified that the method indeed found the global optimum, and even if better mixtures exist in the search space investigated here, we have made great improvements lowering the number of possible candidates, and identified structures superior to the experimentally known structures.

Analysis of Algorithm Robustness

The robustness of the current implementation has also been tested, by analysing the three different runs. Figure 3, shows that the different runs ends up finding the same high fitness structures, by using different routes in the phase space. The 1st run quickly finds the high-fitness structures, and converges after only 20 generations using some building blocks with relatively high fitness, which were found quite early. The 2nd and 3rd run are similar and have slower convergence due to the 2nd-5th best structures changing more slowly. As mentioned, the algorithm has the possibility to reuse already calculated data - in these three runs 28 % of the calculations were skipped, significantly lowering the extra computing time needed to make more trial runs from different populations.

To further test the chosen convergence criteria, we let all three runs continue with two extra generations, to see if new relevant structures entered the population. Afterwards, it was analysed if the top ten structures would have been different with other criteria. By inspection of Figure 3 and 4 it is clear, that the first run was special, and converged very fast. As

1st run			2nd run			3rd run		
Structure	Fitness	Reaction	Structure	Fitness	Reaction	Structure	Fitness	Reaction
Ca4Cu2Y2Cl16	9.12%	[8,2,0]	**Ca4Cu2Y2Cl16**	9.12%	[8,2,0]	**Ca4Cu2Y2Cl16**	9.12%	[8,2,0]
Cu2Sr4Y2Cl16	8.37%	[8,2,0]	**Cu2Sr4Y2Cl16**	8.37%	[8,2,0]	**Cu2Sr4Y2Cl16**	8.37%	[8,2,0]
Ba2Sr6Cl16	7.87%	[8,0]	BaSr7Cl16	8.04%	[8,0]	BaSr7Cl16	8.04%	[8,0]
Ba2Sr5YCl16	7.87%	[8,0]	**Ba2Sr6Cl16**	7.87%	[8,0]	**Ba2Sr6Cl16**	7.87%	[8,0]
Ba3Sr5Cl16	7.72%	[8,0]	**Ba2Sr5YCl16**	7.87%	[8,0]	**Ba2Sr5YCl16**	7.87%	[8,0]
Ba3Sr4YCl16	7.71%	[8,0]	**Ba3Sr5Cl16**	7.72%	[8,0]	**Ba3Sr5Cl16**	7.72%	[8,0]
Ba4Sr4Cl16	7.57%	[8,0]	**Ba3Sr4YCl16**	7.71%	[8,0]	**Ba3Sr4YCl16**	7.71%	[8,0]
Ba4Sr3YCl16	7.56%	[8,0]	Ba4CaSr3Cl16	7.71%	[8,0]	Ba4CaSr3Cl16	7.71%	[8,0]
Ba5Sr3Cl16	7.42%	[8,0]	**Ba4Sr4Cl16**	7.57%	[8,0]	**Ba4Sr4Cl16**	7.57%	[8,0]
Ba5Sr2YCl16	7.42%	[8,0]	**Ba4Sr3YCl16**	7.56%	[8,0]	**Ba4Sr3YCl16**	7.56%	[8,0]

Table 1: Top ten candidates from three different runs, starting from random and thereby different structures. The column "Reaction" shows the predicted observed phases, where 8 signifies octa ammine, 2 di ammine and 0 the empty salt. The highlighted structures are found by all three runs, with the original convergence criteria. The fitness function is defined as the accessible weight percent of hydrogen (wH) released in the specified temperature interval.

discussed in the section "Best Identified Structures", the first run is missing two of the candidates found by the two other runs. Comparing the two last runs, they are more similar, finding the same structures, and do not find new structures in the two extra generations.

From the analysis, it is clear that the number of generations is the most important part of the convergence criteria, significantly increasing the success by requiring that no new structures enters for 6 generations. The third run would have been stopped halfway after 24 generations, if the convergence criteria for instance had been reduced to five stable structures for five generations, only identifying one of the top ten structures. This proves that the convergence criteria are adequate, but comparing top three would actually have been enough in this search space, but would not have lowered the number of structures to test, and requiring stable top five is therefore still recommended. Averaging over the three runs, it is evident that the global success rate is very high (Figure 4), proving the robustness of the algorithm. Therefore one run should in general be enough to find the best candidates, however one should take care if the run converges very fast testing only a small fraction of the total combinations.

Experimental Tests of Selected Candidates

Table 1 reveals many mixtures only containing alkali-earth metals, which are already known to store ammonia both in the pure metal halides and for some mixed materials. Four of the top ten materials are binary metal halides, containing a mixture of barium and strontium chloride in different ratios, resulting in different densities and slightly different release
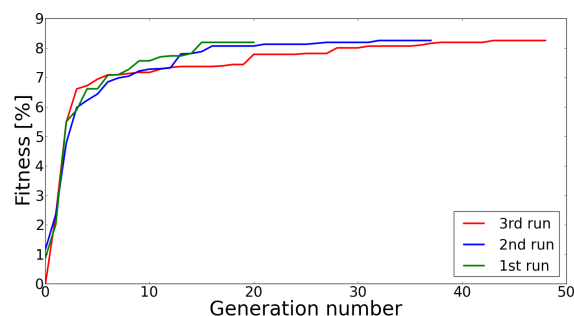

Figure 3: Genetic algorithm convergence for three different runs. It is shown how the average fitness of the top five best stable structures changes as the algorithm runs evolve.

temperatures (Table 1 and Figure 1). We have recently investigated the storage capacities of these Ba/Sr mixtures[19]. As shown in Figure 5, the predicted releases are generally observed, and all materials release all the stored ammonia in the defined temperature interval. The releases for the mixtures are shifted to higher temperatures compared to pure barium chloride, which releases the ammonia at a too low temperature. Furthermore the mixtures display an increased storage capacity as strontium is significantly lighter than barium. $BaSr_7Cl_{16}$ is the only material, which do not show the predicted one-step release from the octa ammine. Despite of this, the material is still interesting, as all the ammonia is released in the defined temperature interval.

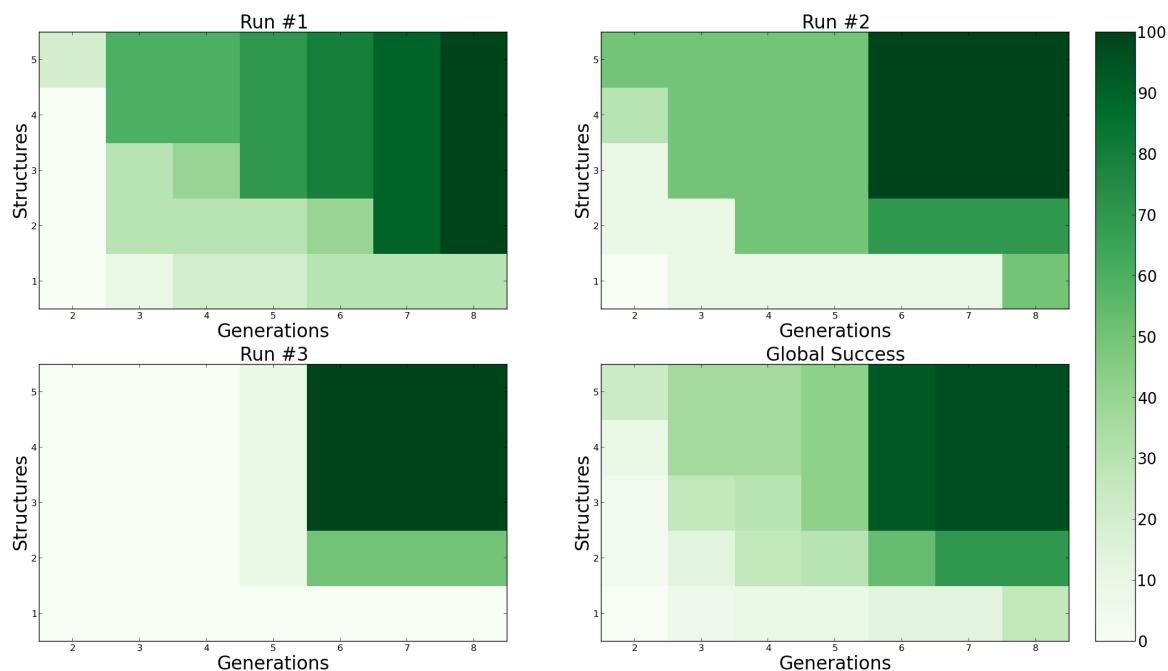Another alkaline-earth mixture, $Ba_4CaSr_3Cl_{16}$, is also found

Figure 4: Success of algorithm with changed convergence criteria, showing which fraction (in percent) of the top 10 structures, that would have been found with different convergence criteria. The chosen criteria was top 5 stable for 6 generations. Run #1-3 shows the success compared to the found structures if the individual run had been converged to top 5 stable in 8 generations. The Global Success is averaging over the three runs comparing to the best top ten structures found in all runs (similar to final top ten for run #2-3, see Table 1).

in the top ten, with a predicted one-step release. This material was synthesised by spray drying and the ammonia storage properties are presented together with the Ba/Sr mixtures and the pure metal chlorides in Figure 5; to our knowledge this is the first reported ternary metal chloride for ammonia storage. The material behaves slightly different compared to the binary metal halides, showing a release in a broader interval, although most of the release is in the expected interval (>95 %). The stability during cycling has also been tested (Figure S1), as this might be expected to be a problem with three different metals, with relatively different atomic radii[54]. Similar to other metal halide ammines, a favourable small change is observed after the first cycle, most probably due to the formation of a porous structure in the material[8]. The 2nd-5th cycles show an slightly faster release due to improved kinetics, and basically no changes are observed between these cycles, verifying that a stable material has been prepared.

The two top candidates, $Ca_4Cu_2Y_2Cl_{16}$ and $Sr_4Cu_2Y_2Cl_{16}$, were also investigated. Because of the use of template structures the mixed materials have an enforced average oxidation state +2, which is not normally observed for pure yttrium chloride. An attempt to synthesize the mixed salt was conducted starting from $CaCl_2$, $CuCl$ and YCl_3, due to the very limited solubility of $CuCl$, synthesis using spray drying was not possible. Planetary ball milling, was therefore employed, starting from the mentioned salts (see supl. info). The obtained mixture was analysed using XRPD, and revealed partial mixing, as the precursors were not visible any more. Complete mixing was, however, not possible and metallic copper was clearly visible. Apart from the peaks associated with metallic copper, the analysis did not reveal any known compounds in a database search. Thus, despite of the known imperfect mixing illustrated by the presence of the Cu peaks, new phases were formed.

Despite the mentioned difficulties and the uncertainties about the constituents, the ammonia storage properties of the sample, were analysed (see sup. info). The material is able to store ammonia and release a large part of it in the predicted temperature interval (~80 %); however, the stored amount of ammonia is lower than the predicted amount, due to the presence of metallic copper. Because of these challenges the other yttrium containing compounds in Table 1 have not yet been tested.

Conclusions

By using genetic algorithms combined with vdW-DF density functional theory calculations, we have identified a number of new, binary and ternary metal chloride ammines with superior storage capacities accessible at temperatures suitable for system integration with PEMFCs. Some of the identified candidates containing a mixture of strontium and barium chloride have previously been reported to release the stored ammonia in the specified interval, proving the accuracy of the employed template-based screening[19].

A ternary metal halide ammine, $Ba_4CaSr_3Cl_{16}$, was also proposed, and found to have a one-step release, releasing the stored ammonia in the desired temperature interval. To our knowledge this is the first reported ternary metal halide for ammonia storage.

New ternary mixtures containing yttrium, copper and either calcium or strontium, $Ca_4Cu_2Y_2Cl_{16}$ and $Sr_4Cu_2Y_2Cl_{16}$, were proposed to have very high storage capacities exceeding 9.1 wt% for the calcium system. Initial tests were also performed for these systems, but a complete synthesis was not possible with neither spray drying nor mechano-chemical. Despite this, the materials obtained from the synthesis were tested, and showed promising storage properties, which are now being investigated further, using different synthesis techniques. Preparation of the mixed salts require high temperatures and
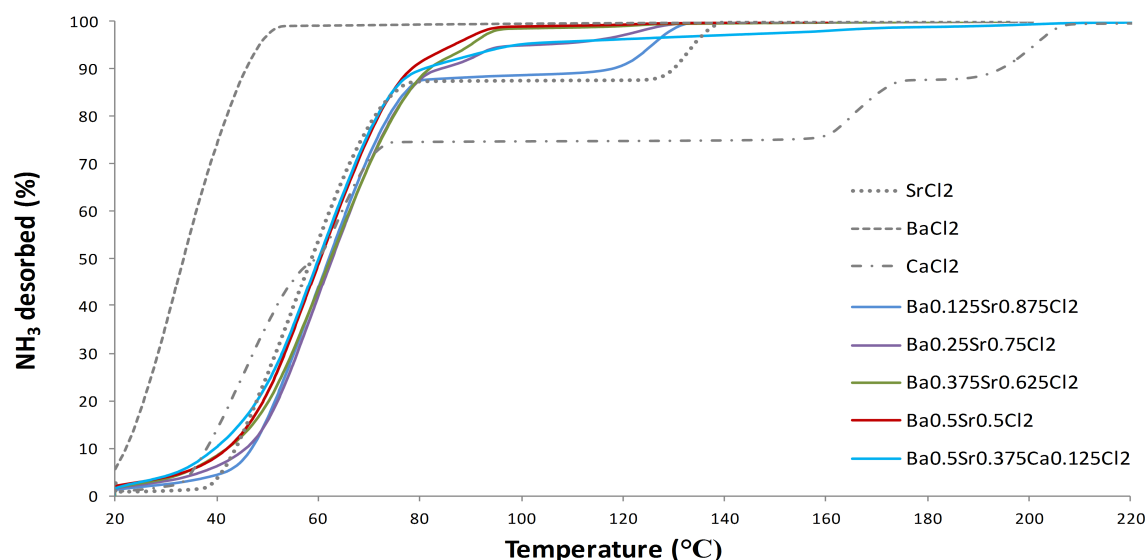

Figure 5: Ammonia temperature programmed desorption (TPD) curves, for selected candidate mixtures containing Ba, Sr and Ca. For comparison the release for the pure salts are also shown. The mixtures only containing Sr and Ba are from Ref. [19].

long-time mechano-chemical synthesis under higher ammonia pressure could lead to higher conversion efficiency.

Acknowledgements

References

1. V. Smil, *Nature*, 1999, **400**, 415.
2. G. Thomas and G. Parks, *Potential roles of ammonia in a hydrogen economy*, U.S. Department of Energy (DOE), 2006.
3. W. Biltz, *Zeitschrift für Anorg. und Allg. Chemie*, 1923, **130**, 93–139.
4. E. Lepinasse and B. Spinner, *Int. J. Refrig.*, 1994, **17**, 309–322.
5. C. H. Christensen, R. Z. Sørensen, T. Johannessen, U. J. Quaade, K. Honkala, T. D. Elmøe, R. Køhler, and J. K. Nørskov, *J. Mater. Chem.*, 2005, **15**, 4106–4108.
6. C. H. Christensen, T. Johannessen, R. Z. Sørensen, and J. K. Nørskov, *Catal. Today*, 2006, **111**, 140–144.
7. A. Klerke, C. H. Christensen, J. K. Nørskov, and T. Vegge, *J. Mater. Chem.*, 2008, **18**, 2304–2310.
8. R. Z. Sørensen, J. S. Hummelshøj, A. Klerke, J. B. Reves, T. Vegge, J. K. Nørskov, and C. H. Christensen, *J. Am. Chem. Soc.*, 2008, **130**, 8660–8.
9. D. Chakraborty, H. N. Petersen, C. Elkjær, A. Cagulada, and T. Johannessen, *Fuel Cells Bull.*, 2009, **2009**, 12–15.
10. R. Lan, J. T. S. Irvine, and S. Tao, *Int. J. Hydrogen Energy*, 2012, **37**, 1482–1494.
11. F. Schüth, R. Palkovits, R. Schlögl, and D. S. Su, *Energy Environ. Sci.*, 2012, **5**, 6278–6289.
12. R. E. Johnsen, P. B. Jensen, P. Norby, and T. Vegge, *J. Phys. Chem. C*, 2014, **118**, 24349–24356.
13. T. D. Elmøe, R. Z. Sørensen, U. Quaade, C. H. Christensen, J. K. Nørskov, and T. Johannessen, *Chem. Eng. Sci.*, 2006, **61**, 2618–2625.
14. H. S. Jacobsen, H. A. Hansen, J. W. Andreasen, Q. Shi, A. Andreasen, R. Feidenhans'l, M. M. Nielsen, K. Ståhl, and T. Vegge, *Chem. Phys. Lett.*, 2007, **441**, 255–260.
15. A. Tekin, J. S. Hummelshøj, H. S. Jacobsen, D. Sveinbjörnsson, D. Blanchard, J. K. Nørskov, and T. Vegge, *Energy Environ. Sci.*, 2010, **3**, 448–456.
16. T. Vegge, R. Z. Sørensen, A. Klerke, J. S. Hummelshøj, T. Johannessen, J. K. Nørskov, and C. H. Christensen, in *Solid state hydrogen storage: Materials and chemistry*, ed. G. Walker, British Welding Research Association, 2008, pp. 533–568.
17. C. Y. Liu and K. Aika, *Ind. Eng. Chem. Res.*, 2004, **3**, 6994–7000.
18. C. Y. Liu and K. Aika, *Ind. Eng. Chem. Res.*, 2004, **43**, 7484–7491.
19. A. Bialy, P. B. Jensen, D. Blanchard, T. Vegge, and U. J. Quaade, *J. Solid State Chem.*, 2015, **221**, 32–36.
20. P. B. Jensen, S. Lysgaard, U. J. Quaade, and T. Vegge, *Phys. Chem. Chem. Phys.*, 2014, **16**, 19732–19740.
21. J. H. Holland, *Adaptation in Natural and Artificial Systems*, University of Michigan Press, 1975, vol. Ann Arbor.
22. S. Forrest, *Science*, 1993, **261**, 872–878.
23. T. Bush, C. Catlow, and P. Battle, *J. Mater. Chem.*, 1995, **5**, 1269–1272.
24. G. Jóhannesson, T. Bligaard, A. Ruban, H. Skriver, K. Jacobsen, and J. Nørskov, *Phys. Rev. Lett.*, 2002, **88**, 255506.
25. L. B. Vilhelmsen, K. S. Walton, and D. S. Sholl, *J. Am. Chem. Soc.*, 2012, **134**, 12807–16.
26. L. B. Vilhelmsen and D. S. Sholl, *J. Phys. Chem. Lett.*, 2012, **3**, 3702–3706.
27. S. Lysgaard, D. D. Landis, T. Bligaard, and T. Vegge, *Top. Catal.*, 2014, **57**, 33–39.
28. A. O. Lyakhov, A. R. Oganov, H. T. Stokes, and Q. Zhu, *Comput. Phys. Commun.*, 2013, **184**, 1172–1182.
29. L. B. Vilhelmsen and B. Hammer, *J. Chem. Phys.*, 2014, **141**, 044711.
30. P. Hohenberg and W. Kohn, *Phys. Rev.*, 1964, **136**, B864–B871.
31. W. Kohn and L. J. Sham, *Phys. Rev.*, 1965, **140**, A1133–A1138.
32. M. Dion, H. Rydberg, E. Schröder, D. C. Langreth, and B. I. Lundqvist, *Phys. Rev. Lett.*, 2004, **92**, 246401.
33. B. McNicol, D. Rand, and K. Williams, *J. Power Sources*, 2001, **100**, 47–59.
34. O. Barbier, L. Arreola-Mendoza, and L. M. Del Razo, *Chem. Biol. Interact.*, 2010, **188**, 319–33.
35. *www.chemicool.com*, 2013.
36. J. J. Mortensen, L. B. Hansen, and K. W. Jacobsen, *Phys. Rev. B*, 2005, **71**, 035109.
37. P. E. Blöchl, *Phys. Rev. B*, 1994, **50**, 17953–17979.
38. P. Haas, F. Tran, and P. Blaha, *Phys. Rev. B*, 2009, **79**, 085104.
39. J. P. Perdew, K. Burke, and M. Ernzerhof, *Phys. Rev. Lett.*, 1996, **77**, 3865–3868.
40. H. J. Monkhorst and J. D. Pack, *Phys. Rev. B*, 1976, **13**, 5188–5192.
41. P. Maragakis, S. A. Andreev, Y. Brumer, D. R. Reichman, and E. Kaxiras, *J. Chem. Phys.*, 2002, **117**, 4651–4658.
42. S. Lysgaard, A. L. Ammitzbøll, R. E. Johnsen, P. Norby, U. J. Quaade, and T. Vegge, *Int. J. Hydrogen Energy*, 2012, **37**, 18927–18936.
43. I. Olovsson, *Acta Crystallogr.*, 1965, **18**, 889–893.
44. I. Hwang and T. Drews, *J. Am. Chem. Soc.*, 2000, **122**, 8486–8489.
45. S. Westman, P. Werner, and T. Schuler, *Acta Chem. Scand. A*, 1981, **35**, 467–472.
46. D. Partin and M. O'Keeffe, *J. Solid State Chem.*, 1991, **183**, 176–183.
47. V. Kanchana, G. Vaitheeswaran, and a. Svane, *J. Alloys Compd.*, 2008, **455**, 480–484.
48. G. Brauer and O. Müller, *Zeitschrift für Anorg. und Allg. Chemie*, 1958, **295**, 218–226.
49. C. Howard, B. Kennedy, and C. Curfs, *Phys. Rev. B*, 2005, **72**, 2–7.
50. A. Leineweber, M. W. Friedriszik, and H. Jacobs, *J. Solid State Chem.*, 1999, **147**, 229–234.
51. S. R. Bahn and K. W. Jacobsen, *Comput. Sci. Eng.*, 2002, **4**, 56–66.
52. D. D. Landis, J. S. Hummelshoj, S. Nestorov, J. Greeley, M. Dulak, T. Bligaard, J. K. Norskov, and K. W. Jacobsen, *Comput. Sci. Eng.*, 2012, **14**, 51–57.
53. J. T. Alander, in *Proceedings Computer Systems and Software Engineering*, IEEE Comput. Soc. Press, 1992, pp. 65–70.
54. R. Shannon, *Acta Crystallogr. Sect. A*, 1976, **32**, 751–767.

Table of Contents Entry

Superior ammonia storage materials are predicted from a computational screening combining DFT calculations with genetic algorithms. Selected candidates with record high capacities were synthesised, and their storage capacities were confirmed.
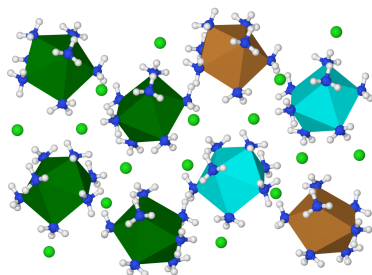
Broader Context

Metal halide ammines are suitable for reversible, high-density ammonia and indirect hydrogen storage. Existing metal halide ammines are not applicable for use as energy carriers for automotive, fuel cell applications, because the ammonia is released at unsuitable temperatures, and often in multiple steps over a broad temperature range. Therefore, there is an interest in finding new mixed materials releasing all ammonia in a narrow temperature interval suitable for system integration with low-temperature polymer electrolyte membrane fuel cells (PEMFC). Using advanced computational search techniques combining Density Functional Theory (DFT) calculations with genetic algorithms, we have identified new superior mixed metal halide ammines, in a search space containing several thousand candidates. Some of the proposed materials have been synthesised, and their ammonia storage properties have been verified. The success of the implemented algorithm is verified by three trial runs capable of finding the same optimal mixtures starting from different random populations, testing less than five percent of the candidates in a search space containing more than 100.000 structures. This approach reduces the number of experimental screening tests, facilitating environmentally friendly and cost-saving computational materials design and optimization, and is easily transferable to other classes of materials.

Supporting Information

Accelerated DFT-Based Design of Materials for Ammonia Storage

Peter Bjerre Jensen,[a,b] Agata Bialy[c], Didier Blanchard[a], Steen Lysgaard,[a] Ulrich J. Quaade[c] and Tejs Vegge*[a]

[a] *Department of Energy Conversion and Storage, Technical University of Denmark, Frederiksborgvej 399, DK-4000 Roskilde, Denmark; E-mail: teve@dtu.dk*
[b] *Center for Atomic-scale Materials Design, Technical University of Denmark, Fysikvej 311, DK-2800 Kgs. Lyngby, Denmark. E-mail: pbjen@dtu.dk*
[c] *Amminex Emmisions Technology A/S, Gladsaxevej 363, DK-2860 Søborg, Denmark; E-mail: ujq@amminex.com*
[*] *Corresponding author: Phone: +45 4677 5818, Fax: +45 4677 5858*

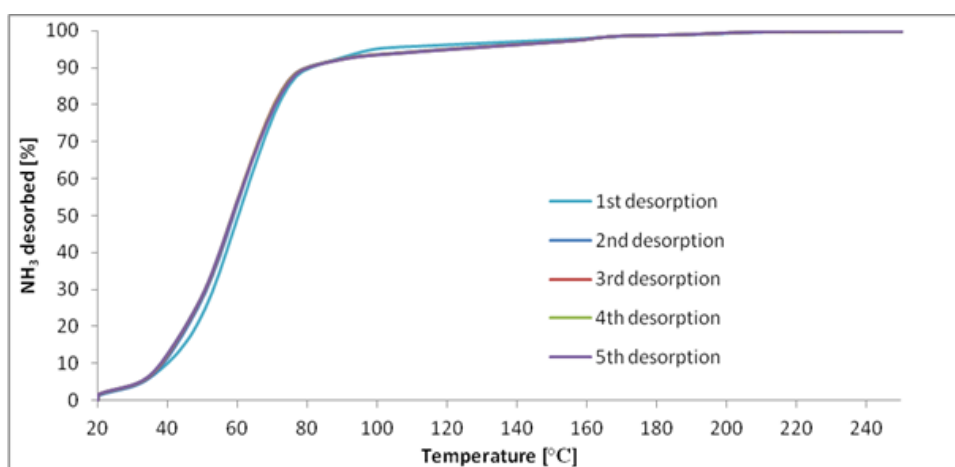## TGA Measurements Showing Stability During Cycling

Figure S1: Cycling experiments for $Ba_4CaSr_3Cl_{16}$, confirming the stability of the mixture.

Alternative Synthesis Procedure for Yttrium Containing Mixtures

Synthesis by Ball Milling

As an alternative synthesis method, not requiring dissolution of the salts, high energy planetary ball milling was employed. Attempts to synthesize the ternary salt were performed by ball milling under an ammonia atmosphere. 4.0 g of the precursor salts (min. purity 99 %), were added to a steel vial along with 25 tungsten carbide balls, resulting in a sample to ball mass ratio of 1:100. The vial with a volume of 250 ml was rotated at 650 rpm for 30 min. on a Fritsch Pulverisette P6.

The dried powders were added to the vial in an argon filled glove box to prevent contact with humidity from air (H_2O and O_2 < 0.1 ppm). Once the vial was tightly sealed, the Ar was purged using a vacuum pump (~10^{-3} mbar) and the vial was filled with NH_3 (5.5 bar). Prior to milling, time was given for the pressure to equilibrate in the vial as the different salts absorbed ammonia. After roughly one hour, the pressure was judged to be constant and adjusted to 5.5 bar NH_3 again. The milling was performed in steps of 2 minutes followed by breaks of 5 minutes to allow the vial to cool down in order to keep its temperature as low as possible. Once the milling was finished, the ammonia was pumped out and the vial emptied in the glove box.

Analysis Using a Sievert's Apparatus

The powder obtained from ball milling is inserted into an autoclave to perform the ammonia cycling. The autoclave is connected to a Sievert's type apparatus, analysing the ammonia content based on measuring the pressure changes in a fixed volume. During absorption of ammonia, the decrease of the pressure in the system is recorded while during the desorption, the increase of the ammonia pressure is recorded.

Typically, a pressure of 1.0 bar was used at the beginning of the desorption, increasing up to 1.7 bar, and a pressure of 2.5 bar was used at the beginning of the absorption, ending at around 1.7 bar when the sample was fully ammoniated. For the desorption, the powder is heated with ramps from 0.5 to 2 °C/min. For the absorption, the sample is kept at room temperature.
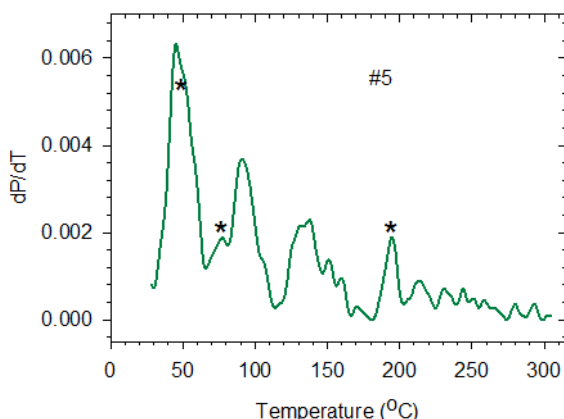

Figure S2: TPD experiment of the mixture obtained, in the first synthesis of $Ca_4Cu_2Y_2Cl_{16}$. The stars indicates possible $CaCl_2$ release events.
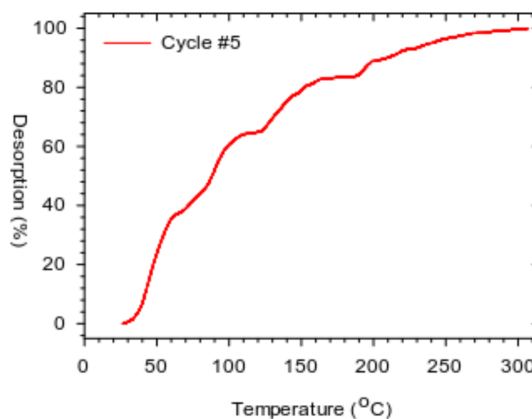

Figure S3: TPD experiment of the mixture obtained, in the first synthesis of $Ca_4Cu_2Y_2Cl_{16}$.